NTNU – Trondheim
Norwegian University of
Science and Technology

Comparing Controllers for Dynamic Positioning of Ships in Extreme Seas

Ole Maurice Røste Rabanal

Master of Science in Cybernetics and Robotics
Submission date: June 2015
Supervisor: Morten Breivik, ITK
Co-supervisor: Asgeir Sørensen, IMT
Astrid H. Brodtkorb, IMT

Norwegian University of Science and Technology
Department of Engineering Cybernetics

Problem Description

During station keeping marine for operations in areas as the North Sea, extreme seas may occur. Operating under such environmental conditions requires a dynamic positioning (DP) system that can handle the strong wind acting on the vessel, when the strong wind simultaneously produces higher and longer waves causing longer periods of oscillations and currents. Such challenges require DP systems with high positioning accuracy and if extreme seas occurs, robust controllers should be able to still maintain position

The aim of this thesis is to develop two different DP controllers and evaluate their behavior in station keeping during extreme seas with the aim of achieving a safer, smarter and greener operation. An operation is safe when the controller is precise, green when the fuel consumption is minimized and smart when the controller achieves both goals simultaneously. The controllers to be tested and compared are proportional-integral-derivative with acceleration feedback (PID-AFB) and sliding-mode control (SMC). PID-AFB has been proven to provide good performance operating in extreme seas by Nguyen et al. (2007) and Brodtkorb et al. (2014), with the controller reacting fast to disturbance forces. However, AFB requires non-noisy acceleration signal measurements, and this may not always be available.

This motivates the testing of other types of controllers in order to investigate if there exists other control strategies with better performance than PID-AFB in extreme seas. SMC has low sensitivity to external disturbances and is robust with respect to plant parameter uncertainties and variations such as the system's inertia and damping matrices. The latter makes the SMC a good candidate to perform just as good as, or better than, PID-AFB in extreme sea conditions. The SMC may suffer from high frequency oscillations known as chattering. Chattering may be caused by unmodeled dynamics or discrete time implementation.

The controllers are to be implemented in the Matlab/Simulink toolbox Marine Cybernetics Simulator (MCSim) for tuning and testing. A nonlinear passive observer (NPO) will be used to ensure good estimates for feedback in both controllers. Final tests involve implementing and testing of the DP control algorithms on a real ship model, Cybership III, in the Marine Cybernetics Laboratory (MCLab) at the Norwegian Marine Technology Research Institute (MARINTEK). The performance of the controllers should be compared with performance metrics in order to determine which control strategies provides the best precision during station keeping. The performance metrics used to measure the performance in MCSim are integral absolute error (IAE), integral time-weighted absolute error (ITAE) and integral squared error (ISE). When testing Cybership III in the model basin, a cost function should be made consisting of the product of each performance metric and the total energy

consumption from the thrusters on Cybership III providing an overall measure of both accuracy and energy consumption.

Summarized problem description:

1. Perform a brief literature review of background material regarding DP in extreme seas, PID-AFB and SMC.
2. Derive mathematical models for DP vessels in normal and extreme seas. Introduce ocean waves, sea states, moving from wave spectra to the time domain and Froude scaling. Use this theory for test cases in MCsim and generate sea states scaled to fit Cybership III for calm and extreme sea states.
3. Derive and implement PID-AFB, SMC, NPO and a reference model in MCSim.
4. Simulate and evaluate the performance of the controllers in MCSim using IAE, ITAE and ISE performance metrics.
5. Implement PID-AFB, SMC, NPO and a reference model for Cybership III with NIVeristand in the MCLab. In addition, an NIVeristand human machine interface should be implemented on the host PC communicating with Cybership III in real-time.
6. Perform test cases and evaluate the performance of the controllers by developing a cost function for every performance metric used in the MCSim test, e.g. the cost for IAE is a product of IAE and the total energy consumption from the thrusters mounted on Cybership III.
7. Compare the performance of the controllers for test cases in MCSim and MCLab. Comment on if MCSim is a realistic simulation platform.

Assignment given: January 15$^{\text{th}}$ 2015
Supervisor: Morten Breivik (ITK)
Co-supervisors: Asgeir J. Sørensen (IMT) and Astrid H. Brodtkorb (IMT)

Abstract

The primary purpose of this study is to develop two different dynamic positioning (DP) controllers for a model-scale supply vessel Cybership III, and determine which control strategy provides a safer, smarter and greener control when the vessel is exposed to extreme seas. DP has since the 1960s contributed to the safety and efficiency of oil-related and other operations for marine vessels. With this computer-controlled system, vessels such as research vessels, supply vessels and cruise ships can automatically maintain position and heading by using propellers when the vessel is exposed to wind, waves and current.

A nonlinear passive observer (NPO), proportional-integral-derivative with acceleration feedback (PID-AFB) controller, sliding-mode control (SMC) and a reference model for Cybership III were derived. Test cases were first performed with the Marine Cybernetics Simulator (MCSim) in calm, harsh and extreme seas. This simulator consists of a high fidelity process plant model of Cybership III in Matlab/Simulink together with models for generation of environmental forces. Secondly, tests in calm and harsh seas were performed on the model vessel in the Marine Cybernetics Laboratory (MCLab) at MARINTEK. The performance for tests in MCSim was evaluated by integral squared error (ISE), integral absolute error (IAE) and integral time-weighted absolute error (ITAE). The measures of performance for tests in the MCLab were performed by using ISE, IAE and ITAE in combination with the energy consumption of the thrusters on Cybership III in order to generate a cost function. This cost function is a new method used to evaluate the performance of the controllers with the aim of achieving a safer operation meaning good accuracy, a greener operation by minimizing energy consumption and a smarter operation by achieving the two latter simultaneously. Other measures of performance used to evaluate controllers on Cybership III and similar vessels in MCLab have as far as the knowledge of the author, only been performed with respect to the error of the positions and heading. This thesis uses a new measure of performance not only evaluating the error, but also the energy consumption during tests, thus evaluating the controller with more realistic performance measures of performance.

The PID-AFB-controller provided the best performance when the vessel was tested in extreme seas in MCSim and was evaluated only by ISE, IAE and ITAE, while the SMC achieved the best performance when tested in calm and harsh seas both in the MCLab and MCSim. The tests performed in MCSim were not comparable with the tests performed in the MCLab and the reasons for this may be inaccurate model parameters, the lack of a proper thruster model, 3D effects of the waves in the basin and reflection on the tank wall. In retrospect of the experiments, Cybership III was found to weight 14% more than modeled in MCSim and hence

the test cases in MCLab was considered to be more credible.

Sammendrag

Det primære formålet med dette studiet er å utvikle to forskjellige dynamisk posisjonerings (DP) regulatorer for et modell-skalert forsyningsskip Cybership III, og bestemme hvilken styringsstrategi som gir en tryggere, smartere og grønnere styring når båten er utsatt for ekstrem sjø. DP har siden 1960-tallet bidratt til sikkerheten og effektiviteten til oljerelaterte og andre operasjoner for marine fartøy. Med dette datakontrollerte systemet, vil fartøy slik som forskningsfartøy, forsyningsskip og cruise skip automatisk kunne holde posisjon og retning ved hjelp av propeller når fartøyet er utsatt for vind, bølger og strøm.

En ulineær passiv tilstands estimator, proporsjonal-integrasjon-derivasjon med akselerasjonstilbakekopling (PID-AFB) regulator, skyve-modus styring (SMC) regulator og en referansemodell for Cybership III ble utledet. Tester ble først utført med Marine Cybernetics Simulatoren (MCSim) i rolig, tøff og ekstrem sjø. Denne simulatoren inneholder en veldig nøyaktig prosessanlegg-modell av Cybership III i Matlab/Simulink sammen med andre modeller laget for å generere miljøkrefter. Dernest, ble tester utført i rolig og tøff sjø på det modell-skalerte fartøyet i Marine Kybernetikk Laboratorium (MCLab) ved MARINTEK. Ytelsen for testene i MCSim ble evaluert av integral kvadrert feil (ISE), integral absolutt feil (IAE) og integral-tidsvektet absolutt feil (ITAE). Ytelsesmålene for testene i MCLab ble utført ved å bruke ISE, IAE og ITAE i kombinasjon med energiforbruket til thrustere på Cybership III til å generere en kostfunksjon. Denne kostfunksjonen er en ny metode brukt til å evaluere ytelsen til regulatorene med målet om å oppnå en tryggere operasjon dvs. god presisjon, en grønnere operasjon ved å minimere energibruk og en smartere operasjon ved å oppnå de to sistnevnte samtidig. Andre ytelsesmål brukt til å evaluere regulatorer på Cybership III og lignende fartøy i MCLab har så langt forfatteren vet, blitt utført bare med hensyn til feilen til posisjonen og retningen. Denne masteroppgaven bruker et nytt mål på ytelse ved å ikke bare evaluere feilen, men også energiforbruket under tester, dermed evaluerer regulatoren med mer realistiske ytelsesmål.

PID-AFB regulatoren ga den beste ytelsen når den ble testet med ekstrem sjø i MCSim og bare evaluert av ISE, IAE og ITAE, mens SMC oppnådde den beste ytelsen når den ble testet i rolig og tøff sjø både MCLab og MCSim. Testene utført i MCSim var ikke sammenlignbare med testene utført i MCLab oggrunner for dette kan være unøyaktige modell parametere, mangel på en skikkelig thruster modell, 3D effekter av bølgene i bassenget og refleksjon i tankveggen. I ettertid av eksperimentene ble Cybership III veid til å være 14% tyngre enn den ble modellert i MCSim og med dette ble testene i MCLab ansett til å være mer troverdige.

Preface

This Master Thesis is the result from my two-year study at the Norwegian University of Science and Technology (NTNU) in Trondheim. The work was done during the spring semester 2015.

First I would like to thank my supervisor Morten Breivik for his guidance throughout this semester. Second I would like to thank Asgeir J. Sørensen for his guidance and for giving me the idea of the primary subject for this thesis. I would like to thank Torgeir Wahl for always being available at the the Norwegian Marine Technology Research Institute for questions and fixing equipment on Cybership III. I would also like to thank the fellow students at GG-44 for providing a positive, rewarding and supporting working environment. A special thanks to Astrid H. Brodtkorb that has been very available for questions and guidance throughout this semester and helpful in the Marine Cybernetics Laboratory.

Department of Engineering Cybernetics at NTNU

June 11th 2015

Ole Maurice Røste Rabanal

Table of Contents

List of Tables

List of Figures

Abbreviations

AFB	=	Centre for Autnomous Marine Operations and Systems
AFB	=	Acceleration Feedback
CPM	=	Control Plant Model
DOF	=	Degree of Freedom
DP	=	Dynamic Positioning
DCMV	=	Dynamics and Control of Marine Vehicles
ECEF	=	Earth-Centered Earth-Fixed
ECI	=	Earth-Centered Inertial
GAS	=	Global Asymptotic Stability
GNC	=	Guidance and Navigation Control
IAE	=	Integral Absolute Error
IMO	=	International Maritime Organization
ISE	=	Integral Squared Error
ITAE	=	Integral Time-weighted Absolute Error
JONSWAP	=	Joint North Sea Wave Project
LF	=	Low-Frequency
LP	=	Low-Pass
LQ	=	Linear Quadratic
MARINTEK	=	Norwegian Marine Technology Research Institute
MCS	=	Motion Capture System
MCLab	=	Marine Cybernetics Laboratory
MCSim	=	Marine Cybernetics Simulator
MIMO	=	Multiple Input and Multiple Output
MPM	=	Modified Pierson-Moskowitz
MSS	=	Marine System Simulator
NED	=	North East Down
NPO	=	Nonlinear Passive Observer
NTNU	=	Norwegian University of Science and Technology
PD	=	Proportional-Derivative
PID	=	Proportional-Integral-Derivative
PID-AFB	=	PID with AFB
RAO	=	Response Amplitude Operators
SMC	=	Sliding-Mode Control
UGAS	=	Uniform Global Asymptotic Stability
UGES	=	Uniform Global Exponential Stability
WF	=	Wave-Frequency
WF	=	Wireless Local Area Network

Symbols

Bold capital letters are matrices while bold small letters are vectors.

Hydrodynamic coefficients

$\boldsymbol{M}$	=	Inertia matrix with added mass
$\boldsymbol{M}_A$	=	Added mass matrix
$\boldsymbol{M}_{Rb}$	=	Rigid-body system inertia matrix
$\boldsymbol{C}_{Rb}(\boldsymbol{\nu})$	=	Rigid-body Coriolis and centripetal matrix
$\boldsymbol{C}_A(\boldsymbol{\nu}_r)$	=	Hydrodynamic Coriolis and centripetal matrix
$\boldsymbol{D}(\boldsymbol{\nu})$	=	Linear and nonlinear damping matrix
$\boldsymbol{G}(\boldsymbol{\eta})$	=	Restoring forces

Control and process variables

$\boldsymbol{\eta}$	=	Generalized position vector
$\boldsymbol{\nu}$	=	Generalized velocity vector
$\boldsymbol{\nu_r}$	=	Generalized relative velocity vector
$\dot{\boldsymbol{\nu}}$	=	Generalized acceleration vector
$\boldsymbol{P}_{b/n}$	=	North (N), East(E), Down(D) position
$\boldsymbol{\Theta}_{nb}$	=	Attitude in roll (ϕ), pitch (θ) and yaw (ψ)
$\boldsymbol{v}^b_{b/n}$	=	Body-fixed linear velocity in surge (u), sway (v) and yaw (w)
$\boldsymbol{\omega}^b_{b/n}$	=	Body-fixed angular velocity in roll (p), pitch (q) and yaw (r)
$\boldsymbol{S}(\boldsymbol{r}^b_g)$	=	Skew-symmetry of vector from body to center of gravity (CG)
$\boldsymbol{R}(\psi)$	=	Rotation matrix related to linear velocity
$\boldsymbol{T}_\Theta$	=	Transformation matrix related to angular velocity
$\boldsymbol{J}_\Theta(\boldsymbol{\eta})$	=	Transformation matrix related to linear and angular velocity
$\boldsymbol{y}$	=	Process measurement vector
$\boldsymbol{\xi}$	=	Wave-frequency motion vector
$\boldsymbol{b}$	=	Bias vector
$\boldsymbol{A}_\omega$	=	System matrix
$\boldsymbol{C}_\omega$	=	Measurement matrix
$\boldsymbol{E}_\omega$	=	Disturbance matrix
$\boldsymbol{\xi}_\omega$	=	Vessel WF position and velocity vector
$\mathbf{w}_{\boldsymbol{\omega}}$	=	Zero-mean Gaussian white noise vector
$\boldsymbol{T}_b$	=	Diagonal matrix of bias of time constants
$\mathbf{v}$	=	Measurement noise vector
$\boldsymbol{\tau}$	=	Control input vector
$\boldsymbol{\tau}_{env}$	=	Vector of environmental forces acting on the vessel
$\boldsymbol{K}_m$	=	Extra inertia matrix from acceleration feedback term

$\boldsymbol{M}^*$	=	Modified inertia matrix
$\boldsymbol{H}$	=	New inertia matrix of the vessel when using acceleration feedback
$\boldsymbol{s}$	=	Sliding surface vector
$\boldsymbol{\eta}_r$	=	Virtual reference vector
$\boldsymbol{\Lambda}$	=	Design matrix representing the bandwith of the SMC
$\boldsymbol{K}_d$	=	Tuning matrix for SMC
$\boldsymbol{K}_s$	=	Tuning matrix that handles wrongly estimated uncertainties for SMC
$\boldsymbol{\Phi}$	=	Boundary layer matrix

Environmental parameters

H_s	=	Significant wave height
ω_c	=	Cut-off frequency
ω_p	=	Peak frequency
T_p	=	Peak period of wave
$S(\omega)$	=	Wave spectrum
A	=	Wave amplitude
β	=	Encounter angle of waves
ϵ	=	Phase of wave

Chapter 1

Introduction

The first oil found in the North Sea was in Ekofisk in 1969, the find was huge and marked the start of Norway's entry into the oil age. At this time, oil tankers used anchors in order to load the oil from the platforms. Anchoring in the wrong places can be dangerous and time consuming in the North Sea, especially if extreme seas occur. In addition to loading oil from rigs to oil tankers, drilling moved into deeper waters and jack-up barges and drillships could not use anchoring anymore. Companies such as Kongsberg Maritime had at that time dynamic positioning (DP) systems on diving vessels and adapted the DP technology quickly to the oil tankers in order to operate in a safer environment. Today, the DP systems are more advanced and companies such as Rolls-Royce, General Electric, Wärtsila and Kongsberg Maritime develops them further. DP systems needed today are of course as in the early 1960s safe, but now also greener. With the precision in order, it is more profitable when the DP system operates greener such that precision and less waste of fuel is achieved simultaneously.

This chapter presents the motivation for this thesis, background involving previous work, main contributions and organization of the thesis.

1.1 Motivation

Marine vessels and operations have to satisfy certain requirements by law in order to have permission to operate in open waters with DP. For example, the International Maritime Organization (IMO) provides an international standard for DP systems on all types of vessels, which involves recommendations of design criteria, necessary equipment, operating requirements and test and documentation systems for the DP systems. Such guidelines have the purpose of reducing the risk to operators, the vessel, other vessels nearby, subsea installations and the environment when

operating in station keeping. For more examples of class societies that have rules for classification of DP systems, see (Sørensen, 2013).

With safety in order, the needs of saving fuel and reducing wear and tear of thrusters are important. In any DP operation including DP in extreme seas, there is a need for a solution that is safer, smarter and greener. The latter means that a vessel is able to maintain position with a small error keeping the operation safe, precise and at the same time not waste more fuel than necessary. In this thesis, DP control systems have been implemented and tested on the model scale supply vessel Cybership III. Trials with robust controllers such as proportional-integral-derivative with acceleration feedback (PID-AFB) have been done before on this vessel, but sliding-mode control (SMC) has never been tested on Cybership III. The need for a robust controller is important when operating in extreme sea conditions because of challenging measurements due to large waves. In addition, the SMC controller is not dependent on acceleration measurements from an accelerometer. Therefore it is especially interesting to find controllers, such as SMC, that may have the same or better performance than a PID-AFB in extreme seas with the motivation of a safer, smarter and greener operation. An illustration of a DP vessel is shown in Figure 1.1.

Figure 1.1: DP vessel, Alphatronmarine (2015).

1.2 Background

MCSim (Marine Cybernetics Simulator), which is a Matlab/Simulink simulator and toolbox (Appendix B.1), has been used for test cases developing hybrid controllers prior to laboratory tests (Nguyen, 2005; Brodtkorb et al., 2014). The work develops hybrid controllers and evaluates their behavior in developing sea states from calm to extreme seas. For a vessel to maintain position during a varying sea state, the control system requires individual tuning for each interval of sea states when operating with a hybrid control system. If a hybrid control system uses three pre-tuned PID controllers with nonlinear passive observers (NPO) for three different sea states, it has the opportunity to switch to the controller with observer that has the best tuning for that particular sea state. With this switching feature, the vessel is able to maintain position with pre-tuned settings for several sea states in a developing sea. In addition to hybrid controllers, MCSim has also been used for testing of other control strategies such as thrust allocation and observer design. MCSim has in this thesis been used to test DP in extreme seas with single controllers in short term sea states. In Figure 1.2, the Matlab/Simulink toolbox and simulator MCSim is shown.

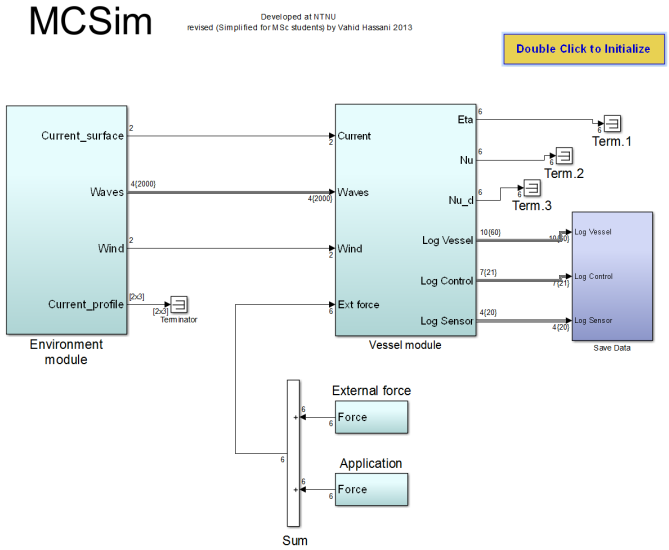

Figure 1.2: MCSim shown in Matlab/Simulink environment.

In extreme seas, waves are higher and have longer periods such that the wave-frequency (WF) motions are found in the same frequency regime as the low-frequency (LF) motions of the vessel. This causes problems with the wave filtering of the WF motions because they cannot be separated from the LF motions. Sørensen et al. (2002) proposes to neglect the wave filter for swell dominated waves

(high sea states) because the observer and controller results in reduced performance and stability problems when the WF motion is filtered. The reason for this is that the wave filter removes parts of the important LF motions of the vessel that the controller should compensate. This have been tested and implemented by Brodtkorb et al. (2014) and Nguyen et al. (2007) with the use of hybrid controllers.

The hybrid controller implemented in both works includes PID-AFB and an NPO without wave filtering. By comparing the hybrid controller with a single PID controller with wave filtering, the aim was to observe if one control strategy had better performance than the other. Simulations were done in a sea state varying from calm to extreme seas and the hybrid controller had the best performance. The results have shown that using an observer without wave filtering in combination with a PID-AFB controller provides improved performance. One reason for choosing this controller over a PID controller is because Lindegaard (2003) has shown it to be more robust than the PID controller.

In order to increase the performance in positioning operations of surface vessels in moderate to rough sea states, Lindegaard (2003) proposed PID-AFB. A chosen mass was multiplied with the measured acceleration in surge and sway and fed back such that the effective inertia of the vessel was increased. By using PID-AFB instead of PID and testing the control system on Cybership II in the Marine Cybernetics Laboratory (MCLab), the precision of the operation was improved i.e. safety was improved. The mass added to the inertia has earlier been chosen different to obtain certain advantages. Fossen et al. (2002) suggests a PID with AFB controller where the effective inertia is increased by including parts of the system's inertia matrix with additional design parameters in feedback with the measured acceleration of the system. The resulting inertia becomes symmetric, which gives the mass in x and y directions equal, resulting in a PID controller independent of the heading angle which is an advantage when tuning the DP system. This controller is, because of Lindegaard (2003), shown to be more robust than the PID controller, still there are other controllers that are known to be more robust than a PID controller.

The SMC is recognized as one of the efficient tools to design robust controllers for complex high-order nonlinear dynamic plants operating under uncertain conditions. The research in this area was initiated in the the former Soviet Union about 50 years ago, and since then the SMC methodology has been receiving much more attention from the international control community within the last two decades (Agrachev et al., 2004). SMC was adapted and used for multiple input and multiple output (MIMO) nonlinear systems by Fossen (1991), with the idea of designing a robust controller in the case of modeling inaccuracies. In extreme seas, large motion couplings in surge, heave, pitch and sway, roll and yaw occurs, and a 3 degree of freedom (DOF) vessel model may be insufficient. This can be solved by using a robust controller. The controller can be made robust in DP by introducing uncertainties of the vessel inertia and damping matrices which is an advantage when controlling large wave motions. Later, Seshagiri and Khalil (2002) presents SMC with integral action that also will be used in this thesis in addition to the work

proposed by Fossen (1991). Compared with PID and PID-AFB, this controller is more tricky to tune and a good start is to compare parts of the SMC controller law with a proportional-derivative (PD) control law. One way to obtain PD gain matrices is to develop a linear quadratic (LQ) controller and use these gain matrices to start tuning with.

The LQ controller is known as a method of providing feedback gains stabilizing a defined system (Hespanha, 2009). However, the automated technique of providing gains that is satisfactory may be a challenge. Bryson (2002) shows how to predetermine the desired maximum squared value of the states and control input. Generating the best possible gain matrices for a system has been useful for this thesis when tuning PID-AFB and SMC.

1.3 Main Contributions

The aim of this thesis was to develop two different DP controllers with an NPO operating in extreme seas and determine which control strategy provided the best performance leading to a safer and greener operation, by being smart. A test case with good accuracy of position and heading constitutes a safe operation, test cases with low energy consumption are green and a controller is smart when achieving both goals simultaneously. Extreme seas is in this thesis defined as very high sea states with significant wave height $H_s \geq 9$m and peak wave frequency $\omega_p \leq 0.46$ rad/s as shown in Table 2.1. In Chapter 2-3, the peak wave frequency is used together with the significant wave height to describe sea states, while in the rest of the chapters presenting the results and parameters for test cases the peak period of wave T_p is used. In this thesis, the controllers and observer with and without wave filtering are presented more thoroughly. A reference model is briefly described and thrust allocation of Cybership III is found in Appendix B.4.1. All components shown in Figure 1.3 describing a conventional DP vessel are developed in this thesis, except of the vessel model.

1. SMC, PID-AFB, NPO and a reference model are developed in the Matlab/Simulink simulator and toolbox MCSim. The controllers are tested with different tuning strategies.

2. Measures of performance for tests in MCSim are performed in order to determine which control strategies provide the best performance in extreme seas. The performance metrics are Integral Absolute Error (IAE), Integral Time-weighted Absolute Error (ITAE) and Integral Squared Error (ISE). These performance metrics evaluate only the error of the vessel determines only if an operation is safe. It is not possible to determine if a control strategy provides a green operation in MCSim i.e. energy saving operation, because it does not exist any measure of energy consumption due to the lack of thruster and motor models.

3. SMC, PID-AFB, NPO and a reference model are developed for Cybership

III in the MCLab at the Norwegian Marine Technology Research Institute (MARINTEK) with the software NIVeristand that converts Matlab/Simulink models to C-code readable for an on board computer on Cybership III. In addition, a human machine interface (HMI) is developed for real-time change of settings for controllers, reading measurements and enable/disable of thrusters.

4. Measures of performance for tests cases in the MCLab are performed in order to determine which control strategies provide the best performance in the highest sea state possible to generate in the model basin. The performance are now evaluated by a cost function for each performance metric used when evaluating the results from MCSim. When the cost function is evaluated with respect to IAE, the cost function is a product of IAE and the total energy consumed by the three thrusters on Cybership III. This cost function now evaluates the performance with respect to both the error and energy consumption. This measure of performance has as far as the author of this thesis is concerned not been done before when testing controllers in MCLab. The controllers are evaluated to not only be safer, but also greener. A smart controller is both safe and green.

5. Results from the test cases performed in MCSim and the MCLab are compared and discussed. The precision of the simulator MCSim relative to Cybership III and waves generated in the MCLab is discussed.

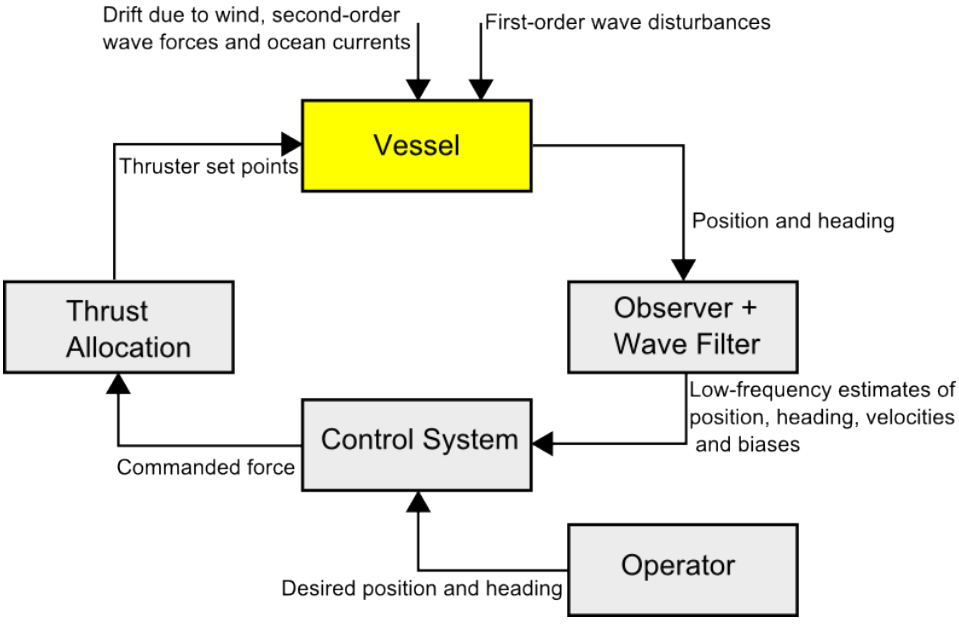

Figure 1.3: Illustration of conventional DP system.

1.4 Organization of the Thesis

In Chapter 2, the mathematical modeling of marine vessels and ocean waves are presented. This chapter covers reference frames, kinematics, kinetics, control plant models for regular and extreme seas, definitions of sea states, sea states from wave spectrum to the time domain and Froude scaling.

Chapter 3 first describes a conventional NPO with its properties, then this observer is modified for extreme seas.

Design methods and stability analysis of PID-AFB and SMC are covered in Chapter 4. This chapter also describes a reference model and an LQ tuning strategy is used for tuning the SMC and PID-AFB.

All simulations of Cybership III performed in the Matlab/Simulink simulator MCSim are described in Chapter 5. First, the simulation setup is described, then the test cases and tuning are shown and finally the results with a brief discussion are presented.

The experiments in the model basin are shown in Chapter 6. The laboratory facilities are first briefly described, then the test cases, tuning, results and a brief discussion are presented. Towards the end of this chapter, an extensive comparison of the test cases performed in MCSim and the MCLab is discussed.

In Chapter 7 the thesis is concluded, lessons learned from the work with MCSim and Cybership III are commented and further work are proposed.

The bibliography after Chapter 7 includes all references.

All digital attachments are described in Appendix A.

Appendix B covers extra information regarding the experiments in the MCLab and MCSim. This involves additional information about the MCSim software, simulation results from test cases in MCSim, MCLab setup and equipment used for test cases and additional concerning Cybership III including thrust allocation.

The performance metrics shown in Chapter 5 and 6 are described in detail in Appendix C. The cost function used for evaluation of the control strategies developed in Chapter 6 is described here together with the performance metrics IAE, ISE and ITAE.

Passivity analysis for an NPO is derived in Appendix D.

Chapter 2

Mathematical Modeling

This section looks at the mathematical modeling of marine vessels and ocean waves. The mathematical modeling consists of reference frames, kinematics, kinetics and the 3 DOF control plant model of the vessel for regular and extreme sea. The following section involves a description of the different sea states defined by Price and Bishop (1974) and Froude scaling of waves with respect to the dimensions of Cybership III. In addition, a brief description of moving from a wave spectrum to the time domain is shown.

2.1 Ocean Waves

2.1.1 Sea States

A sea state can be described by a wave spectrum $S(\omega, \psi)$, which is a function of the wave frequency ω and wave direction ψ, and is often used to describe irregular waves. The wave spectrum is divided into a frequency spectrum $S(\omega)$ that describes energy distribution over frequencies and a directional spreading function $D(\psi, \omega)$ which is a function of direction and frequency. These are often simplified to be a function of only direction and hence:

$$S(\omega, \psi) = S(\omega)D(\psi, \omega). \tag{2.1}$$

The frequency spectrum is a function of significant wave height and the peak wave frequency. Significant wave heights H_s[1] with their peak wave frequency ω_p are illustrated in the Joint North Sea Wave Project (JONSWAP) spectrum in Figure

[1]The significant wave height is the mean wave height of the one-third highest waves, also denoted $H_{1/3}$ (Fossen, 2011)

2.1. Other spectra such as the Modified Pierson-Moskowitz (MPM) spectrum and Torsethaugen spectrum are also used to describe ocean waves. The MPM spectrum should only be used for a fully developed sea with large (infinite) depth, no swell and unlimited fetch. For nonfully developed seas with swell, the JONSWAP or Torsethaugen spectra are recommended (Fossen, 2011; Torsethaugen, 2004).

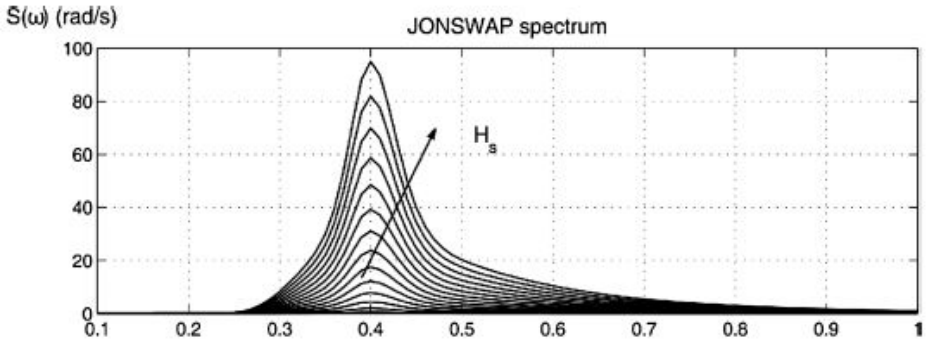

Figure 2.1: JONSWAP spectrum for $\omega_p = 0.4$ rad/s and $H_s = 3, 4, ..., 14$ m (Fossen, 2011).

The different sea states are listed in Table 2.1 and as the sea develops from sea state code 0 to 9 one can observe an increase of H_s and a decrease of the peak wave frequency. Increasing the height and periods of the waves to the extreme leads to severe thrust losses due to ventilation and in-and-out-of-water effects for marine vessels and this is not taken into account in this thesis. Such losses may be compensated for by implementing robust thruster control similar to wheel slip control on cars (Smogeli et al., 2008).

Table 2.1: Definition of sea state codes (Price and Bishop, 1974).

Sea state code	**Description of sea**	**Significant wave height** H_s [m]	**Peak wave frequency** ω_p [rad/s]	**Probability Northern North Atlantic** [%]
0	Calm	0	1.29	None
1	Calm	0-0.1	1.29-1.11	6.0616
2	Smooth	0.1-0.5	1.11-0.93	None
3	Slight	0.5-1.25	0.93-0.79	21.5683
4	Moderate	1.25-2.5	0.79-0.68	40.9915
5	Rough	2.5-4.0	0.68-0.60	21.2383
6	Very rough	4.0-6.0	0.60-0.53	7.0101
7	High	6.0-9.0	0.53-0.46	2.6931
8	Very high	9.0-14.0	0.46-0.39	0.4346
9	Phenomenal	over 14.0	Less than 0.39	0.0035

2.1.2 From Wave Spectra to the Time Domain

The Matlab/Simulink simulator used for this thesis, MCSim, is equipped with an environment module that can generate current, waves and wind by specifications from the user. The waves generated are specified prior initialization of the MCSim model. Fossen (2011) proposes methods for moving from a wave spectrum to forces in the time domain. First, a wave spectrum is specified by parameters such as significant wave height H_s and peak wave frequency ω_p. Then the wave amplitude A has to be generated, so that:

$$A = \sqrt{2S(\omega)\Delta\omega}, \tag{2.2}$$

where $\Delta\omega$ is the constant difference between the frequencies. The amplitude is used when creating a time domain realization of the wave spectra :

$$\xi = \sum_{k=1}^{N}\sum_{i=1}^{M} = \sqrt{2S(\omega_k, \beta_i)\Delta\omega\Delta\beta}cos(\omega_k + \epsilon_k), \tag{2.3}$$

where β is the angle the waves encounters the vessel and ϵ is the phase. The wave amplitude describes the current sea state and by using wave force response amplitude operators (RAO) for the vessel, an amplitude can be used to generate wave-induced forces used in the modeling of the vessel WF and LF motions. The RAOs are dependent of the weight, gravity, hull of the vessel, etc. For more details, see (Fossen, 2011, Chapter 8)

2.1.3 Froude Scaling

Table 2.1 cannot be used directly to adjust the environmental model in MCSim without scaling the significant wave height H_s and peak wave frequency ω_p to the model. Vessels with geometrical and kinematic similarity, and similarity in Froude number in model and full scale ensures similarity between inertia and gravity forces (Steen, 2014). Surface waves are gravity waves, hence equality in Froude number gives similar wave forces acting on the down scaled model and full scale model. According to Fossen (2011), the following holds for the Froude number:

$$Fn := \frac{U}{\sqrt{gL}} \tag{2.4}$$

$$\Updownarrow$$

$$Fn_{model} = Fn_{fullscale}, \tag{2.5}$$

where U is the craft speed, L is the overall submerged length of the craft and g is the acceleration of gravity.

The vessel scale ratio $L_{fullscale}$ in full scale relative to the ship equals L_{model} relative to the model with scaling factor α_s:

$$\begin{aligned} L_{model} &= \alpha_s L_{fullscale} \\ \alpha_s &= \frac{L_{model}}{L_{fullscale}}. \end{aligned} \tag{2.6}$$

This leads to the scaled significant wave height:

$$H_{s,model} = \alpha_s H_{s,fullscale}, \tag{2.7}$$

and peak wave period of wave

$$T_{p,model} = \sqrt{\alpha_s} T_{p,fullscale}. \tag{2.8}$$

The model scale Cybership III is a 1:30 down scaled model of a supply vessel with mass $m = 76$ kg , length $L = 2.275$ m, breadth $B = 0.437$ m and draught $T = 0.153$ m.

2.2 Marine Vessels

2.2.1 Reference Frames

Reference frames are used to analyze the motion of marine crafts in 6 DOF. Primary, there are reference frames with origin at the center of the earth and geographic reference frames with respect to either the body of a vessel or to the surface of the Earth. As proposed by Fossen (2011), the reference are frames convenient to define when analyzing the motion of a marine craft in 6 DOF. The earth-centered and geographic reference frames are illustrated in Figure 2.2. The following reference frames are used for DP in this thesis. Fossen (2011) proposed:

Definition 2.1. *The North-East-Down(NED) coordinate system* $\{n\} = (x_n, y_n, z_n)$ *with origin* 0_n *is defined relative to the Earth's reference ellipsoid. The x axis of this system points towards true North, the y axis points towards East while the z axis points downwards normal to the Earth's surface. This reference frame can be defined as the tangent plane on the surface of the Earth moving with the craft with different axes than the body-fixed reference frame.*

Definition 2.2. *The body-fixed reference frame* $\{b\} = (x_b, y_b, z_b)$ *with origin* 0_b *is a coordinate frame fixed to the body. The position and orientation of the craft are described with respect to the inertial reference frame (NED) while the linear and angular velocities are expressed in the body-fixed coordinate system.*

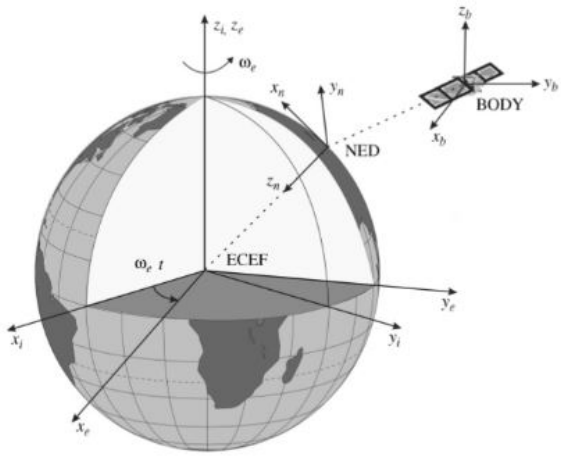

Figure 2.2: The earth-centered earth-fixed (ECEF), earth-centered inertial (ECI), north-east-down (NED) and body-fixed reference frames (Fossen, 2011).

2.2.2 Kinematics

Kinematics describes the vessel with coordinates in order to determine position and orientation. The position and orientation are described by vectors that have the size relative to the number of DOF. The marine craft 6 DOF kinematic equations can be written on matrix form as:

$$\dot{\boldsymbol{\eta}} = \boldsymbol{J}_{\Theta}(\boldsymbol{\eta})\boldsymbol{\nu}, \tag{2.9}$$

where $\dot{\boldsymbol{\eta}}$ is the velocity expressed in NED, $\boldsymbol{J}_{\Theta}$ transforms the body-fixed velocity $\boldsymbol{\nu}$ to the NED frame. In addition, $\boldsymbol{\eta}$ is the position and attitude vector, which is illustrated in Figure 2.3.

The position and orientation is translated from the body-fixed reference frame to the NED frame by the transformation matrix $\boldsymbol{J}_{\Theta}(\boldsymbol{\eta})$.

$$\dot{\boldsymbol{\eta}} = \boldsymbol{J}_{\Theta}(\boldsymbol{\eta})\boldsymbol{\nu} \tag{2.10}$$

$$\Updownarrow \tag{2.11}$$

$$\begin{bmatrix} \dot{\boldsymbol{P}}_{b/n} \\ \dot{\boldsymbol{\Theta}}_{nb} \end{bmatrix} = \begin{bmatrix} \boldsymbol{R}_b^n(\boldsymbol{\Theta}_{nb}) & \boldsymbol{0}_{3\text{x}3} \\ \boldsymbol{0}_{3\text{x}3} & \boldsymbol{T}_{\Theta}(\boldsymbol{\Theta}_{nb}) \end{bmatrix} \begin{bmatrix} \boldsymbol{v}_{b/n}^b \\ \boldsymbol{\omega}_{b/n}^b \end{bmatrix}. \tag{2.12}$$

According to (2.12) the following are related through the transformation matrices. Let $\boldsymbol{R}_b^n(\boldsymbol{\Theta}_{nb}) : \mathcal{S}^3 \to SO(3)$ denote the rotation matrix relating the linear velocity vector $\boldsymbol{v}_{b/n}^b = \begin{bmatrix} u & v & w \end{bmatrix}^\top$ to the Euler angles $\boldsymbol{\Theta}_{nb} = \begin{bmatrix} \phi & \theta & \psi \end{bmatrix}^\top$. The transformation matrix $\boldsymbol{T}_{\Theta}(\boldsymbol{\Theta}_{nb})$ relates the angular velocity vector $\boldsymbol{\omega}_{b/n}^b = \begin{bmatrix} p & q & r \end{bmatrix}^\top$ to the Euler rate vector $\dot{\boldsymbol{\Theta}}_{nb} = \begin{bmatrix} \dot{\phi} & \dot{\theta} & \dot{\psi} \end{bmatrix}^\top$.

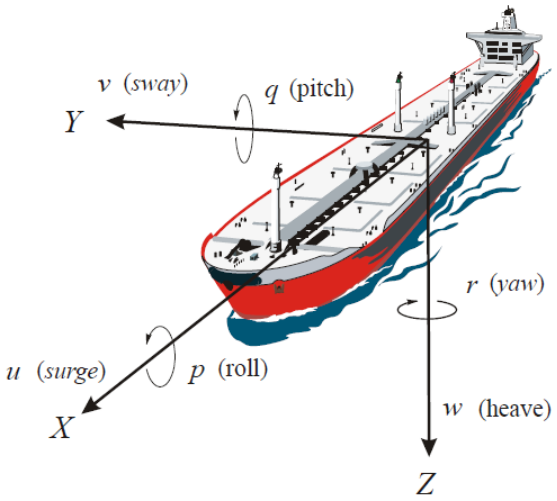

Figure 2.3: Definition of surge, sway, heave, roll, pitch and yaw modes of motion in body-fixed frame (Fossen, 2011).

2.2.3 Kinetics

Kinetics describes the motions of the vessel due to forces from the environment and thrusters. The 6 DOF rigid-body equations of motion can be written on matrix form as:

$$\underbrace{\boldsymbol{M}_{RB}\dot{\boldsymbol{\nu}} + \boldsymbol{C}_{RB}(\boldsymbol{\nu})\boldsymbol{\nu}}_{\text{rigid-body forces}} + \underbrace{\boldsymbol{M}_{A}\dot{\boldsymbol{\nu}}_r + \boldsymbol{C}_{A}(\boldsymbol{\nu}_r)\boldsymbol{\nu}_r + \boldsymbol{D}(\boldsymbol{\nu}_r)\boldsymbol{\nu}_r}_{\text{hydrodynamic forces}} + \underbrace{\boldsymbol{g}(\boldsymbol{\eta}) + \boldsymbol{g}_0}_{\text{hydrostatic forces}} = \boldsymbol{\tau} + \boldsymbol{\tau}_{env}, \tag{2.13}$$

where $\boldsymbol{M}_A$ and $\boldsymbol{M}_{RB}$ are the added mass and rigid body matrices. $\boldsymbol{C}_{RB}(\boldsymbol{\nu})$ and $\boldsymbol{C}_A(\boldsymbol{\nu}_r)$ are the rigid body Coriolis and added mass matrix. The hydrodynamic damping matrix consists of a linear and nonlinear part so that $\boldsymbol{D}(\boldsymbol{\nu}_r) = \boldsymbol{D} + \boldsymbol{D}_n(\boldsymbol{\nu}_r)$, with $\boldsymbol{\nu}_r = \boldsymbol{\nu} - \boldsymbol{\nu}_c$ as the relative velocity when the vessel is exposed ocean current.

Rewriting (2.13) to:

$$\boldsymbol{M}\dot{\boldsymbol{\nu}}_r + \boldsymbol{C}(\boldsymbol{\nu}_r)\boldsymbol{\nu}_r + \boldsymbol{D}(\boldsymbol{\nu}_r)\boldsymbol{\nu}_r + \boldsymbol{g}(\boldsymbol{\eta}) + \boldsymbol{g}_0 = \boldsymbol{\tau} + \boldsymbol{\tau}_{env}, \tag{2.14}$$

where this equation is included in a high fidelity process plant model[2] that gives an accurate description of vessel motion and is used for controller testing.

[2]The Matlab/Simulink toolbox and simulator MCSim has a process plant model which is a comprehensive model of Cybership III with environmental disturbances and control inputs.

2.2.4 3 DOF Control Plant Model

The control plant model is a simplificaton of (2.14) capturing only the most important vessel dynamics. This model is used for model-based control design and stability analysis and is described in 3 DOF for DP surface vessels. The total model of the marine vessel dynamics is separated into a low-frequency (LF) model and a wave-frequency (WF) model by superposition (Sørensen, 2013). The nonlinear LF equations of motion consists of second-order mean, slowly-varying wave, current and wind loads. The WF model is mainly for motions due to first-order wave loads. The reason for separating the system in two simplified models is for the purpose of model-based observer and controller design. A vessel operating with DP is dependent on moving in the horizontal plane and heave, roll and pitch motions are neglected. By this reduction, the model may be insufficient when exposed to extreme seas due to large motion couplings in surge, heave, pitch and sway, roll and yaw that occurs.

With low-speed maneuvering, the velocities $\boldsymbol{\nu}$ and $\boldsymbol{\nu}_r$ may assumed to be small such that $\boldsymbol{C}_{RB}(\nu)\boldsymbol{\nu}$ and $\boldsymbol{C}_A(\boldsymbol{\nu}_r)\boldsymbol{\nu}_r$ can be neglected. Firstly, the 6 DOF equations of motion in (2.14) are reduced to 3 DOF:

$$\dot{\boldsymbol{\eta}} = \boldsymbol{R}(\psi)\boldsymbol{\nu} \tag{2.15}$$

$$\boldsymbol{M}\dot{\boldsymbol{\nu}} + \boldsymbol{D}\boldsymbol{\nu} + \boldsymbol{G}\boldsymbol{\eta} = \boldsymbol{\tau}, \tag{2.16}$$

under the assumption of small roll and pitch angles. Sørensen (2013) suggests to assume that $\boldsymbol{G}\boldsymbol{\eta} \approx \boldsymbol{0}_{3\times 3}$ for freely floating vessels. When operating with approximately zero velocity, station keeping, the rigid body and hydrodynamic centripetal and Coriolis matrices becomes $\boldsymbol{C}(\boldsymbol{\nu}_r) \approx \boldsymbol{0}_{3\times 3}$ due to multiplication with the velocity $\boldsymbol{\nu} \approx \boldsymbol{0}$. Furthermore the nonlinear damping also becomes $\boldsymbol{D}_n(\boldsymbol{\nu}_r) \approx 0$ when station keeping and $\boldsymbol{\nu} \approx \boldsymbol{0}$.

The following control plant model comprises the 3 DOF LF and WF motions, a bias model and the measurement of the vessel:

$$\dot{\boldsymbol{\xi}} = \boldsymbol{A}_{\boldsymbol{\omega}}\boldsymbol{\xi} + \boldsymbol{E}_{\boldsymbol{w}}\mathbf{w}_{\boldsymbol{w}} \tag{2.17a}$$

$$\dot{\boldsymbol{\eta}} = \boldsymbol{R}(\psi)\boldsymbol{\nu} \tag{2.17b}$$

$$\dot{\boldsymbol{b}} = -\boldsymbol{T}_b^{-1}\boldsymbol{b} + \boldsymbol{E}_{\boldsymbol{b}}\mathbf{w}_{\boldsymbol{b}} \tag{2.17c}$$

$$\boldsymbol{M}\dot{\boldsymbol{\nu}} = -\boldsymbol{D}\boldsymbol{\nu} + \boldsymbol{R}^\top(\psi)\boldsymbol{b} + \boldsymbol{\tau} \tag{2.17d}$$

$$\boldsymbol{y} = \boldsymbol{\eta} + \boldsymbol{C}_{\boldsymbol{w}}\boldsymbol{\xi} + \mathbf{v}. \tag{2.17e}$$

Each part of (2.17) are described in the following subsections.

Low-frequency model

In (2.17b) and (2.17d), the 3 DOF DP equations of motion are designed for station keeping and low-speed maneuvering. These are intended for observer and controller design where $\boldsymbol{\eta} = \begin{bmatrix} N & E & \psi \end{bmatrix}^\top$ is the position and heading vector, $\boldsymbol{\nu} = \begin{bmatrix} u & v & r \end{bmatrix}^\top$ is the velocity vector, $\boldsymbol{b} \in \mathbb{R}^3$ is the bias vector representing slowly-varying environmental forces and $\boldsymbol{\tau} = \begin{bmatrix} \tau_x & \tau_y & \tau_\psi \end{bmatrix}^\top$ is the control input vector.

When operating with 3 DOF, the transformation matrix $\boldsymbol{J}_\Theta(\boldsymbol{\eta})$ from (2.9) reduces to $\boldsymbol{R}_b^n(\boldsymbol{\Theta}_{nb}) = \boldsymbol{R}_{z,\psi}\boldsymbol{R}_{y,\theta}\boldsymbol{R}_{x,\phi} \approx \boldsymbol{R}_{z,\phi}$ and $\boldsymbol{T}_\Theta(\boldsymbol{\Theta}_{nb}) \approx \boldsymbol{I}_{3\text{x}3}$. The result of neglecting the elements corresponding to heave, roll and pitch gives:

$$\dot{\boldsymbol{\eta}} = \boldsymbol{R}(\psi)\boldsymbol{\nu}, \quad \text{with} \quad \boldsymbol{R}(\psi) = \begin{bmatrix} c\psi & -s\psi & 0 \\ s\psi & c\psi & 0 \\ 0 & 0 & 1 \end{bmatrix}, \tag{2.18}$$

where $c\psi = cos(\psi)$ and $s\psi = sin(\psi)$.

Wave-frequency model

The WF motions from (2.17a) are caused by first-order wave loads acting on the vessel that in regular sea states are filtered out by an observer. The WF model is designed and driven by white noise processes that consists of uncoupled harmonic oscillators with damping. An approximation of the wave spectrum can be done by a second-order system (Fossen, 2011). Such system can be transformed to the time domain and shown in state space form as shown in (2.17a) and (2.17e) where $\mathbf{w}_\omega \in \mathbb{R}^3$ is a zero-mean Gaussian white noise vector and $\boldsymbol{\xi}_\omega \in \mathbb{R}^6$ is the vessel WF position and velocity vector. The system matrix $\boldsymbol{A}_\omega \in \mathbb{R}^{6\text{x}6}$ consists of the peak wave frequency ω_p and the damping ratio λ. The disturbance matrix is written as $\boldsymbol{E}_\omega \in \mathbb{R}^{6\text{x}3}$ and the measurement matrix is written as $\boldsymbol{C}_\omega \in \mathbb{R}^{3\text{x}6}$.

The following are the matrices describing the linear WF model:

$$\boldsymbol{A}_\omega \begin{bmatrix} \mathbf{0}_{3\text{x}3} & \boldsymbol{I}_{3\text{x}3} \\ -\boldsymbol{\Omega}^2 & -2\boldsymbol{\Lambda}\boldsymbol{\Omega} \end{bmatrix}, \; \boldsymbol{C}_\omega = \begin{bmatrix} \mathbf{0}_{3\text{x}3} & \boldsymbol{I}_{3\text{x}3} \end{bmatrix}, \; \boldsymbol{E}_\omega = \begin{bmatrix} \mathbf{0}_{3\text{x}3} \\ \boldsymbol{K}_\omega \end{bmatrix}, \tag{2.19}$$

with the wave frequencies $\boldsymbol{\Omega} = diag\{\omega_1, \omega_2, \omega_3\}$, relative damping ratios $\Lambda = diag\{\zeta_1, \zeta_2, \zeta_3\}$ and $\boldsymbol{K}_\omega = diag\{K_{\omega 1}, K_{\omega 2}, K_{\omega 3}\}$. In high sea states with long wave lengths, Table 2.1, the WF motions are neglected as shown in (2.20a)-(2.20d).

Bias model

This model represents slowly-varying environmental forces like ocean currents, second-order wave drift forces, mean wind and unmodeled dynamics from reducing the CPM from 6 to 3 DOF. The bias model used in (2.17c) is the first order

Markov model. Alternatively, one can design the bias model as a Wiener process, $\dot{\boldsymbol{b}} = \boldsymbol{E}_b \mathrm{w}_b$. The reason for not using a Wiener process in regular seas is because when designing an NPO, use of the Markov model will result in exponential stability, see Section 3.1. The wiener process is applied to the control plant model for extreme seas as explained in the next section.

The bias model (2.17c) is driven by the zero-mean Gaussian white noise vector $\mathbf{w}_b \in \mathbb{R}^3$, the diagonal matrix of bias time constants $\boldsymbol{T}_b \in \mathbb{R}^{3\mathrm{x}3}$ and $\boldsymbol{E}_b \in \mathbb{R}^{3\mathrm{x}3}$ is a diagonal scaling matrix.

2.2.5 Control Plant Model in Extreme Seas

In sea states with wave periods from 5-9 seconds that correspond to sea state codes 1-5, the DP control system counteracts low frequency LF wave motions caused by wind, current and slowly-varying wave loads in order to hold the desired position. It is common to use wave filtering to filter out the WF motions from the measurements caused by first-order wave loads in order to avoid wear and tear of the propulsion system.

As the waves becomes higher and the sea state code increases, the periods of the waves becomes longer and WF motions can be found in the vessel LF frequency regime. This causes the problem of separating LF from WF wave motions and if an observer with a wave filter is used, the wave filter will remove important LF vessel motions leading to poor estimates and unsatisfactory control. The large vessel motions due to high waves gives a challenge when the objective is to maintain position. Swell waves are large with long periods and is most likely present with the waves generated by the wind (Fossen, 2011). Sørensen et al. (2002) proposes to reformulate the observer by neglecting the wave filtering to give better control of the vessel.

Control plant model for DP in extreme seas (Sørensen, 2013):

$$\dot{\boldsymbol{\eta}} = \boldsymbol{R}(\psi)\boldsymbol{\nu} \tag{2.20a}$$

$$\dot{\boldsymbol{b}} = \boldsymbol{E_b}\mathbf{w_b} \tag{2.20b}$$

$$\boldsymbol{M}\dot{\boldsymbol{\nu}} + \boldsymbol{D}\boldsymbol{\nu} = \boldsymbol{R}^\top(\psi)\boldsymbol{b} + \boldsymbol{\tau} \tag{2.20c}$$

$$\boldsymbol{y} = \boldsymbol{\eta} + \mathbf{v}. \tag{2.20d}$$

Environmental forces are a challenge for marine vessels and with the general mathematical modeling of ocean waves and marine vessels in order, the next step in making a DP system is for the vessel to be able to tackle such forces. Recall Figure 1.3 where the environmental forces acting on the vessel are illustrated. The measurements from the vessel are treated by an observer with a wave filter. In the next chapter, a very common observer used in DP systems is presented and modeled.

Chapter 3

Observer Design

An observer is presented in this chapter, first as a conventional nonlinear passive observer (NPO), then the observer is modified for vessel operation in extreme seas.

The observer is an important part of a DP system because of its capabilities of state estimation and filtering. It is common to filter out measurement noise that will have a negative effect on the controller. If sensors become faulty or too expensive, the observer can perform state estimation to reconstruct measurements. If the vessel experiences signal losses because of sensor fail, one can use dead reckoning and trust the predicted model in the observer. The observer divides the motion of the marine vessel in a WF and LF motion. The WF motion is for most DP applications filtered out in order to reduce wear and tear of the actuators and fuel costs.

3.1 Nonlinear Passive Observer

The reason for using an NPO instead of the Kalman filter or other types of observers is because it is more convenient to implement and it has its advantages. The Kalman filter requires linearization 36 times for every 10 degree of yaw angle which can be avoided by using other observers such as an NPO. In addition, an NPO includes wave filtering, bias and velocity estimation . The NPO has may have less tuning parameters than the Kalman filter. An NPO guarantees global asymptotic stability (GAS) by passivity design while the Kalman filter does not. This chapter is based on Fossen and Strand (1999) and Fossen (2011).

In order to prove passivity, Fossen (2011) proposes the following assumptions:

Assumption 1: Neglect position and heading noise, $\boldsymbol{\omega} = 0$ and $\boldsymbol{v} = 0$. If the zero-mean Gaussian white noise terms are neglected from the observer Lyapunov

analysis, the error dynamics will be uniform global asymptotically/exponentially stable (UGAS/UGES). If not, the error dynamics will become uniformly ultimately bounded (UUB). This assumption may not be realistic in reality.

Assumption 2: Assume a small amplitude of the wave induced yaw motion. $\boldsymbol{R}(\mathrm{y}_3) = \boldsymbol{R}(\psi) \implies \mathrm{y}_3 = \psi + \psi_\omega \approx \psi$. The magnitude of the wave-induced yaw disturbance is normally less than five degrees in extreme sea conditions, sea state codes 5-9 from Price and Bishop (1974), and less than one degree during ship operations in regular sea states below sea state code 4.

Copying the dynamics of (2.17a)-(2.17e), and using Assumption 1 and 2 results in:

$$\dot{\boldsymbol{\xi}} = \boldsymbol{A}_{\boldsymbol{\omega}}\boldsymbol{\xi} \tag{3.1a}$$
$$\dot{\boldsymbol{\eta}} = \boldsymbol{R}(\mathrm{y}_3)\boldsymbol{\nu} \tag{3.1b}$$
$$\dot{\boldsymbol{b}} = -\boldsymbol{T}_b^{-1}\boldsymbol{b} \tag{3.1c}$$
$$\boldsymbol{M}\dot{\boldsymbol{\nu}} = -\boldsymbol{D}\boldsymbol{\nu} + \boldsymbol{R}^\top(\mathrm{y}_3)\boldsymbol{b} + \boldsymbol{\tau} \tag{3.1d}$$
$$\boldsymbol{y} = \boldsymbol{\eta} + \boldsymbol{C}_{\boldsymbol{w}}\boldsymbol{\xi}. \tag{3.1e}$$

With the DP observer model (3.1a)-(3.1e) the observer equations can be written as:

$$\dot{\hat{\boldsymbol{\xi}}} = \boldsymbol{A}_\omega\hat{\boldsymbol{\xi}} + \boldsymbol{K}_1(\boldsymbol{\omega}_0)\tilde{\mathbf{y}} \tag{3.2a}$$
$$\dot{\hat{\boldsymbol{\eta}}} = \boldsymbol{R}(\mathrm{y}_3)\hat{\boldsymbol{\nu}} + \boldsymbol{K}_2\tilde{\mathbf{y}} \tag{3.2b}$$
$$\dot{\hat{\boldsymbol{b}}} = -\boldsymbol{T}_b^{-1}\hat{\boldsymbol{b}} + \boldsymbol{K}_3\tilde{\mathbf{y}} \tag{3.2c}$$
$$\boldsymbol{M}\dot{\hat{\boldsymbol{\nu}}} = -\boldsymbol{D}\hat{\boldsymbol{\nu}} + \boldsymbol{R}^\top(\mathrm{y}_3)\hat{\boldsymbol{b}} + \boldsymbol{\tau} + \boldsymbol{R}^\top(\mathrm{y}_3)\boldsymbol{K}_4\tilde{\mathbf{y}}_{\mathbf{3}} \tag{3.2d}$$
$$\hat{\mathbf{y}} = \hat{\boldsymbol{\eta}} + \boldsymbol{C}_\omega\hat{\boldsymbol{\xi}}, \tag{3.2e}$$

where $\tilde{\mathbf{y}}$ is the estimation error $\mathbf{y}-\hat{\mathbf{y}}$ and $\boldsymbol{K}_1(\boldsymbol{\omega}_0)$, $\boldsymbol{K}_2, \boldsymbol{K}_3$ and $\boldsymbol{K}_4$ are the observer gain matrices. $\boldsymbol{T}_b$ represents the low-pass (LP) filtering of the bias estimation, chosen to be $\boldsymbol{T}_b = diag\{T_1, T_2, T_3\}$. By using (3.2c) with LP filtering instead of a pure integrator of the white noise term $\boldsymbol{K}_3\tilde{\mathbf{y}}$, exponential stability is ensured (Fossen, 2011). Passivity analysis is shown in Appendix D.1.

In order to ensure passivity and relate the observer gains to the dominating wave response frequencies, the following tuning rules by Fossen (2011) are chosen:

$$\boldsymbol{K}_i(\omega_i) = -2(\zeta_{ni} - \lambda_i)\frac{\omega_{ci}}{\omega_i}, \quad i = 1, 2, 3 \tag{3.3}$$
$$\boldsymbol{K}_i(\omega_{pi}) = 2\omega_i(\zeta_{ni} - \lambda_i), \qquad i = 4, 5, 6 \tag{3.4}$$
$$\boldsymbol{K}_i = \omega_{ci}, \qquad i = 7, 8, 9, \tag{3.5}$$

where $\omega_{ci} > \omega_i$ is the filter cut-off frequencies and $\zeta_{ni} > \zeta_i$ is a tuning parameter set between 0.1-1.0. As proposed by Sørensen (2013), one should notice that $\boldsymbol{A}_\omega$ is also dependent of the actual sea state through the parameter ω_i and is often set equal to the wave peak frequency $\omega_{pi} \approx \frac{2\pi}{T_{pi}}$. When tuning $\boldsymbol{K}_3$ in (3.8), the gain parameters $k_{10} - k_{12}$ are chosen sufficiently high to ensure proper bias estimation.

The following observer gain matrices correspond to (3.3)-(3.5):

$$\boldsymbol{K}_1 = \begin{bmatrix} diag\{k_1, k_2, k_3\} \\ diag\{k_4, k_5, k_6\} \end{bmatrix} \tag{3.6}$$

$$\boldsymbol{K}_2 = diag\{k_7, k_8, k_9\} \tag{3.7}$$

$$\boldsymbol{K}_3 = diag\{k_{10}, k_{11}, k_{12}\} \tag{3.8}$$

$$\boldsymbol{K}_4 = diag\{k_{13}, k_{14}, k_{15}\}. \tag{3.9}$$

The transfer function of the observer gains consists of three decoupled transfer functions:

$$\boldsymbol{H}(s) = diag\{h_1(s), h_2(s), h_3(s)\}. \tag{3.10}$$

In Figure 3.1, the transfer function $h_1(s)$ in surge is illustrated. The plots show an NPO where the wave filtering of first-order waves are shown. The environmental forces are described at different frequencies as shown in the figure. At low frequencies, the NPO cancels out mean wave drift forces, ocean currents and wind by integral action. $\frac{1}{T_i}$ is shown at $\omega = 0.01$ rad/s in the figure. This illustrates that the bias time constant to cancel the bias are found at this low frequency and has to be chosen to operate within this area when designing the observer. The notch cancels the first-order wave forces at the peak frequency $\omega_p = 0.8976$ rad/s. If the notch found place at frequencies below $\omega_p < 0.1$ rad/s, problems that are to be discussed may occur.

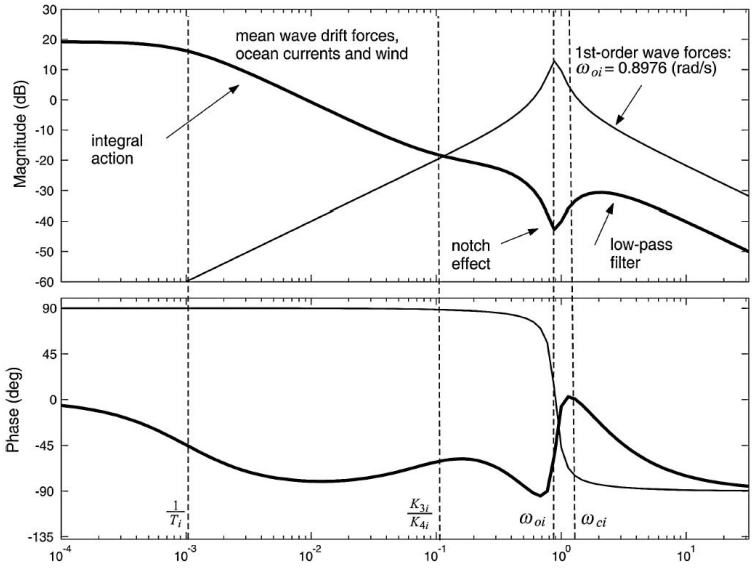

Figure 3.1: Bode plot of NPO and environmental forces acting on the vessel showing the notch effect (Fossen, 2011).

When experiencing high waves with long wave periods in extreme sea conditions, an NPO filters out important LF measurements that are supposed to be compensated for by the DP controller. Recall that in extreme seas, the waves are higher and have longer wave periods such that WF motions, first-order waves, are in the same frequency regime as the LF motions of the vessel. This causes the NPO not being able to separate the WF motions from the LF motions. Thus the notch effect will be within the bandwidth of the DP controller (Sørensen et al., 2002) and important LF motions and bias are filtered out.

The following observer without wave filtering is proposed by Sørensen et al. (2002) for extreme seas:

$$\dot{\hat{\boldsymbol{\eta}}} = \boldsymbol{R}(\mathrm{y}_3)\hat{\boldsymbol{\nu}} + \boldsymbol{K}_2\tilde{\mathbf{y}} \tag{3.11a}$$

$$\dot{\hat{\boldsymbol{b}}} = -\boldsymbol{T}_b^{-1}\hat{\boldsymbol{b}} + \boldsymbol{K}_3\tilde{\mathbf{y}} \tag{3.11b}$$

$$\boldsymbol{M}\dot{\hat{\boldsymbol{\nu}}} = -\boldsymbol{D}\hat{\boldsymbol{\nu}} + \boldsymbol{R}^\top(\mathrm{y}_3)\hat{\boldsymbol{b}} + \boldsymbol{\tau} + \boldsymbol{R}^\top(\mathrm{y}_3)\boldsymbol{K}_4\tilde{\mathbf{y}}_{\mathbf{3}} \tag{3.11c}$$

$$\hat{\mathbf{y}} = \hat{\boldsymbol{\eta}}. \tag{3.11d}$$

The NPO deals with the position and heading measurements, which may be noisy, and separates them in a LF and WF motion of the vessel. In extreme sea states the wave filter is neglected, while in the more calm sea states with lower peak periods of the waves, the WF motions are found outside of the LF frequency regime and have to be dealt with by the wave filter. The LF motion of the vessel is then used by the control system as shown in the DP overview Figure 1.3. In this figure,

the desired positions and heading are illustrated as a result of a choice made by the operator. When an operator chooses desired position and heading, a reference model processes the desired set points prior the control system starts procesing them. In the next chapter the control system, reference model and an LQ tuning strategy are presented.

Chapter 4

Control Design and Stability Analysis

This chapter involves control design and stability analysis of PID-AFB control and SMC. The kinetic 3 DOF equation of motion (2.17d) is used throughout this chapter where the controllers that generates the commanded force $\boldsymbol{\tau}_c$[1] are derived. At the end of this chapter and a reference model is made so that it is possible to use setpoints when controlling the vessel. An LQ tuning strategy that can be adapted to SMC and PID-AFB tuning is presented. The Matlab script and Simulink model of the work presented in this chapter are digitally attached to the thesis.

4.1 PID Control with Acceleration Feedback

The conventional PID controller has a proportional, derivative and integral part. The proportional part ensures that the input changes proportionally with the error of the desired $\boldsymbol{\eta}_d$ and actual position and heading $\boldsymbol{\eta}$. The integral-part has its main purpose to cancel the stationary deviation caused by slowly-varying forces acting on the vessel such as waves, wind and current. The derivative-part is proportional to the velocity and reduces the dynamical deviation and counteracts changes and oscillations in the state.

The PID-AFB controller is different from the conventional PID controller due to an extra inertia $\boldsymbol{K}_m$ that is fed back with measured acceleration and added to the

[1] The commanded force generated by the controller is referred to as τ_c while u is the thruster setpoints, see Appendix B.4.1 and Figure 1.3. The commanded force τ_c is referred to as τ throughout this chapter.

system intertia matrix $\boldsymbol{M}$. This makes the system less sensitive to external disturbances and hence more robust. The commanded force from (2.17d) is generated by the following control law:

$$\boldsymbol{\tau} = \boldsymbol{R}(\psi)^\top \boldsymbol{\tau}_{PID} - \boldsymbol{K}_m \dot{\boldsymbol{\nu}}, \tag{4.1}$$

with (4.2)

$$\boldsymbol{\tau}_{PID} = -\boldsymbol{K}_p \tilde{\boldsymbol{\eta}} - \boldsymbol{R}(\psi)\boldsymbol{K}_d \boldsymbol{\nu} - \boldsymbol{K}_i \int_0^t \tilde{\boldsymbol{\eta}}(\tau)\, \mathrm{d}\tau. \tag{4.3}$$

The error is written as $\tilde{\boldsymbol{\eta}} = \boldsymbol{\eta} - \boldsymbol{\eta}_d$. The gain matrices $\boldsymbol{K}_p$, $\boldsymbol{K}_d$ and $\boldsymbol{K}_i$ belong to the PID-part of the controller. The AFB gain matrix $\boldsymbol{K}_m$ is chosen as proposed in Fossen et al. (2002) where $\boldsymbol{K}_m = \boldsymbol{M}^* + \Delta\boldsymbol{K} > \boldsymbol{0}$ with $\Delta\boldsymbol{K} = \Delta\boldsymbol{K}^\top \geq \boldsymbol{0}$ is to be multiplied with the measured acceleration. The waves encounter the vessel at the bow, such that the only acceleration measurements from the accelerometer used is for surge and sway. The acceleration $\dot{\boldsymbol{\nu}}$ is to be filtered by an LP-filter if necessary. This is explained in sections 5.1.1 and 6.1.2.

By including the new inertia $\boldsymbol{K}_m$ in feedback with the measured acceleration, a new virtual inertia $\boldsymbol{H}$ is made:

$$\boldsymbol{H} = \boldsymbol{M} + \boldsymbol{K}_m. \tag{4.4}$$

Now choosing the AFB gain matrix as the modified inertia matrix $\boldsymbol{M}^*$ and with design parameters ΔK_{11} and ΔK_{22} as shown in (4.5). An advantage when tuning the controller is to choose $\Delta K_{11} = \Delta K_{22}$ such that the controller is independent of the heading angle. The design parameter $\Delta K = \Delta K_{11} = \Delta K_{22}$ is in chapters 5-6 tuned with different amounts of mass [2] in order to find the best tuning strategy for a safer, smarter and greener control of the vessel.

$$\boldsymbol{K}_m = \begin{bmatrix} K_{11} & K_{12} & 0 \\ K_{21} & K_{22} & 0 \\ K_{31} & K_{32} & 0 \end{bmatrix} = \begin{bmatrix} \mathrm{X}_{\dot{u}} + \Delta K_{11} & 0 & 0 \\ 0 & \mathrm{Y}_{\dot{v}} + \Delta K_{22} & 0 \\ 0 & \mathrm{N}_{\dot{v}} - \mathrm{Y}_{\dot{r}} & 0 \end{bmatrix}. \tag{4.5}$$

The gain matrix parameters K_{11}, K_{12}, K_{21}, K_{22}, K_{31} and K_{32} are chosen as shown in (4.5) such that $\boldsymbol{H} = \boldsymbol{H}^\top$. With the symmetry of the new inertia as shown in (4.6), the design parameters can be used for tuning as long as they are chosen the same in order to maintain an independent heading angle.

$$\boldsymbol{H} = \begin{bmatrix} m + \Delta K & 0 & 0 \\ 0 & m + \Delta K & mx_g - \mathrm{Y}_{\dot{r}} \\ 0 & mx_g - \mathrm{Y}_{\dot{r}} & I_z - \mathrm{N}_{\dot{r}} \end{bmatrix}. \tag{4.6}$$

[2] The AFB gain matrix parameter ΔK is measured in kg.

By applying (4.1) to (2.17d), the resulting closed loop is:

$$\begin{aligned}&\boldsymbol{H}\dot{\boldsymbol{\nu}} + (\boldsymbol{D} + \boldsymbol{K}_d^\star)\boldsymbol{\nu} + \boldsymbol{R}^\top(\psi)\boldsymbol{K}_p\tilde{\boldsymbol{\eta}} + \boldsymbol{R}^\top(\psi)\boldsymbol{K}_i \int_0^t \tilde{\boldsymbol{\eta}}(\tau)\ \mathrm{d}\tau \\ &= \boldsymbol{R}^\top(\psi)\boldsymbol{b},\end{aligned} \tag{4.7}$$

with $\boldsymbol{K}_d^\star = \boldsymbol{R}^\top(\psi)\boldsymbol{K}_d\boldsymbol{R}(\psi)$. With $\boldsymbol{H} = \boldsymbol{H}^\top > \boldsymbol{0}$ and $\boldsymbol{K}_p = \boldsymbol{K}_p^\top > \boldsymbol{0}$, the Lyapunov function candidate (LFC) can be chosen as done by Fossen (2011):

$$V = \frac{1}{2}\boldsymbol{\nu}^\top\boldsymbol{H}\boldsymbol{\nu} + \frac{1}{2}\tilde{\boldsymbol{\eta}}^\top\boldsymbol{K}_p\tilde{\boldsymbol{\eta}}, \tag{4.8}$$

where the bias is assumed to be canceled out by the integral action such that:

$$\dot{V} = \boldsymbol{\nu}^\top\boldsymbol{H}\dot{\boldsymbol{\nu}} + \dot{\tilde{\boldsymbol{\eta}}}^\top\boldsymbol{R}^\top(\psi)\boldsymbol{K}_p\tilde{\boldsymbol{\eta}} = \boldsymbol{\nu}^\top\boldsymbol{H}\dot{\boldsymbol{\nu}} + \dot{\boldsymbol{\eta}}^\top\boldsymbol{R}^\top(\psi)\boldsymbol{K}_p\tilde{\boldsymbol{\eta}} \tag{4.9}$$

$$= \boldsymbol{\nu}^\top(\boldsymbol{H}\dot{\boldsymbol{\nu}} + \boldsymbol{R}^\top(\psi)\boldsymbol{K}_p\tilde{\boldsymbol{\eta}}), \tag{4.10}$$

resulting in:

$$\dot{V} = -\boldsymbol{\nu}^\top[\boldsymbol{D} + \boldsymbol{K}_d^\star]\boldsymbol{\nu}. \tag{4.11}$$

With no bias and integral action, $\dot{V}$ is negative semi-definite and stability can be proven by applying Krasovskii-LaSalle's Theorem (Khalil, 2002). By defining the set $\Omega := \{\boldsymbol{x} \in \mathbb{R}^3 |\ \boldsymbol{\nu} = \boldsymbol{0}\}$ of all points for when $\dot{V}(\tilde{\boldsymbol{\eta}}, \boldsymbol{\nu}) \equiv \boldsymbol{0}$ and $\dot{\boldsymbol{\eta}} = \boldsymbol{0}$, the velocity is found to be $\boldsymbol{\nu} = \boldsymbol{0}$, leading to $\boldsymbol{\eta} = \boldsymbol{0}$. Achieving $\boldsymbol{\nu} \equiv 0$ implies that $\boldsymbol{H}\dot{\boldsymbol{\nu}} = -\boldsymbol{R}^\top(\psi)\boldsymbol{K}_p\tilde{\boldsymbol{\eta}}$, such that the system cannot get stuck at any other point than $\tilde{\boldsymbol{\eta}} = \boldsymbol{0}$ and hence the system is GAS.

4.2 Sliding-mode Control

The SMC makes a simplification of replacing the higher-order tracking problem by a first order stabilization problem. The aim of the controller is to account for parameter uncertainties in mass and damping, unmodeled dynamics such as structural resonant modes, neglected time-delays, etc. (Slotine and Li, 1991). This section is inspired by Fossen (2011) and Fossen (1991).

Firstly, a measure of tracking has to be defined:

$$\boldsymbol{s} := \dot{\tilde{\boldsymbol{\eta}}} + 2\boldsymbol{\Lambda}\tilde{\boldsymbol{\eta}} + \boldsymbol{\Lambda}^2 \int_0^t \tilde{\boldsymbol{\eta}}(\tau)d\tau, \tag{4.12}$$

where $\boldsymbol{s}$ is the sliding surface dependent of the position and heading error $\tilde{\boldsymbol{\eta}}$ and the velocity error $\dot{\tilde{\boldsymbol{\eta}}} \approx \dot{\boldsymbol{\eta}}$. The tuning parameter $\boldsymbol{\Lambda} > 0$ represents the bandwidth of the controller.

Now defining a virtual reference vector $\boldsymbol{\eta}_r$ satisfying:

$$\boldsymbol{s} = \dot{\boldsymbol{\eta}} - \dot{\boldsymbol{\eta}}_r, \;\; \dot{\boldsymbol{\eta}}_r = \dot{\boldsymbol{\eta}}_d - 2\boldsymbol{\Lambda}\tilde{\boldsymbol{\eta}} - \boldsymbol{\Lambda}^2 \int_0^t \tilde{\boldsymbol{\eta}}(\tau) d\tau \tag{4.13}$$

and

$$\dot{\boldsymbol{s}} = \ddot{\boldsymbol{\eta}} - \ddot{\boldsymbol{\eta}}_r. \tag{4.14}$$

When $\boldsymbol{s} = \boldsymbol{0}$, the equation describes a sliding surface with exponentially stable dynamics.

In Figure 4.1, a scalar example of the sliding surface is illustrated. The SMC consists of two parts. The first part is the reaching part, where the trajectory starting outside the surface moves towards the sliding surface. The second part is where the trajectory moves along the line $s = 0$ towards the equilibrium. The tuning parameter ϕ describes the thickness of the boundary layer and will be explained in more detail when discussing the control law in (4.26).

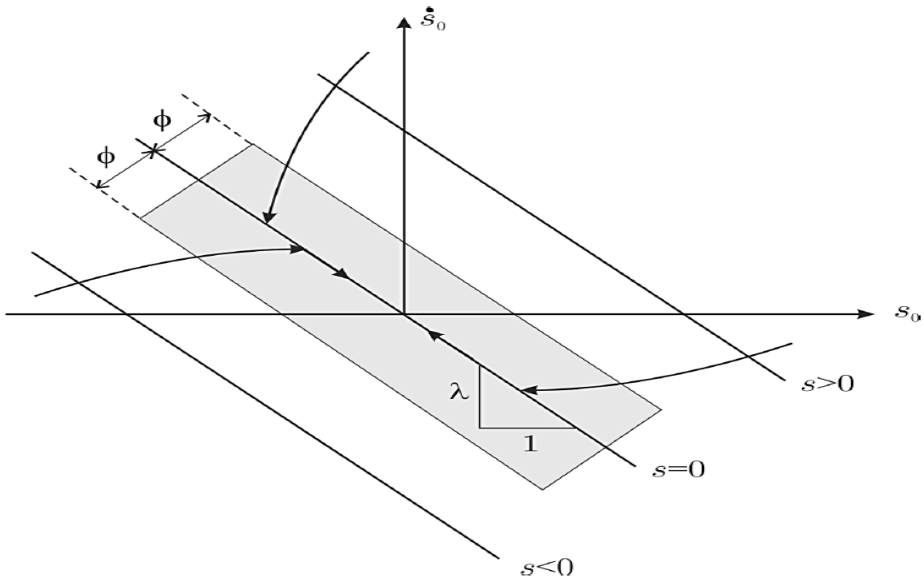

Figure 4.1: Graphical interpretation of the sliding surface $s = \dot{s}_0 + \lambda s_0$ and boundary layer $\phi > 0$ (Fossen, 2011).

The equations of motion are described in NED, as it is control of the position and heading that is of interest. The equations of motion are according to (Fossen, 2011, Chapter 7):

$$\boldsymbol{M}^\star(\boldsymbol{\eta})\ddot{\boldsymbol{\eta}} + \boldsymbol{D}^\star(\boldsymbol{\eta})\dot{\boldsymbol{\eta}} = \boldsymbol{\tau}^\star, \tag{4.15}$$

with

$$\boldsymbol{M}^{\star}(\boldsymbol{\eta}) = \boldsymbol{R}(\psi)\boldsymbol{M}\boldsymbol{R}^{\top}(\psi) \tag{4.16}$$
$$\boldsymbol{D}^{\star}(\boldsymbol{\eta}) = \boldsymbol{R}(\psi)\boldsymbol{D}\boldsymbol{R}^{\top}(\psi) \tag{4.17}$$
$$\boldsymbol{\tau}^{\star} = \boldsymbol{R}(\psi)\boldsymbol{\tau}, \tag{4.18}$$

where $\boldsymbol{\tau}$ is defined in (4.26).

Control law

Fossen (1991) derived a control law for MIMO SMC of underwater vehicles. This can be used to derive a control law for the 3 DOF DP SMC. The LFC is chosen to be:

$$V = \frac{1}{2}\boldsymbol{s}^{\top}\boldsymbol{M}^{\star}\boldsymbol{s}, \quad \boldsymbol{M}^{\star} = \boldsymbol{M}^{\star\top} > \boldsymbol{0}. \tag{4.19}$$

Using the skew-symmetry property $\boldsymbol{s}^{\top}(\dot{\boldsymbol{M}} - \boldsymbol{C}^{\star})\boldsymbol{s} = \boldsymbol{0}$ with $\boldsymbol{C}^{\star} = \boldsymbol{0}$ and due to low velocities in station keeping:

$$\dot{V} = \boldsymbol{s}^{\top}\boldsymbol{M}^{\star}\dot{\boldsymbol{s}}. \tag{4.20}$$

Inserting (4.14) into (4.20) yields:

$$\dot{V} = \boldsymbol{s}^{\top}\boldsymbol{M}^{\star}(\ddot{\boldsymbol{\eta}} - \ddot{\boldsymbol{\eta}}_r) = \boldsymbol{s}^{\top}(-\boldsymbol{M}^{\star}\ddot{\boldsymbol{\eta}}_r - \boldsymbol{D}^{\star}\dot{\boldsymbol{\eta}}_r + \boldsymbol{\tau}^{\star}) \tag{4.21}$$
$$= -\boldsymbol{s}^{\top}\boldsymbol{D}^{\star}\boldsymbol{s} + \boldsymbol{s}^{\top}(-\boldsymbol{M}^{\star}\ddot{\boldsymbol{\eta}}_r - \boldsymbol{D}^{\star}\dot{\boldsymbol{\eta}}_r + \boldsymbol{\tau}^{\star}). \tag{4.22}$$

Now simplifying this expression by transforming the virtual reference velocity $\boldsymbol{\nu}_r$ and acceleration $\dot{\boldsymbol{\nu}}_r$ from the NED to BODY frame:

$$\boldsymbol{\nu}_r = \boldsymbol{R}^{\top}(\psi)\dot{\boldsymbol{\eta}}_r \tag{4.23}$$
$$\dot{\boldsymbol{\nu}}_r = \boldsymbol{R}^{\top}(\psi)(\ddot{\boldsymbol{\eta}}_r - \dot{\boldsymbol{R}}(\psi)\boldsymbol{\nu}_r). \tag{4.24}$$

At small motions, $\dot{\boldsymbol{R}}(\psi) = \boldsymbol{0}_{3\text{x}3}$ and (4.22) can be written as:

$$\dot{V} = -\boldsymbol{s}^{\top}\boldsymbol{D}^{\star}\boldsymbol{s} + \boldsymbol{R}(\psi)\boldsymbol{s}^{\top}(-\boldsymbol{M}\dot{\boldsymbol{\nu}}_r - \boldsymbol{D}\boldsymbol{\nu}_r + \boldsymbol{\tau}). \tag{4.25}$$

Recall that in implementation, the integral part of the sliding surface $\boldsymbol{s}$, $\boldsymbol{\Lambda}^2 \int_0^t \tilde{\boldsymbol{\eta}}(\tau)d\tau$, from (4.12) is multiplied with the gain matrix $\boldsymbol{K}_d$ and added separate to the sum of commanded forces. This is illustrated towards the end of this section in Figure 4.2. With this in mind the commanded control force are written as:

$$\boldsymbol{\tau} = \underbrace{\hat{\boldsymbol{M}}\dot{\boldsymbol{\nu}}_r + \hat{\boldsymbol{D}}\boldsymbol{\nu}_r}_{\text{Feedforward term}} - \underbrace{\boldsymbol{R}^\top(\psi)\boldsymbol{K}_d\boldsymbol{s}}_{\text{PD-controller}} - \underbrace{\boldsymbol{K}_s . \times sgn(\boldsymbol{R}^\top(\psi)\boldsymbol{s})}_{\text{Robustifying term}}, \tag{4.26}$$

where $\hat{\boldsymbol{M}}$ is a chosen estimate of the system's inertia matrix $\boldsymbol{M}$ and $\hat{\boldsymbol{D}}$ is an estimate of the system's damping matrix $\boldsymbol{D}$. The gain matrix $\boldsymbol{K}_d$ is meant for tuning and is comparable with the derivative gain matrix used in PD control. The tuning matrix $\boldsymbol{K}_s$ is chosen as shown in (4.28) with $.\times$ as the Schur product. Chattering is known to occur when using the $sgn(\boldsymbol{R}^\top(\psi)\boldsymbol{s})$ function causing oscillations around zero, the solution for solving this was to use a hyperbolic tangent function $tanh(\boldsymbol{\Phi}^{-1}\boldsymbol{R}^\top(\psi)\boldsymbol{s})$ in order to reduce wear and tear of the vessel actuators. This function has the advantage of producing a smooth control input. The boundary layer matrix $\boldsymbol{\Phi}$ is tunable and describes the boundary layer thickness for every DOF. The result of using $\boldsymbol{K}_s$ with the hyperbolic tangent function with the sliding surface $\boldsymbol{s}$ is that it compensates for the uncancelled inexact estimation of the inertia $\hat{\boldsymbol{M}}$ and $\hat{\boldsymbol{D}}$ providing more robustness to the controller.

For simplicity, the integral action shown in (4.26) is assumed to still be a part of the sliding surface $\boldsymbol{s}$. With this in mind and by including $\boldsymbol{\tau}$, the following is derived:

$$\dot{V} = -\boldsymbol{s}^\top(\boldsymbol{D}^\star + \boldsymbol{K}_d)\boldsymbol{s} + \boldsymbol{R}(\psi)\boldsymbol{s}^\top(\tilde{\boldsymbol{M}}\dot{\boldsymbol{\nu}}_r + \tilde{\boldsymbol{D}}\boldsymbol{\nu}_r) - \boldsymbol{K}_s^\top|\boldsymbol{R}(\psi)^\top\boldsymbol{s}|, \tag{4.27}$$

with $\tilde{\boldsymbol{M}} = \hat{\boldsymbol{M}} - \boldsymbol{M}$.

Choosing $\boldsymbol{K}_s$ as:

$$\boldsymbol{K}_s \geq |\tilde{\boldsymbol{M}}\dot{\boldsymbol{\nu}}_r + \tilde{\boldsymbol{D}}\boldsymbol{\nu}_r| + \delta,\ \delta > 0, \tag{4.28}$$

results in

$$\dot{V} \leq -\boldsymbol{s}^\top(\boldsymbol{D}^\star + \boldsymbol{K}_d)\boldsymbol{s} - \delta(\boldsymbol{R}(\psi)\boldsymbol{s}). \tag{4.29}$$

The controller can be seen as a feedback linearizing controller with correction possibilities of the mass and damping matrices. Further, the choice of $\boldsymbol{K}_s$ handles the model uncertainties and forces $\dot{V}$ to stay negative semidefinite, hence the controller can be called robust. When $(\boldsymbol{D}^\star + \boldsymbol{K}_d) > \boldsymbol{0}$, $\boldsymbol{s}$ is bounded and $\dot{V}$ is uniformly continous, the sliding surface $\boldsymbol{s} \to \boldsymbol{0}$ and $\tilde{\boldsymbol{\eta}} \to \boldsymbol{0}$ when $t \to \infty$ by Barbalat's lemma (Khalil, 2002; Fossen, 1991).

Using (4.12) directly when implementing the SMC in MCSim, results in a stationary deviation of the sliding surface $\boldsymbol{s}$. This means that the integral action should be separated from $\boldsymbol{s}$, still be a part of (4.13) and included individually to the commanded forces $\boldsymbol{\tau}$. The contributions are still summarized when generating the total commanded force such that this implementation is not shown in the deriving of the control law in (4.26). In Figure 4.2, the separation is shown, box 2 and 3 are together the product of the sliding surface $\boldsymbol{s}$ with and without the integral part and the gain matrix $\boldsymbol{K_d}$ as written in (4.26).

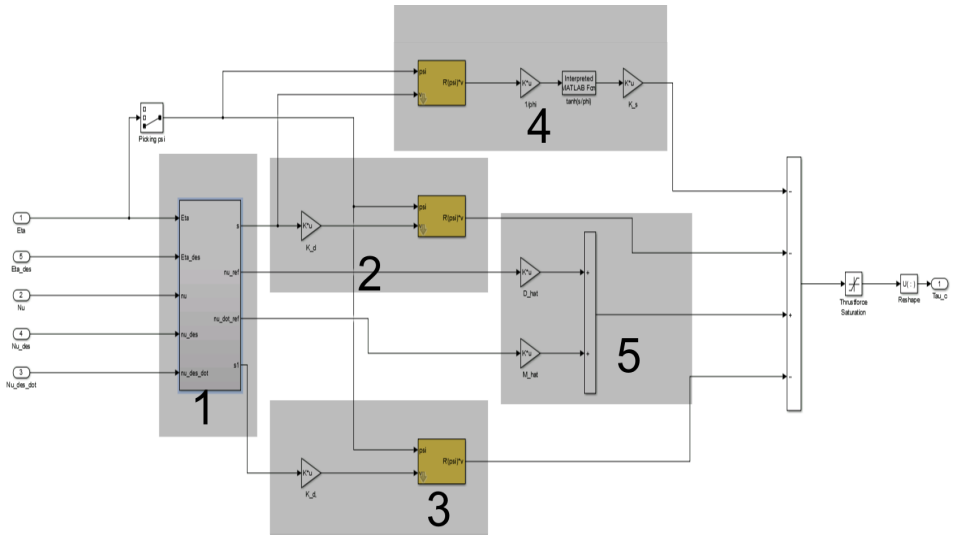

Figure 4.2: Illustration of SMC implementation in MCSim. Box 1 represents the subsystem generating the sliding surface $\boldsymbol{s}$, the virtual reference velocity $\boldsymbol{\nu}_r$ and virtual reference acceleration $\dot{\boldsymbol{\nu}}_r$. Box 2 represents (4.12) without the integral part, multiplied with $\boldsymbol{K}_d$ and box 3 represents the integral part from (4.12) multiplied with $\boldsymbol{K}_d$. Box 4 shows the correcting term $\boldsymbol{K}_s$. $\times\, tanh(\boldsymbol{\Phi}^{-1}\boldsymbol{R}^{\top}(\psi)\boldsymbol{s})$. Box 5 consists of the estimated inertia and damping $\hat{\boldsymbol{M}}$ and $\hat{\boldsymbol{D}}$ multiplied with the virtual acceleration and velocity.

4.3 Reference Model

The reference model generates a smooth reference trajectory making the control of the vessel easier because of the non-infinite derivative that appears in a normal set point change. This prevents the values of the P, I and D gains of the PID controller to change at a high rate. The natural frequency $\boldsymbol{\Omega}$ is tuned in order to achieve the desired transient behavior and the bandwidth of the reference model is chosen lower than the bandwidth of the motion control system in order to obtain adequate tracking performance and stability (Fossen, 2011). In addition, it is suggested to

use a first order LP filter in cascade with a mass-damper-spring system:

$$\frac{\eta_{di}}{r_i^n}(s) = \frac{\omega_{ni}^2}{(1+T_i s)(s^2 + 2\zeta_i \omega_{ni} s + \omega_{ni}^2)} \quad (i = 1, ..., n). \tag{4.30}$$

Working with 3 DOF, the reference model is :

$$\boldsymbol{\eta}_d^{(3)} + (2\boldsymbol{\Delta} + \boldsymbol{I})\boldsymbol{\Omega}\ddot{\boldsymbol{\eta}}_d + (2\boldsymbol{\Delta} + \boldsymbol{I})\boldsymbol{\Omega}^2\dot{\boldsymbol{\eta}}_d + \boldsymbol{\Omega}^3\boldsymbol{\eta}_d = \boldsymbol{\Omega}^3\boldsymbol{r}^n, \tag{4.31}$$

with the tuned natural frequencies

$$\boldsymbol{\Omega} = \begin{bmatrix} \omega_{n1} & 0 & 0 \\ 0 & \omega_{n2} & 0 \\ 0 & 0 & \omega_{n3} \end{bmatrix} \tag{4.32}$$

and relative damping

$$\boldsymbol{\Delta} = \begin{bmatrix} \zeta_{n1} & 0 & 0 \\ 0 & \zeta_{n2} & 0 \\ 0 & 0 & \zeta_{n3} \end{bmatrix}. \tag{4.33}$$

The desired velocity and acceleration have been saturated by trials such that the SMC can use them in the process of generating virtual velocity and acceleration:

$$\boldsymbol{\nu}_{max} = \begin{bmatrix} 1 & 0.5 & 0.5 \end{bmatrix}^\top \tag{4.34}$$

and

$$\dot{\boldsymbol{\nu}}_{max} = \begin{bmatrix} 0.01 & 0.01 & 0.01 \end{bmatrix}^\top. \tag{4.35}$$

The reference model that is used for both controllers derived in this chapter is implemented in MCSim is shown in Figure 4.3. By tuning the LP-filter part of the reference model, the time constants can be adjusted such that chosen set points ramp up faster or slower to the final value. Saturations have been made for the desired acceleration and velocity and when developing the SMC control law, the desired velocity and acceleration are used in order to generate virtual reference velocity and acceleration.

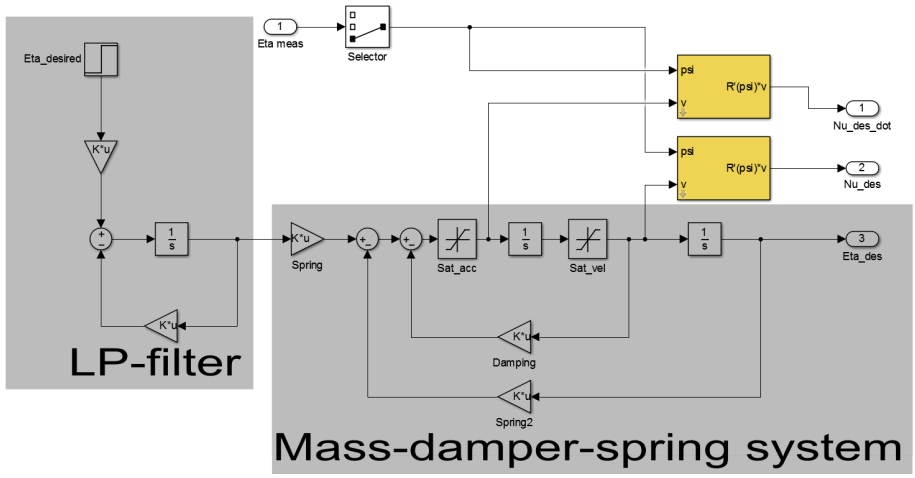

Figure 4.3: Reference model in MCSim. LP-filter on the left hand side. Mass-damper-spring system on the right side.

In a DP system, the operator is interested in choosing the desired positions and heading of the vessel. This information is dealt with by the reference model such that the control system receives processed set points. Processing the set points means that they are delayed and smoothed such that the vessel does not have to compensate for suddenly large errors between actual and desired positions and heading at once, but rather sets points building up to a final value over a time chosen by design. The result of using a reference model are smooth vessel motions when changing set points during operations such as station keeping e.g. making readjustments of position and heading during station keeping.

The controller's goal are to reach the set points, no error, and hold this position and heading by constantly generating a commanded force for each DOF, $\boldsymbol{\tau}_c$. These commanded forces are sent to the thruster allocation part of the DP system as shown in Figure 1.3. The thrust allocation distributes the commanded forces to thruster set points $\boldsymbol{u}$ such that each thruster can produce the right amount of force in the right direction e.g. desired revolutions per minute(rpm) for thruster propellers. In Appendix B.4.1, the thrust allocation for the DP system developed for Cybership III is described.

4.4 LQ-Based Tuning Rules

This section describes how to generate gain matrices that are to be compared with the gain matrices computed by the method that Fossen (2011) proposed for PID-AFB, see Section 5.1.2. The steps for finding the LQ gain matrices in this section

are inspired by Hespanha (2009) and Bryson (2002).

The procedure of calculating the optimal gains resulting in the gain matrices $\boldsymbol{K}_p$ and $\boldsymbol{K}_d$ involves solving the Riccati equation. The integral part has to be tuned individually.

The equations of motion (2.17b) and (2.17d) without bias are to be formulated in state space with the control force vector consisting of the LQ and integral part:

$$\boldsymbol{\tau} = \boldsymbol{\tau}_{LQ} + \boldsymbol{\tau}_{integral}, \tag{4.36}$$

where $\boldsymbol{\tau}_{LQ}$ is the PD part of the controller and the linearized control plant model written as:

$$\begin{bmatrix} \dot{\boldsymbol{\eta}} \\ \dot{\boldsymbol{\nu}} \end{bmatrix} = \begin{bmatrix} \boldsymbol{0}_{3\text{x}3} & \boldsymbol{I}_{3\text{x}3} \\ \boldsymbol{0}_{3\text{x}3} & \boldsymbol{M}^{-1}\boldsymbol{D} \end{bmatrix} \begin{bmatrix} \boldsymbol{\eta} \\ \boldsymbol{\nu} \end{bmatrix} + \begin{bmatrix} \boldsymbol{0}_{3\text{x}3} \\ -\boldsymbol{M}^{-1} \end{bmatrix} \boldsymbol{\tau}_{LQ}. \tag{4.37}$$

Now the closed loop error dynamics are:

$$\dot{\boldsymbol{x}} = \underbrace{\begin{bmatrix} \boldsymbol{0}_{3\text{x}3} & \boldsymbol{I}_{3\text{x}3} \\ \boldsymbol{0}_{3\text{x}3} & \boldsymbol{M}^{-1}\boldsymbol{D} \end{bmatrix}}_{\boldsymbol{A}} \boldsymbol{x} + \underbrace{\begin{bmatrix} \boldsymbol{0}_{3\text{x}3} \\ -\boldsymbol{M}^{-1} \end{bmatrix}}_{\boldsymbol{B}} \boldsymbol{u}_{LQ} \tag{4.38}$$

$$\boldsymbol{e} = \underbrace{\begin{bmatrix} \boldsymbol{I} & \boldsymbol{0}_{3\text{x}3} \end{bmatrix}}_{\boldsymbol{C}} \boldsymbol{x}, \tag{4.39}$$

with $\boldsymbol{u}_{LQ} = \boldsymbol{\tau}_{LQ}$, $\boldsymbol{e} = \boldsymbol{\eta} - \boldsymbol{\eta}_d$, $\dot{\boldsymbol{e}} = \boldsymbol{\nu} - \boldsymbol{\nu}_d$ and $\boldsymbol{x} = \begin{bmatrix} \boldsymbol{e} & \dot{\boldsymbol{e}} \end{bmatrix}^\top$.

The optimal feedback control gains are found by minimizing the cost function:

$$\begin{aligned} J &= \min_{\boldsymbol{u}_{LQ}} \Big\{ \frac{1}{2} \int_0^T (\boldsymbol{y}^\top \boldsymbol{\mathcal{Q}} \boldsymbol{y} + \boldsymbol{u}_{LQ}^\top \boldsymbol{R} \boldsymbol{u}_{LQ}) dt \Big\} \\ &= \min_{\boldsymbol{u}_{LQ}} \Big\{ \frac{1}{2} \int_0^T (\boldsymbol{x}^\top \boldsymbol{C}^\top \boldsymbol{\mathcal{Q}} \boldsymbol{C} \boldsymbol{x} + \boldsymbol{u}_{LQ}^\top \boldsymbol{R} \boldsymbol{u}_{LQ}) dt \Big\}, \end{aligned} \tag{4.40}$$

with the weighting matrices $\boldsymbol{R} = \boldsymbol{R}^\top > \boldsymbol{0}$ and $\boldsymbol{\mathcal{Q}} = \boldsymbol{\mathcal{Q}}^\top > \boldsymbol{0}$.

The controllability matrix has full row rank:

$$\mathcal{C} = \begin{bmatrix} \boldsymbol{B} & \boldsymbol{AB} & ... & \boldsymbol{A}^5\boldsymbol{B} \end{bmatrix}. \tag{4.41}$$

The optimal control law is:

$$\boldsymbol{u}_{LQ} = -\boldsymbol{R}^{-1}\boldsymbol{B}^\top \boldsymbol{P}_\infty \boldsymbol{x} = -\boldsymbol{K}\boldsymbol{x}, \tag{4.42}$$

with $\boldsymbol{K} = \begin{bmatrix}\boldsymbol{K}_p & \boldsymbol{K}_d\end{bmatrix}$as the gain matrices. The Riccati equation is :

$$\boldsymbol{P}_\infty \boldsymbol{A} + \boldsymbol{A}^\top \boldsymbol{P}_\infty - \boldsymbol{P}_\infty - \boldsymbol{P}_\infty \boldsymbol{B}\boldsymbol{R}^{-1}\boldsymbol{B}^\top \boldsymbol{P}_\infty + \boldsymbol{C}^\top \boldsymbol{\mathcal{Q}}\boldsymbol{C} = \boldsymbol{0}, \tag{4.43}$$

where $\boldsymbol{P}_\infty$ as the stationary solution of the Riccati equation.

Bryson (2002) suggests to tune the weighting matrices $\boldsymbol{R}$ and $\boldsymbol{\mathcal{Q}}$ as the inverse of the desired maximum squared values of the forces τ^2_{max} and deviation of the states $x^2_{max,i}$:

$$\boldsymbol{R} = diag\{r_i\}, i = 1, ..., 3,\ r_i = \frac{1}{\tau^2_{max,i}} \tag{4.44}$$

$$\boldsymbol{Q} = diag\{q_i\}, i = 1, .., 3,\ q_i = \frac{1}{x^2_{max,i}}. \tag{4.45}$$

The gain matrix $\boldsymbol{K}$, the solution of the Riccati equation $\boldsymbol{P}$ and the eigenvalues are obtained by using the Matlab function *lqr*. Choosing the same eigenvalues for the PID-AFB as the SMC makes the controllers more comparable and provides a more similar basis for tuning.

The controllers, observer and reference model are tested in Chapter 5 and 6. The following chapter describes testing of Cybership III in MCSim.

Chapter 5

Simulations in MCSim

This chapter describes the simulations of Cybership III performed in MCSim by presenting settings for generating waves and test cases, tuning of controllers, results of the test cases and a discussion of the results. The results for each test case are presented in Section 5.2 by illustrating the position and attitude of the vessel with best controller performance and comparing the different tuning strategies with each other by the performance metrics IAE, ITAE and ISE, see Appendix C. Energy consumption is not included in the performance metrics because the power system for Cybership III is not modeled in MCSim and hence achieving a "greener" control is not possible. The measures of performance presented in this chapter evaluates the precision of the controller. Towards the end of this chapter an overall discussion is presented in Section 5.3.

5.1 Simulation Setup

In Section 5.1 the simulation setup, test cases and tuning of the controllers are described. The simulation setup involves a choice of wave parameters and defining of test cases. The tuning presents tuning parameters chosen for each test case with SMC and PID-AFB.

5.1.1 Test Cases

The only environmental forces used in the simulations were wave forces. By adjusting parameters in the environmental module in MCSim, the wave forces were chosen as similar as possible to the waves that were planned to be generated in the MCLab, see Chapter 6. Table 5.1 describes the settings of the parameters

for generating wave forces in MCSim. The significant wave heights H_s and peak period of waves T_p shown in tables 5.2-5.3 are scaled by Froude scaling, see Section 2.1.3, correct to the model Cybership III. A scaled significant wave height is: $H_{s,model} = \alpha_s H_{s,fullscale}$, with the scaling factor $\alpha_s = 0.0290$. The peak period of wave had to be scaled by $T_{p,model} = \sqrt{\alpha_s} T_{p,fullscale}$ and is related to the peak wave frequency by $\omega_p = \frac{2\pi}{T_p}$. The peak wave frequencies has been chosen in the observer with respect to Table 2.1 and scaled.

Table 5.1: Wave settings in MCSim for test cases.

Symbols	Description of symbol	Specified value
H_s	Significant wave height	Varying
ω_p	Peak frequency	Varying
ψ	Wave encounter direction	0° (fore)
s	Spreading factor for direction	4
γ	Peak parameter for JONSWAP spectrum	3.3
ω_c	Cutoff frequency for JONSWAP spectrum	2.5
	Cutoff direction for JONSWAP spectrum	0
n_{waves}	Number of waves	500
n_{freq}	Number of frequency components	100
n_{dir}	Number of wave directions	10
	Random frequencies	yes
	Random directions	10

Table 5.2 describes test case 1 where the PID-AFB was tested. Test case 2 was done with the SMC and is shown in Table 5.3. In tables 5.2 and 5.3, each test case are described by significant wave height H_s, peak period of wave T_p, extra mass ΔK added to the inertia $\boldsymbol{M}$ and uncertainties of the sinertia and damping matrices $\boldsymbol{M}$ and $\boldsymbol{D}$. The sea state parameters are constant during simulations, i.e. the sea state does not change. The measured accelerations in surge and sway for test cases performee in MCSim were fetched from the high fidelity process plant model and filtered by an LP filter with $T = 9$ s because of noisy measurements. All tables regarding test cases and tuning in this chapter are split with horizontal lines in order to clearly show which test cases were done in the same sea state.

Test case a-b in tables 5.2 and 5.3 corresponds to sea state code 1 (calm) from Table 2.1. These test cases was done with the wave filter enabled and tested with the extra mass $\Delta K = (0, 30)$ kg for tuning purposes and for pure interest to check if this would improve the performance. Test cases c-g in the tables are equivalent to sea state code 5 (rough) and the wave filter was not enabled for these test cases. The extra mass ΔK was used as a tuning parameter and was chosen to be tested for $\Delta K = (0, 10, 30, 50)$ kg. This extra mass corresponds to an increase of the inertia of the vessel making the system believe the inertia is larger than in reality. The same tuning parameters were used on test case g-j and these test cases corresponds to sea state code 9 (phenomenal). The only differences between tables 5.2 and 5.3 are the tuning parameters for the controllers i.e. ΔK and uncertainties $\hat{\boldsymbol{M}}$ and

$\hat{\boldsymbol{D}}$. In Table 5.3 an overestimations of the inertia $\boldsymbol{M}$ and damping $\boldsymbol{D}$ of the vessel were done with model uncertainties of $+10\%, +30\%, +40\%, +50\%$.

Table 5.2: Test case 1, parameters used for testing with PID-AFB in MCSim. Arrows and vertical lines indicates repetitive values.

Case	**Significant wave height,** H_s [m]	**Peak period of wave** T_p [s]	**Extra mass** ΔK [kg]
1a	0.03	1.5	0
1b	|	|	30
1c	0.1	1.5	0
1d			10
1e	↓	↓	30
1f			40
1g			50
1h	0.26	2.3	0
1i			10
1j	↓	↓	30
1k			40
1l			50

Table 5.3: Test case 2, parameters used for testing with SMC in MCSim. Arrows and vertical lines indicates repetitive values.

Case	**Significant wave height,** H_s [m]	**Peak period of wave** T_p [s]	**Uncertainty in** $\boldsymbol{M}$ **and** $\boldsymbol{D}$ [%]
2a	0.03	1.5	0
2b	|	|	+30
2c	0.1	1.5	0
2d			+10
2e	↓	↓	+30
2f			+40
2g			+50
2h	0.26	2.3	0
2i			+10
2j	↓	↓	+30
2k			+40
2l			+50

5.1.2 Tuning

Fossen (2011) suggested tuning methods for PID-AFB by using the total added mass and inertia of the craft $\boldsymbol{M}$, damping $\boldsymbol{D}$, an extra inertia $\boldsymbol{K}_m$, the natural

frequency ω_n and damping ζ. The SMC had to be tuned differently and it was therefore useful to calculate the best possible gain matrices with LQ optimal control tuning, see section 4.4. In addition to finding reasonable gain matrices for the SMC, calculating the LQ gain matrices gave an intuition and a reference to the PID-AFB gain matrices obtained by the tuning rules of Fossen (2011). By comparison and testing of the gain matrices obtained from the two above mentioned methods, reasonable gains were chosen.

PID with Acceleration Feedback

The PID-AFB was tuned by comparison of the LQ control gain matrices and the gain matrices obtained by the tuning method proposed by Fossen (2011). The latter was done by specifying the natural frequency and damping of the system and solve for:

$$\boldsymbol{K}_p = (\boldsymbol{M} + \boldsymbol{K}_m)\Gamma \tag{5.1}$$

$$\boldsymbol{K}_d = 2\Upsilon\Gamma(\boldsymbol{M} + \boldsymbol{K}_m) - \boldsymbol{D} \tag{5.2}$$

with Υ as the damping matrix and Γ as the matrix with the natural frequencies. The integral action was tuned as $\boldsymbol{K}_i = \frac{1}{10}\boldsymbol{K}_p$. Solving (5.1) and (5.2) led to the following gain matrices:

$$\boldsymbol{K}_p = \begin{bmatrix} 15 & 0 & 0 \\ 0 & 36 & 0 \\ 0 & 0 & 4 \end{bmatrix}, \quad \boldsymbol{K}_d = \begin{bmatrix} 105 & 0 & 0 \\ 0 & 179 & 0 \\ 0 & 0 & 19 \end{bmatrix}, \boldsymbol{K}_i = \begin{bmatrix} 0.47 & 0 & 0 \\ 0 & 0.99 & 0 \\ 0 & 0 & 0.11 \end{bmatrix} \tag{5.3}$$

The LQ control approach is described in Section 4.4 and the gain matrices were found by choosing (4.44) and (4.45) as:

$$\boldsymbol{R} = \begin{bmatrix} 0.1 & 0 & 0 \\ 0 & 0.1 & 0 \\ 0 & 0 & 0.0833 \end{bmatrix} \tag{5.4}$$

$$\tag{5.5}$$

and

$$\boldsymbol{Q} = \begin{bmatrix} 10 & 0 & 0 & 0 & 0 & 0 \\ 0 & 10 & 0 & 0 & 0 & 0 \\ 0 & 0 & 11.4548 & 0 & 0 & 0 \\ 0 & 0 & 0 & 0 & 0 & 0 \\ 0 & 0 & 0 & 0 & 0 & 0 \\ 0 & 0 & 0 & 0 & 0 & 0 \end{bmatrix}. \tag{5.6}$$

By usng the Matlab function *lqr* with the matrices (5.4) and (5.6), the following gain matrices were found:

$$\boldsymbol{K}_p = \begin{bmatrix} 10 & 0 & 0 \\ 0 & 9 & 0 \\ 0 & 0 & 11 \end{bmatrix}, \quad \boldsymbol{K}_d = \begin{bmatrix} 53 & 0 & 0 \\ 0 & 67 & 0 \\ 0 & 0 & 32 \end{bmatrix} \text{ and } \boldsymbol{K}_i = \begin{bmatrix} 1 & 0 & 0 \\ 0 & 0.9 & 0 \\ 0 & 0 & 1.1 \end{bmatrix}. \quad (5.7)$$

The gain matrices used in the test cases for PID-AFB are shown in Table 5.4.

Table 5.4: Tuning for test case 1, PID-AFB in MCSim. Arrows and vertical lines indicates repetitive values.

Case	$\boldsymbol{K}_p$	$\boldsymbol{K}_d$	$\boldsymbol{K}_i$
1a	diag{7.1 5.2 4.5}	diag{13 30 14}	diag{0.47 0.45 0.097}
1b	|	|	|
1c	diag{9.6 6.6 6.5}	diag{16.8 35 19.1}	
1d	↓	↓	↓
1e	↓	↓	↓
1f	↓	↓	↓
1g	↓	↓	↓
1h	↓	↓	↓
1i	↓	↓	↓
1j	↓	↓	↓
1k	↓	↓	↓
1l	↓	↓	↓

The gain matrices chosen by trial and error tuning were more similar to the gain matrices found by the LQ tuning. The derivative gain matrices found by both tuning methods were too large and had to be reduced. The proportional gain matrices found from both methods were closely related to the ones used for the simulations in MCSim. The gain matrix $\boldsymbol{K}_i$ was after tuning more similar to the gain matrix found by in (5.3), however it is often chosen to be $\frac{1}{10}\boldsymbol{K}_p$.

Sliding-mode Control

The gain matrices for the SMC were found by comparing the traditional PD control law derived from (4.42) with parts of the SMC law. The control law for the controller (4.26) has in the following equation been simplified such that it was comparable with a PD control law. By choosing the SMC gain matrices with respect to the PID-AFB gain matrices, the controllers become comparable in test cases:

$$\boldsymbol{\tau}_{PID} = -\boldsymbol{K}_p\tilde{\boldsymbol{\eta}} - \boldsymbol{K}_d\dot{\boldsymbol{\eta}} - \boldsymbol{K}_i \int_0^t \tilde{\boldsymbol{\eta}}(\tau)d\tau, \tag{5.8}$$

$$\boldsymbol{\tau}_{Sliding} = -\boldsymbol{K}_d(\dot{\boldsymbol{\eta}} + 2\boldsymbol{\Lambda}\tilde{\boldsymbol{\eta}} + \boldsymbol{\Lambda}^2 \int_0^t \tilde{\boldsymbol{\eta}}(\tau)d\tau), \tag{5.9}$$

where

$$\boldsymbol{K}_{d,PID} = \boldsymbol{K}_{d,sliding} \tag{5.10}$$

and (5.11)

$$\boldsymbol{K}_{p,PID} = 2\boldsymbol{K}_{d,sliding}\boldsymbol{\Lambda} \implies \boldsymbol{\Lambda} = \frac{\boldsymbol{K}_{p,PID}}{2\boldsymbol{K}_{d,sliding}}. \tag{5.12}$$

By applying (5.10)-(5.12) with the gain matrices found in Table 5.4, the gain matrices $\boldsymbol{\Lambda}$ and $\boldsymbol{K}_d$ were found. The gain matrix $\boldsymbol{K}_s$ was found by satisfying (4.28) in combination with tuning. In addition, the boundary layer matrix $\boldsymbol{\Phi}$ was found by tuning and are shown in Table 5.5 among the rest of the gain matrices.

Table 5.5: Tuning for test case 2, SMC in MCSim. Arrows and vertical lines indicates repetitive values.

Case	$\boldsymbol{\Lambda}$	$\boldsymbol{K}_d$	$\boldsymbol{K}_s$	$\boldsymbol{\Phi}$
2a	diag{0.27 0.08 0.16}	diag{13 30 14}	diag{1 1 1}	diag{1 1 2}
2b	|	|	diag{5 1.3 1.8 }	|
2c	diag{0.28 0.09 0.72}	diag{16 30 19}	diag{1 1 1}	↓
2d	↓	↓	diag{2 1.3 1.5}	↓
2e	↓	↓	diag{5 1.5 1.8}	↓
2f	↓	↓	diag{6 3 2}	↓
2g	↓	↓	diag{7 4 2.2}	↓
2h	↓	↓	diag{1 1 1}	↓
2i	↓	↓	diag{2 1.3 1.5}	↓
2j	↓	↓	diag{5 1.5 1.8}	↓
2k	↓	↓	diag{6 3 2}	↓
2l	↓	↓	diag{7 4 2.2}	↓

5.2 Results

The results of test case 1 and 2 for PID-AFB and SMC are presented in this section. Measures of performance were done by using ITAE, ISE and IAE and are summarized in tables in sections 5.2.1 and 5.2.2. By using these performance metrics, the best tuning strategy with respect to position and heading precision can be found. Rows marked yellow indicate that this particular test case provides better performance than the other test cases for that sea state. Section 5.2.1 presents test

cases done by PID-AFB and Section 5.2.2 presents the test cases done with SMC. By testing the SMC strategies with the same sea states and eigenvalues of the controller gain matrices as the PID-AFB control, they can be compared with the measures of performance. Most of the position and heading figures from test case 1 and 2 looks very similar, those that were mentioned and not shown in the following sections are found in Appendix B.2.

5.2.1 Test Case 1, PID with Acceleration Feedback

Test case 1b, 1g and 1l provided the best performance for the PID-AFB compared to the other test cases in the specific sea states. The test cases that provided best performance are presented in this section. These test cases had one tuning strategy in common, they had an extra mass $\Delta K > 0$ kg added to the acceleration feedback inertia gain. In Figure B.1, the position and heading of Cybership III are shown when the vessel was exposed to waves with significant wave height of $H_s = 0.03$ m and peak period of the wave $T_p = 1.5$ s. The green dotted line is the measured position and heading, while the black line is the NPO estimates of the LF positions and heading. The desired position and heading $\boldsymbol{\eta}_d = \begin{bmatrix} 0 & 0 & 0 \end{bmatrix}^\top$ are shown with a red line in all plots. The wave filter removes first-order waves such that Cybership III does not have to compensate for all first-order wave induced motions.

From time 0-20 seconds in the simulations from this section and the next as shown in figures B.1-B.5 and 5.1-5.3, an overshoot was experienced. This overshoot appeared in all test cases done in MCSim and was caused by the initialization of the waves and controller and waves encountering the vessel at $\psi = 0°$. The observer estimated a bias ramping up to 1.5 N from time 5-35 seconds and the integral-part of the PID-AFB controller compensated for this bias. The east position oscillates around 0.005 m which is minimal, while the heading shows more steady behavior.

Figure B.2 shows test case 1g with $\Delta K = 50$ kg. In this sea state, the wave filter was disabled because it can filter out important LF motions. It may look like the estimates were not exactly the same as the measured states, this is not the case. Figures B.2 and B.3 show test case 1g, first in full simulation time, then in the interval 150-300 seconds. The north position oscillates around $N = \pm 0.05$ m while the east position oscillates with $E = \pm 0.01$ and the north position has a larger error than the east position because the waves encounters the vessel at $\psi = 0°$ giving the control system a harder job to counteract waves in this direction.

The final sea state tested in MCSim was extreme with $H_s = 0.26$ m and $T_p = 2.3$ s. This corresponds to sea state code 9 that is found in full scale to be a significant wave height of $H_s = 9$ m with peak period of $T_p = 13.5$ s. The best tuning strategy was to increase the extra inertia with $\Delta K = 50$ kg as shown in Figure 5.1. Figure 5.2 shows the same test case with a shorter time horizon. The wave filter was disabled and the estimated LF measurements were very close to the measured due to no wave filtering. The north position oscillates with $N = \pm 0.1$ m and this error

is clearly a result of the increased wave height and change of peak period of wave. This corresponds to oscillations of $N = \pm 3$ m in full scale[1] for the supply vessel.

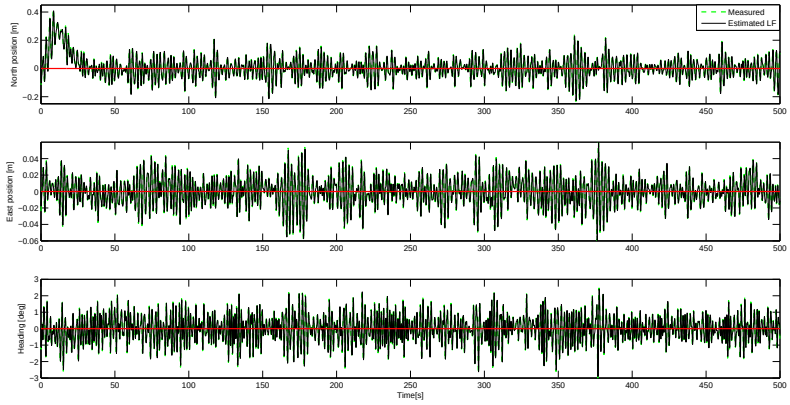

Figure 5.1: Positions and heading in test case 1l. Significant wave height $H_s = 0.26$ m and peak period of wave $T_p = 2.3$ s. PID-AFB control with $\Delta K = 50$ kg.

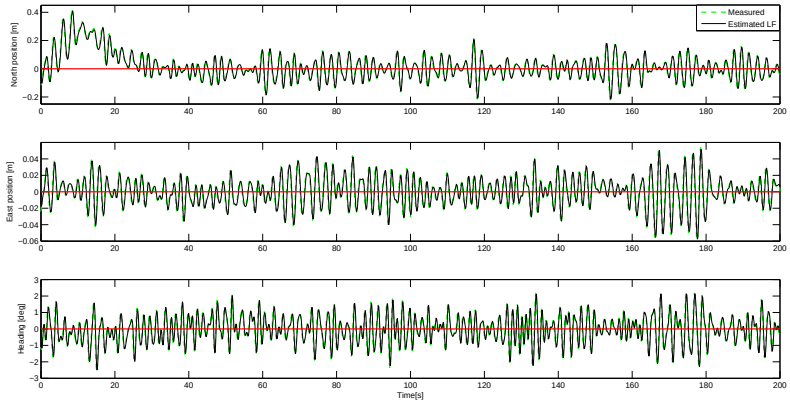

Figure 5.2: Positions and heading in test case 1l with short time horizon. Significant wave height $H_s = 0.26$ m and peak period of wave $T_p = 2.3$ s. PID-AFB control with $\Delta K = 50$ kg.

Test case 1 evaluated by IAE, ITAE and ISE is shown in tables 5.6-5.8. As shown in Table 5.6, the tuning strategy used for test cases 1g and 1l using $\Delta K = 50$ kg was the most accurate when simulating the sea states with $H_s = 0.1$ m and

[1] A position oscillating with ± 0.1 m in MCSim is in full scale found as $0.1 \times 30 = 3$ m for Cybership III

$T_p = 1.5$ s and $H_s = 0.26$ m and $T_p = 0.23$ s. In tables 5.7 and 5.8, it is shown that the yellow marked test cases achieved best accuracy of the desired position and heading.

Table 5.6: IAE for test case 1, PID-AFB in MCSim.

Case	**North** [m]	**East** [m]	**Heading** [rad/s]	**Total**
1a	2.58	0.60	0.85	4.03
1b	2.55	0.59	0.85	3.99
1c	11.42	2.07	3.00	16.49
1d	11.35	2.06	3.01	16.42
1e	11.24	2.05	3.01	16.29
1f	11.18	2.06	3.01	16.24
1g	11.14	2.07	3.00	16.20
1h	29.84	6.92	5.62	42.38
1i	29.54	6.87	5.61	42.01
1j	28.96	6.81	5.61	41.39
1k	28.70	6.81	5.62	41.13
1l	28.45	6.80	5.63	40.87

Table 5.7: ITAE for test case 1, PID-AFB in MCSim.

Case	**North** [m] 10^3	**East** [m] 10^3	**Heading** [rad/s] 10^3	**Total** 10^3
1a	0.561	0.149	0.210	0.920
1b	0.552	0.147	0.210	0.909
1c	1.953	0.515	0.747	3.217
1d	1.938	0.512	0.747	3.197
1e	1.910	0.512	0.747	3.168
1f	1.897	0.512	0.747	3.157
1g	1.889	0.511	0.746	3.147
1h	6.791	1.693	1.351	9.836
1i	6.709	1.677	1.350	9.737
1j	6.557	1.664	1.351	9.574
1k	6.492	1.666	1.352	9.511
1l	6.429	1.663	1.355	9.448

Table 5.8: ISE for test case 1, PID-AFB in MCSim.

Case	North [m]	East [m]	Heading [rad/s]	Total
1a	0.0234	0.0011	0.0023	0.0268
1b	0.0231	0.0011	0.0023	0.0265
1c	0.9587	0.0137	0.0289	1.0013
1d	0.9566	0.0136	0.0289	0.9991
1e	0.9562	0.0134	0.0289	0.9985
1f	0.9544	0.0136	0.0289	0.9969
1g	0.9540	0.0136	0.0289	0.9965
1h	3.2513	0.1539	0.0988	3.5040
1i	3.1993	0.1520	0.0987	3.4500
1j	3.0949	0.1493	0.0988	3.3430
1k	3.0505	0.1492	0.0991	3.2988
1l	3.0014	0.1485	0.0992	3.2491

5.2.2 Test Case 2, Sliding-mode Control

Test case 2a was performed with the SMC with 0% uncertainty of the system's inertia and damping matrices $\boldsymbol{M}$ and $\boldsymbol{D}$ and is shown in Figure B.4. The north and east positions were not so oscillatory, except of the the overshoot in north position. The wave filter works as expected and removes the first-order wave induced motions. At time 470 seconds and towards the end of the simulation, the heading tends to become more oscillatory. A reason for this may be the vessel being exposed to a wave train of larger waves making the heading control more difficult.

Figure B.5 shows the SMC with 0% uncertainty of the estimated system matrices $\hat{\boldsymbol{M}}$ and $\hat{\boldsymbol{D}}$ assuming perfect knowledge of the real system matrices $\boldsymbol{M}$ and $\boldsymbol{D}$. This test case was done when the vessel was exposed to the second sea state tested, harsh. In this test case the wave filter was not enabled and the positions and heading were more oscillatory. Test case 2h is shown in Figure 5.3. The north position oscillates with $N = \pm 0.1$ m, east position with $E = \pm 0.05$ m and the heading oscillates around $\psi = \pm 2°$. By this observation it is clearly seen that this sea state is more harsh than the latter.

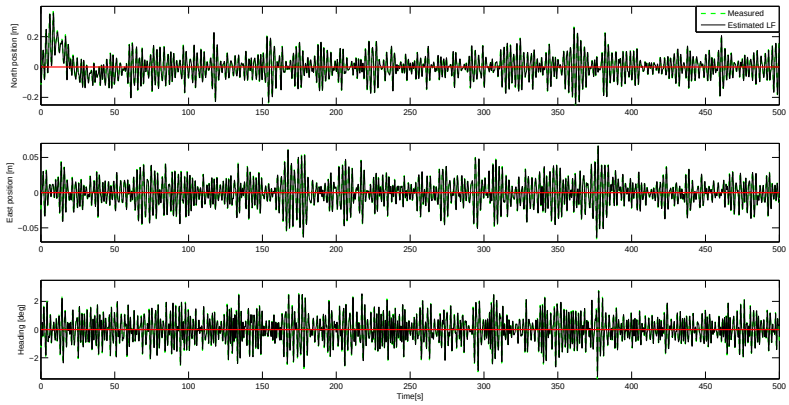

Figure 5.3: Positions and heading in test case 2h. Significant wave height $H_s = 0.26$ m and peak period of wave $T_p = 2.3$ s. SMC with 0% uncertainty of $\boldsymbol{D}$ and $\boldsymbol{M}$.

In tables 5.9-5.11, the test cases providing the best performance are marked with yellow lines. The SMC with estimated inertia and damping matrices $\hat{\boldsymbol{M}}$ and $\hat{\boldsymbol{D}}$ chosen to be exactly the same as the system matrices $\boldsymbol{M}$ and $\boldsymbol{D}$ in the process plant model showed best performance in almost every measure of performance. The only deviation was test case 2d in Table 5.11 where the estimated inertia and damping matrices were chosen to be +10% larger than expected. The differences between 2d and 2c in Table 5.11 are marginal in east and heading and in north position, the difference is found to be 0.0058 m.

As seen in Table 5.9, test case 2c provided the best performance for IAE and ITAE in that particular sea state with 0% uncertainties of the the inertia and damping matrices $\boldsymbol{M}$ and $\boldsymbol{D}$. When testing with the extreme seas, test case 2h, also with 0% uncertainties, was best out of 2h-2l. This tuning strategy also had the best performance for ITAE in Table 5.10. In , test case 2c was not the best as observed in tables 5.9 and 5.10 for SMC.

Table 5.9: IAE for test case 2, SMC in MCSim.

Case	North [m]	East [m]	Heading [rad/s]	Total
2a	2.45	0.59	0.85	3.89
2b	2.46	0.59	0.85	3.90
2c	10.40	2.12	3.24	15.76
2d	10.42	2.13	3.29	15.81
2e	10.48	2.13	3.30	15.91
2f	10.51	2.13	3.31	15.95
2g	10.54	2.13	3.32	15.99
2h	29.45	7.21	6.36	43.01
2i	29.54	7.22	6.39	43.15
2j	29.71	7.24	6.42	43.36
2k	29.80	7.25	6.43	43.47
2l	29.87	7.25	6.44	43.56

Table 5.10: ITAE for test case 2, SMC in MCSim.

Case	North [m] 10^3	East [m] 10^3	Heading [rad/s] 10^3	Total 10^3
2a	0.561	0.146	0.209	0.916
2b	0.560	0.146	0.210	0.916
2c	1.965	0.528	0.805	3.300
2d	1.971	0.529	0.811	3.312
2e	1.979	0.529	0.820	3.319
2f	1.979	0.529	0.823	3.332
2g	1.983	0.530	0.827	3.339
2h	6.963	1.765	1.538	10.267
2i	6.984	1.768	1.544	10.297
2j	7.026	1.773	1.552	10.352
2k	7.046	1.775	1.555	10.377
2l	7.065	1.777	1.558	10.400

Table 5.11: ISE for test case 2, SMC in MCSim.

Case	North [m]	East [m]	Heading [rad/s]	Total
2a	0.0187	0.0011	0.0023	0.0221
2b	0.0190	0.0011	0.0023	0.0224
2c	0.5616	0.0146	0.0336	0.6097
2d	0.5558	0.0145	0.0340	0.6043
2e	0.5572	0.0147	0.0347	0.6066
2f	0.5623	0.0148	0.0349	0.6120
2g	0.5625	0.0150	0.0353	0.6128
2h	0.0563	0.0150	0.0353	3.2471
2i	2.9541	0.1668	0.1262	3.2641
2j	2.9973	0.1680	0.1287	3.2940
2k	3.0138	0.1685	0.1129	3.3115
2l	3.0235	0.1688	0.1296	3.3219

5.2.3 Summarized Performance

The test cases a and b in calm seas for the SMC and PID-AFB were primary meant for tuning purposes. However, they were included as a part of the results to investigate if the tuning strategies used for extreme seas has a pattern when tested in sea states with smaller waves and peak periods of waves as well.

For test case 1b, the PID-AFB where $\Delta K = 30$ kg showed best performance. Test case 2a was SMC with 0% uncertainty of $\hat{\boldsymbol{M}}$ and $\hat{\boldsymbol{D}}$ had the best performance out of 2a and 2b for the first sea state. When comparing the best control strategy of test case 1b and 2a, test case 2a had the best performance in two out of three measures of performance as shown in tables 5.6-5.11. A comparison of the best control strategies from test case 1 and 2 for the harsh and extreme sea states are shown in figures 5.4-5.9. These figures shows plots of the test cases compared by the measures of performance IAE, ITAE and ISE with the results from tables 5.6-5.11.

Test cases 1c-1g and 2c-2g correspond to when the vessel was exposed to the harsh sea state with waves with $H_s = 0.1$ m and peak period of wave $T_p = 1.5$ s. Figure 5.4 shows a comparison of test case 1g and 2c with respect to IAE. The SMC provides best precision in north position. The PID-AFB shows better performance in Figure 5.5 where the measure of performance was done with ITAE.

In Figure 5.6, subplot 1 shows that the ISE in north position are clearly better for the SMC than PID-AFB when exposed to waves with $H_s = 0.1$ m and $T_p = 1.5$ s. However, the PID-AFB has better performance in the east position and heading than the SMC. The ISE evaluation of the north position was improved by 0.3982 m when using SMC and this difference was so dominating that even though the PID-AFB shows better performance in two out three DOF, the total error is smaller

when using SMC. The PID-AFB provided best performance in position and heading with respect to the ITAE as shown in in Figure 5.5. Overall, the SMC was the most precise controller with respect to ISE and IAE for this sea state. The error for the PID-AFB has a quick increase in 5.6 from time 0-20 seconds. This is illustrated by the black thin line and is most likely caused by the PID-AFB having a much larger overshoot than the SMC and overall worse performance in surge.

Figure 5.7-5.9 shows the results from the tests performed in extreme seas with $H_s = 0.26$ m and $T_p = 2.3$ s. The tuning strategy with $\Delta K = 50$ kg in test case 1l was overall better than SMC with 0% uncertainty.

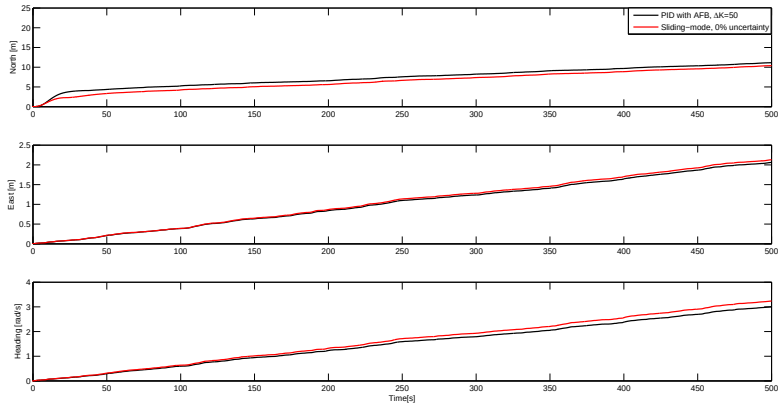

Figure 5.4: Comparison of test cases 1g and 2c with respect to IAE. Significant wave height $H_s = 0.1$ m and peak period of wave $T_p = 1.5$ s. SMC is shown in the red line and PID-AFB in the black.

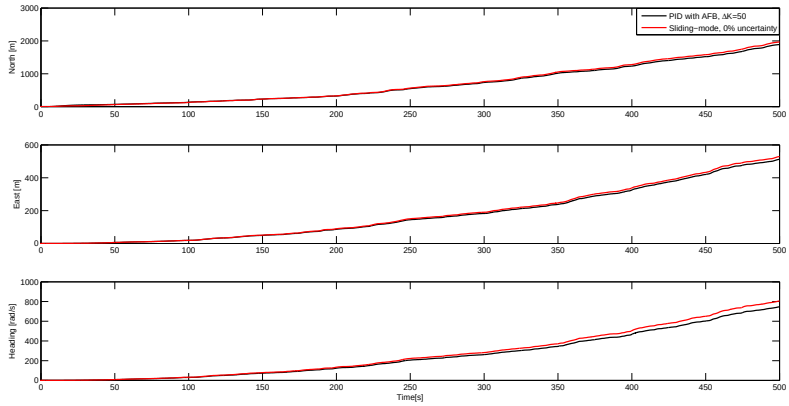

Figure 5.5: Comparisons of test case 1g and 2c with respect to ITAE. Significant wave height $H_s = 0.1$ m and peak period of wave $T_p = 1.5$ s. SMC is shown in the red line and PID-AFB in the black.

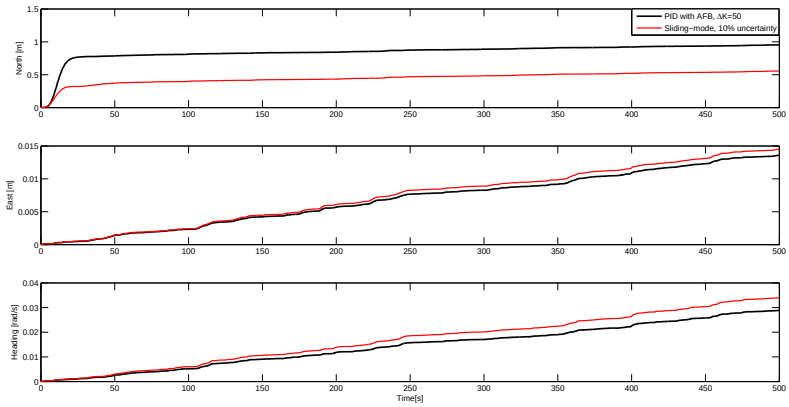

Figure 5.6: Comparison of test cases 1g and 2d with respect to ISE. Significant wave height $H_s = 0.1$ m and peak period of wave $T_p = 1.5$ s. SMC is shown in the red line and PID-AFB in the black.

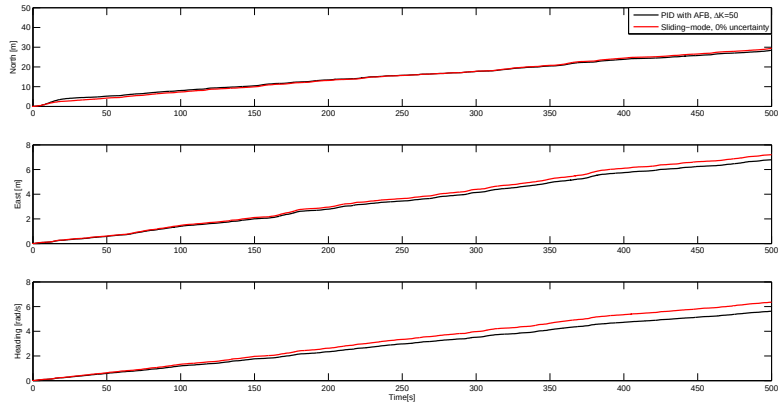

Figure 5.7: Comparison of test cases 1g and 2c with respect to IAE. Significant wave height $H_s = 0.26$ m and peak period of wave $T_p = 2.3$ s. SMC is shown in the red line and PID-AFB in the black.

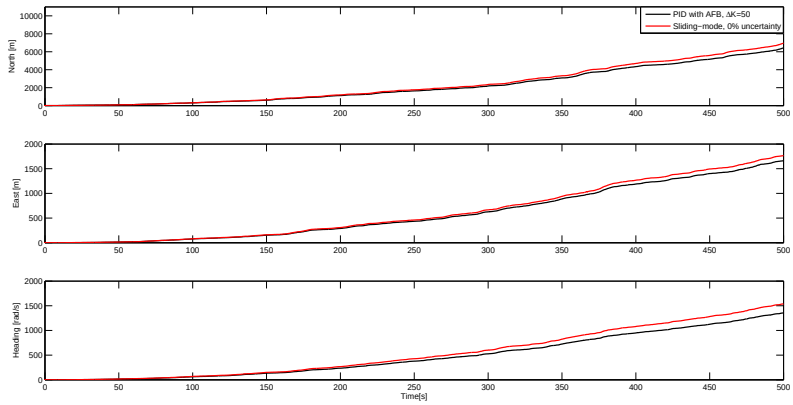

Figure 5.8: Comparison of test cases 1g and 2c with respect to ITAE. Significant wave height $H_s = 0.26$ mand peak period of wave $T_p = 2.3$ s. SMC is shown in the red line and PID-AFB in the black.

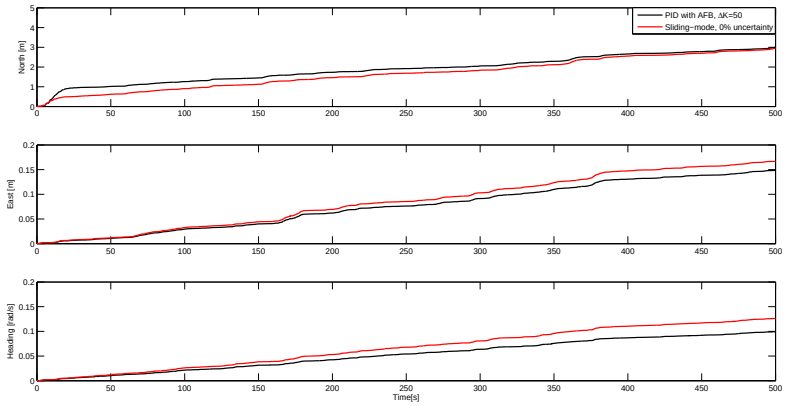

Figure 5.9: Comparison of test cases 1g and 2c with respect to ISE. Significant wave height $H_s = 0.26$ m and peak period of wave $T_p = 2.3$ s. SMC is shown in the red line and PID-AFB in the black.

5.3 Discussion

The control strategies that showed best performance when evaluated by the performance metrics IAE, ITAE and ISE in MCSim, are shown in Table 5.12. The controllers were tested for three sea states with respect to the performance metrics that evaluates if the controllers performs accurately enough with safety in order.

Table 5.12: Best performance for PID-AFB and SMC in MCSim summarized. The gray marked rows are test cases evaluated by the same performance metrics.

Performance Metrics	**Case**	**Sea State**	**Controller Type**	**Extra Mass/ Uncertainty** [kg] / [%]	**Total**
IAE	1b		PID-AFB	30	3.99
IAE	2a	$H_s = 0.03$ m	SMC	0	3.89
ITAE	1b	$T_p = 1.5$ s	PID-AFB	30	909
ITAE	2a		SMC	0	916
ISE	1b		PID-AFB	30	0.0265
ISE	2a		SMC	0	0.0221
IAE	1g		PID-AFB	50	16.20
IAE	2c	$H_s = 0.1$ m	SMC	40	15.76
ITAE	1g	$T_p = 1.5$ s	PID-AFB	50	3147
ITAE	2c		SMC	40	3300
ISE	1g		PID-AFB	50	0.9965
ISE	2d		SMC	40	0.6043
IAE	1l		PID-AFB	50	40.87
IAE	2h	$H_s = 0.26$ m	SMC	40	43.01
ITAE	1l	$T_p = 2.3$ s	PID-AFB	50	9448
ITAE	2h		SMC	40	10267
ISE	1l		PID-AFB	50	3.2491
ISE	2h		SMC	40	3.24

The test cases 1a-1b and 2a-2b for the calm sea state has shown that the SMC had the best performance when measuring IAE and ISE as shown in Table 5.12. The PID-AFB provided better preicision over time and therefore achieving better performance when evaluated by ITAE. The control strategy used to achieve the best overall performance with the SMC for the test cases performed in calm seas was when expecting the inertia and damping of the vessel to be perfectly correct. This was done by assuming 0% uncertainty of the matrices $\hat{\boldsymbol{M}}$ and $\hat{\boldsymbol{D}}$ assuming they were exactly the same as the inertia and damping matrices $\boldsymbol{M}$ and $\boldsymbol{D}$ modeled in the process plant model. It is believed that the reason for the good performance may be because the estimated inertia matrix and damping matrix $\hat{\boldsymbol{M}}$ and $\hat{\boldsymbol{D}}$ used by the SMC (4.26) were exactly the same as those describing the high fidelity process plant model in the 3 DOF. With no uncertainty, the $\boldsymbol{K}_s$ term in (4.28) does not have to be increased due to no potential inexact estimations of the system

matrices . By only using the sliding surface $\boldsymbol{s}$ and tuning $\boldsymbol{\Lambda}$ and $\boldsymbol{K_d}$ resulting in the only contribution to the commanded force $\boldsymbol{\tau}_c$, the controller can be seen as a PD controller with no robustness. The K_s term is increased when the estimated system matrices $\hat{\boldsymbol{M}}$ and $\hat{\boldsymbol{D}}$ are increased in order to increase the robustness of the control if the estimates was to be wrongly estimated in the feed forward part of the controller (4.26).

The second sea state for testing was the harsh, with $H_s = 0.1$ m and a peak period of wave $T_p = 1.5$ s. With this test case the wave filter was disabled as proposed by Sørensen et al. (2002) and shown in Chapter 3. For test case 1 compared with test case 2, PID-AFB provided better performance in east position and heading in all the comparison plots shown in figures 5.4-5.6. The SMC provided an overall better performance because the north position contributed to a better total performance when the east position and heading errors were much smaller than the north position error. An example of this was Figure 5.6 where the difference between test case 1g and 2d in north position was 0.3982 m and the two remaining measurements had differences such as 0.0009 m in east position and 0.0051 rad/s in heading corresponding to 0.29°. By this, the north position measurements evaluated by the performance metrics, dominated the small errors in east and heading measurements.

The third and last sea state for testing was with $H_s = 0.26$ m and $T_p = 2.3$ s that in full scale is equivalent with a significant wave height of $H_s = 9$ m and peak period of wave $T_p = 13.5$ s. This sea state corresponds to the most extreme of all tested in MCSim. The SMC did not provide better performance than PID-AFB in any of the test cases done in this sea state. As the PID-AFB has been referred to as a robust controller, it has shown to still be comparable with the performance for the SMC. The difference in performance with respect to IAE, ITAE and ISE was not large, but clear enough. It was not expected that the SMC with no uncertainties would be the tuning strategy providing the best performance for all test cases, except of the extreme, compared with the PID-AFB. However, the PID-AFB has shown best performance with the acceleration feedback gain (4.5) as large as ever tested by using the tuning parameter $\Delta K = 50$ kg in the extreme sea state. Recall that the latter tuning strategy had a north position oscillating with $N = \pm 0.1$ m that is equivalent with oscillations of $N = \pm 3$ m in full scale. The full scale vessel has a length of 68 m and when exposed to large waves, it is crucial to maintain a steady heading of the vessel to avoid waves encountering the vessel at port and starboard side. By evaluating the performance of the vessel with the performance metrics IAE, ITAE and ISE as done in this chapter, the results only concludes if operations were safe or not. This is not sufficient in order to determine if the control strategy is smart enough by achieving a more green operation and at the same time being accurate. The results achieved in this chapter were only providing information about precision and robustness and not energy consumption.

Lindegaard (2003) showed that by using AFB with a very low gain matrix applied improved the performance of Cybership II in the MCLab. Brodtkorb et al. (2014) and Nguyen et al. (2007) applied AFB with a low gain matrix in order to have

a robust controller to test Cybership III with in extreme seas. Cybership II is smaller than Cybership III with the length of $L = 1.255$ m compared to $L = 2.275$ m. The former PID-AFB performance tests done on Cybership III and the similar vessel Cybership II, were performed with low AFB gain matrices and compared only by evaluating the error. The result of applying an increased gain matrix with the AFB in this thesis shows that by increasing the tuning parameter ΔK, the performance can be improved even more than done before. However, these results were based on tests in MCSim where the energy consumption from the thrusters not were included as a part of the performance metrics and it will be interesting to see if the same performance are obtained when testing the controllers on Cybership III in the MCLab at MARINTEK.

The following chapter presents the experiments in the MCLab.

Chapter 6

Experiments in MCLab

This chapter describes the experimental test cases done in MCLab by presenting the settings and test cases, tuning of controllers, results of the test cases and a discussion of the results. The results for each test case are presented in Section 6.2 by illustrating the position and attitude of the best working controllers and comparing the different tuning strategies with each other by a cost function. The cost function is developed by including energy consumption as a performance metric in addition to the IAE, ITAE ISE and evaluating the product of each performance metric with the total energy consumption from the thrusters on Cybership III. By including the energy consumption together with the performance metrics used in Chapter 5, the "greener" performance can be evaluated together with the measure of accuracy i.e. one overall measure. In Section 6.3 a discussion of the results from test cases in the MCLab is shown and to the end, an overall comparison of test cases performed in MCSim and MCLab is discussed.

6.1 Experimental Setup

In Section 6.1 the experimental setup, test cases and tuning of the controllers are described. The experimental setup involves a choice of wave parameters and defining test cases. The tuning presents tuning parameters chosen for each test case with SMC and PID-AFB.

6.1.1 Laboratory Facilities

The MCLab is equipped with a DHI Wave Synthesizer wave flap where among different types of waves, irregular waves can be generated by choosing wave parameters

for the desired sea states. To track the position of Cybership III, a Qualisys motion capture system (MCS) is mounted at the end of the model basin area used for the test cases. This MCS has to be calibrated prior laboratory tests. A host PC is used for reading measurements, adjusting settings for the controllers and enable/disable of thrusters. In addition, a joystick connected to the vessel by Bluetooth can be used to manually control the vessel and enable/disable the thrusters. The waves are generated by pre-modeling waves and specifying them in the wave generator PC. An illustration of the communication between the different units in the MCLab is shown in Figure 6.1. For more information about the MCLab and Cybership III, see appendices B.3-B.4.

The objective for all test cases in the model basin is for Cybership III to maintain position at $\boldsymbol{\eta} = \begin{bmatrix} 0 & 0 & 0 \end{bmatrix}^\top$. This corresponds to maintin position at the center of the basin and 2 meters away from the DHI Wave Synthesizer wave flap.

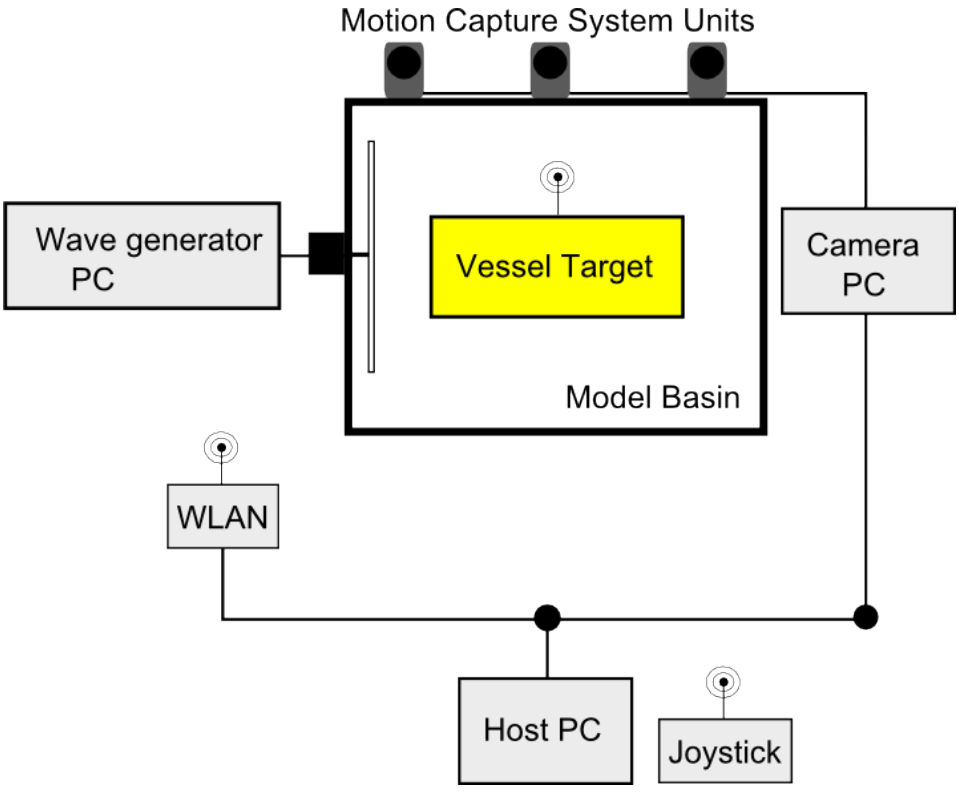

Figure 6.1: Illustration of the communication between all units in the MCLab.

6.1.2 Test Cases

Test case 3 and 4 was done in the MCLab with waves as the only environmental forces generated. The test cases was performed with two different sea states, the first sea state was calm with $H_s = 0.03$ m and $T_p = 0.8$ s Test case 3 and 4 was done in the MCLab with waves as the only environmental forces generated. The test cases was performed with two different sea states, the first sea state was calm with $H_s = 0.03$ m and $T_p = 0.8$ s. The second sea state tested in the MCLab was with $H_s = 0.1$ m and $T_p = 1.5$ s and is referred to as harsh. The measured acceleration used for the AFB in the PID-AFB controller was barely filtered due to very good measurements and the resulting maximum measured variance of the acceleration was $a = \pm 0.0004\ m/s^2$.

Test case 3 is shown in Table 6.1 was performed with the tuning parameter $\Delta K = (0, 10, 30, 50)$ kg. This tuning parameter provides an extra virtual mass to the vessel that the control system has to take in to account during DP. Test case 4 in Table 6.2 was tested with the following estimates of the inertia $\boldsymbol{M}$ and damping $\boldsymbol{D}$ matrices of the vessel , 0%, +10%, +30%,+40% and +50%. This table shows that the test cases performed in the MCLab were only exact and overestimations of the inertia and damping of the vessel $\boldsymbol{M}$ and $\boldsymbol{D}$. The reason for not testing underestimations of the inertia and damping was because during tuning in the simulator MCSim, the performance of the vessel was not obviously any better with overestimations than underestimations of the inertia and damping. Due to limited time in the MCLab, it was necessary to choose either underestimation or overestimation of the inertia and damping matrices of the vessel. Overestimating these matrices when the vessel was exposed to large waves with long peak periods of the waves seemed like a reasonable choice considering the PID-AFB strategy was to increase the inertia.

Table 6.1: Test case 3, parameters used for testing with PID-AFB in MCLab. Arrows and vertical lines indicates repetitive values.

Case	**Significant wave height,** H_s [m]	**Peak period of wave** T_p [s]	**Extra mass** ΔK [kg]
3a	0.03	0.8	0
3b	|	|	30
3c	0.1	1.5	0
3d			10
3e	↓	↓	30
3f			50

Table 6.2: Test case 4, parameters used for testing with SMC in MCLab. Arrows and vertical lines indicates repetitive values.

Case	Significant wave height, H_s [m]	Peak period of wave T_p [s]	Uncertainty in $\boldsymbol{M}$ and $\boldsymbol{D}$ [%]
4a	0.03	0.8	0
4b	|	|	+30
4c	0.1	1.5	0
4d	↓	↓	+10
4e	↓	↓	+20
4f	↓	↓	+40
4g	↓	↓	+50

6.1.3 Tuning

PID with Acceleration Feedback

Choosing gain matrices when testing Cybership III in the MCLab was not straightforward because the gain matrices from Section 5.1.2 were too large. The test cases shown in Table 6.1 were done with two different settings of the gain matrices $\boldsymbol{K}_p$, $\boldsymbol{K}_d$ and $\boldsymbol{K}_i$. The reason these gain matrices were different from the gain matrices chosen for the MCSim test cases is because they provided too aggressive control when they were tested on Cybership III in the MCLab. Therefore the tuning had to be done manually and the result was gain matrices incomparable with those found in tables 5.4 and 5.5. One reason for the large difference between the gain matrices could be the lack of a model for the thruster dynamics for Cybership III in the MCSim DP loop. Second, the vessel model, in particular $\boldsymbol{M}$ and $\boldsymbol{D}$, may be inaccurate.

The main challenge when tuning the vessel in the MCLab was finding reasonable gains in order to avoid the vessel becoming unstable and to achieve steady state. The gain matrices from MCSim tests was too large resulting in aggressive control and unstable behavior. The trick was to start low and increase slowly, especially when the vessel initial position was too far away from the reference. The reason for this was because the vessel compensated too much for the large error. Thus low gain matrices made it possible for the vessel to advance into the desired position. The gain matrices for the test cases are shown in Table 6.3.

Table 6.3: Tuning for test case 3, PID-AFB in MCLab.

Case	$\boldsymbol{K}_p$	$\boldsymbol{K}_d$	$\boldsymbol{K}_i$
3a	diag{1.1 1 0.5}	diag{5 5 5}	diag{0.03 0.06 0.03}
3b	|	|	|
3c	diag{1.5 1 0.5}	diag{8 8 8}	diag{0.05 0.1 0.05}
3d			
3e	↓	↓	↓
3f			

Sliding-mode Control

To start with, the gain matrices from Table (5.10) together with (5.10) and (5.12) were used to find gain matrices for the SMC. These gain matrices did not provide satisfactory performance and they had to be adjusted. By starting with low gain matrices as was done when tuning the PID-AFB in the model basin, the gain matrices ended up very low. The tuning matrix $\boldsymbol{\Lambda}$, Table 6.4, was very sensitive to errors and tuning was done with caution. First $\boldsymbol{\Lambda}$ was tuned, then $\boldsymbol{K}_d$ was tuned. After increasing the uncertainty of the vessel, the tuning matrix $\boldsymbol{K}_s$ was increased so that (4.28) was satisfied. Table 6.4 lists the final gain matrices achieved.

Table 6.4: Tuning for test case 4, SMC in MCLab.

Case	$\boldsymbol{\Lambda}$	$\boldsymbol{K}_d$	$\boldsymbol{K}_s$	$\boldsymbol{\Phi}$
4a	diag{0.03 0.01 0.2}	diag{5 5 3}	diag{1 1 1}	diag{1 1 2}
4b	|	|	diag{5 1.3 1.8}	|
4c	diag{0.06 0.03 0.02}	diag{13 12 5}	diag{1 1 1}	
4d			diag{2 1.5 1.5}	
4e	↓	↓	diag{5 1.3 1.8}	↓
4f			diag{6 3 2}	
4g			diag{7 4 2.2}	

6.2 Results

The results from test case 3 and 4 for PID-AFB and SMC are presented in this section. Test case 3a-3b and 4a-4b was meant to test the performance of the controllers as a tuning prior Cybership III was tested with higher waves and longer periods of the waves . These test cases were tested with $H_s = 0.03$ m and $T_p = 0.8$ s. The main test cases were 3c-3f and 4c-4g and they were tested with $H_s = 0.1$ m and $T_p = 1.5$ s. This sea state corresponds to a downscale of sea state code 5 in Table 2.1. The reason for not generating larger waves than $H_s = 0.1$ m with peak

period of waves $T_p = 1.5$ was due to limitations with the DHI Synthesizer wave flap.

When performing test cases in the MCLab, the desired position corresponding to $\boldsymbol{\eta}_d = \begin{bmatrix} 0 & 0 & 0 \end{bmatrix}^\top$ had to be adjusted such that the vessel had a distance of 2m away from the wave flap in order to achieve realistic waves corresponding to the settings made for the wave flap. This change of set points has been fixed in the figures showing the desired positions and heading $\boldsymbol{\eta}_d = \begin{bmatrix} 0 & 0 & 0 \end{bmatrix}^\top$. In addition, the reference model was experienced to be too slow when ramping up to the final desired set points. Therefore the reference model that worked in MCSim had to be speed up by tuning the time constants in the LP-filter part of the reference model. The reference model is shown in Figure 4.3.

In order to determine which tuning strategies had the best performance, a cost function was made where the product of the total energy consumption from the three thrusters mounted on Cyberhip III and ITAE, IAE and ISE was evaluated. The cost function and measures of performance are described in Appendix C.1. When the cost is low, the product of the energy consumption and error is low and hence a precise and energy saving control i.e. greener control. All test cases has been summarized in tables 6.5-6.10 where the best tuning strategy for each sea state has been marked yellow and the total cost is shown in the right column. The test cases that provided best performance out of the PID-AFB and SMC test cases are shown in figures 6.2-6.5 with plots of measured position and heading.

6.2.1 Test Case 3, PID with Acceleration Feedback

Test cases 3b and 3e had the best performance for all the PID-AFB test cases. Figure 6.2 shows the position and heading of Cyberhip III during test case 3b. The extra inertia was chosen to be $\Delta K = 30$ kg and this made the control system believe the vessel had a larger inertia. The position and heading oscillates around the set point $\boldsymbol{\eta}_d = \begin{bmatrix} 0 & 0 & 0 \end{bmatrix}^\top$ with a deviation for the north position of $N = \pm 0.05$ m, east position by $E = \pm 0.05$ m and heading with $\psi = \pm 2°$. From time 200-360 seconds, the vessel is exposed to a wave train of very small waves leading to very good performance and low error compared with the time series from 0 to 200 seconds.

Figure 6.3 shows test case 3e with $\Delta K = 30$ kg as the extra mas added to the vessel. The current sea state has higher waves with a longer peak period of the waves, thus larger oscillation of the position and heading around the set point. This plot shows how the vessel can behave quite differently dependent on what kind of waves that has been produced by the DHI Synthesizer wave flap. From 0-50 seconds, very small waves encounters the vessel. Suddenly, a wave train of large waves has been generated and acts on the vessel. This can be seen in the positions and more clearly in the heading from 150-350 seconds.

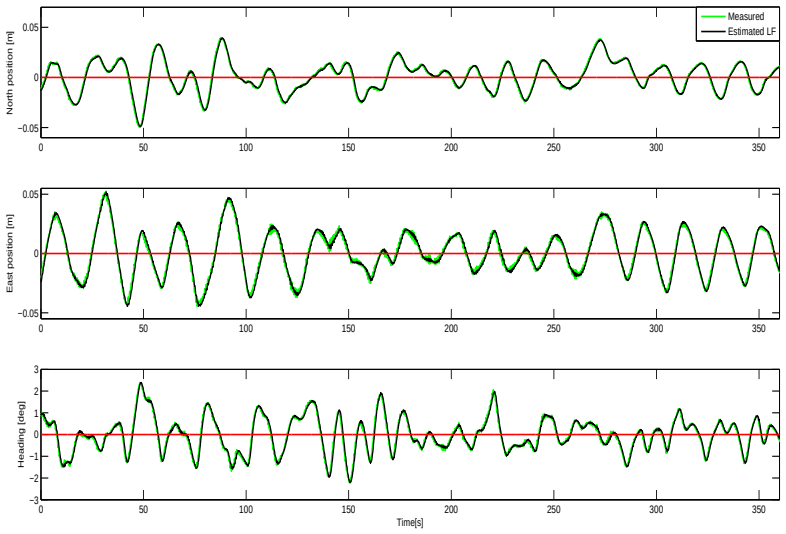

Figure 6.2: Positions and heading in test case 1l. Significant wave height $H_s = 0.03$ m and peak period of wave $T_p = 0.8$ s. PID-AFB control with $\Delta K = 30$ kg.

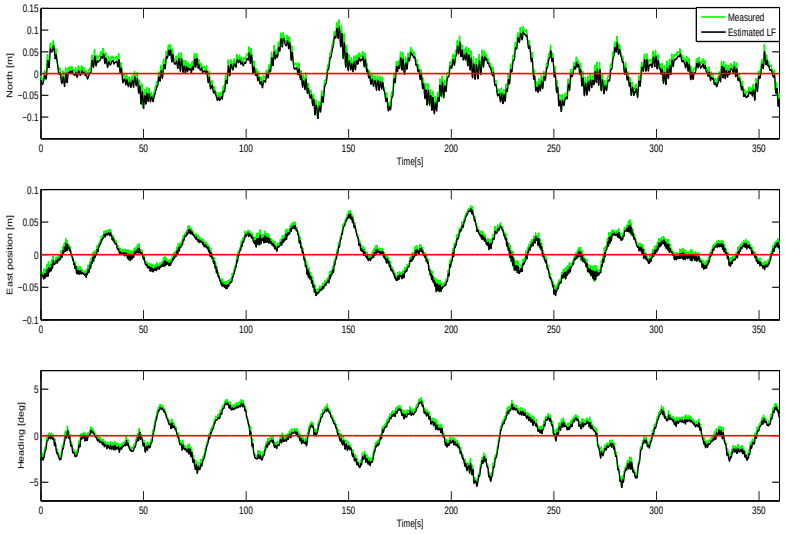

Figure 6.3: Positions and heading in test case 1l. Significant wave height $H_s = 0.1$ m and peak period of wave $T_p = 1.5$ s. PID-AFB control with $\Delta K = 30$ kg.

In tables 6.5-6.7 the costs J_{IAE}, J_{IAE}, and J_{IAE} for test case 3 are summarized. Test case 3b as shown in Figure 6.2 was the best test case with PID-AFB for the calm sea state, while 3e had the lowest cost out of test cases 3c-3f. The tuning strategy with the choice of $\Delta K = 30$ kg gave the best performance when generating the cost with respect to IAE, ITAE and ISE for both sea states tested as shown in tables 6.5-6.7.

Table 6.5: Cost J_{IAE} for test case 3, PID-AFB in MCLab.

Case	Cost in North	Cost in East	Cost in Heading	Total
3a	1.94	1.54	1.20	4.68
3b	0.69	0.87	0.62	2.18
3c	3.65	1.84	3.04	8.53
3d	3.11	1.73	2.39	7.23
3e	2.73	1.80	2.48	7.01
3f	3.24	1.83	2.71	7.78

Table 6.6: Cost J_{ITAE} for test case 3, PID-AFB in MCLab.

Case	Cost in North	Cost in East	Cost in Heading	Total 10^3
3a	337	256	201	0.794
3b	115	142	99	0.356
3c	664	347	492	1.503
3d	582	323	408	1.310
3e	484	310	473	1.267
3f	583	339	464	1.386

Table 6.7: Cost J_{ISE} for test case 3, PID-AFB in MCLab.

Case	Cost in North	Cost in East	Cost in Heading	Total
3a	0.08	0.05	0.34	0.47
3b	0.01	0.02	0.01	0.04
3c	0.21	0.05	0.14	0.4
3d	0.16	0.05	0.10	0.31
3e	0.13	0.06	0.10	0.29
3f	0.19	0.06	0.13	0.38

6.2.2 Test Case 4, Sliding-mode Control

Figure 6.4 shows the positions and heading measured and estimated from test case 4a when SMC was tested with no uncertainty of the system's inertia and damping matrices assuming perfect knowledge of them. The position has a very low variance, but the heading does not have the same oscillations as in test case 3b. The heading is influenced by a bias of 0.5 N acting on the vessel as seen in time 125-250 seconds and from time 250-300 seconds. By observing the east position in the same time intervals as the heading, it is seen that the east position is influenced by the same bias. The oscillations in east position and heading changed simultaneously and this is an example of how the DOFs to the vessel are coupled.

Figure 6.5 shows test case 4f with +40% overestimated inertia $\hat{\boldsymbol{M}}$ and and damping $\hat{\boldsymbol{D}}$ of the vessel. The controller is able to maintain a stable oscillation around the set point for the positions and heading. From 100-230 seconds, the heading has a very low variance around the set point and this can be seen in following tables.

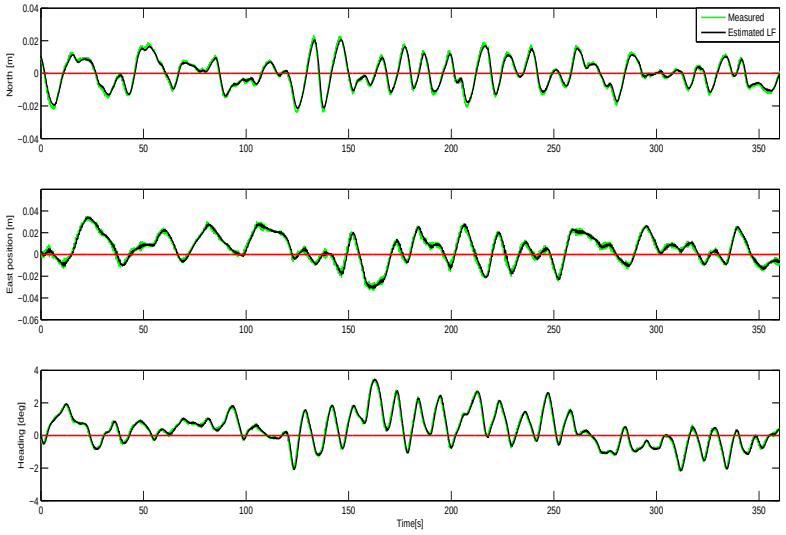

Figure 6.4: Positions and heading in test case 4a. Significant wave height $H_s = 0.03$ m and peak period of wave $T_p = 0.8$ s. SMC with 0% uncertainty of $\boldsymbol{D}$ and $\boldsymbol{M}$.

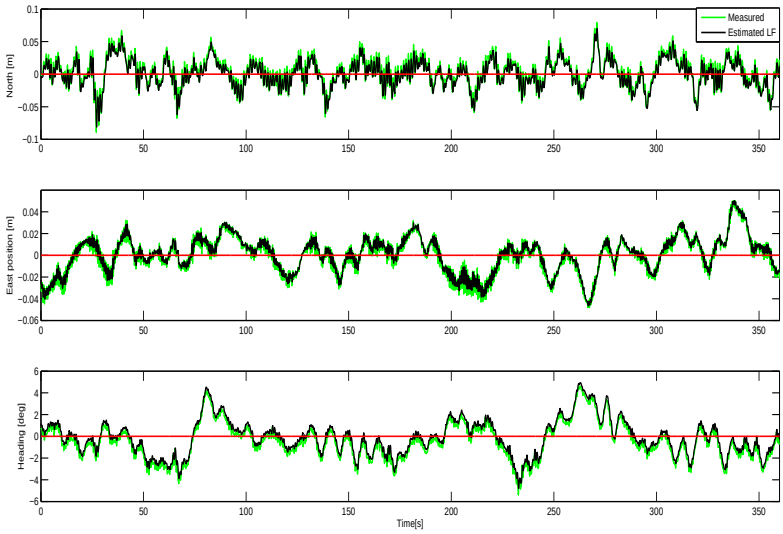

Figure 6.5: Positions and heading in test case 4f. Significant wave height $H_s = 0.1$ m and peak period of wave $T_p = 1.5$ s. SMC with +40% uncertainty of $\boldsymbol{D}$ and $\boldsymbol{M}$.

In tables 6.8-6.10 test case 4 is summarized. The tuning strategy used in 4a showed better results than 4b as shown in Table 6.8 and the total difference in cost was 0.16. In Table 6.10, test case 4b with 30% uncertainty of the inertia and damping matrices gave the best performance and the difference between test case 4a and 4b was marginal with the cost of 0.01. Test case 4f with 40% uncertainty gave the best performance with all three cost functions.

Table 6.8: Cost J_{IAE} for test case 4, SMC in MCLab.

Case	Cost in North	Cost in East	Cost in Heading	Total
4a	0.36	0.52	0.67	1.55
4b	0.42	0.62	0.67	1.71
4c	1.96	1.60	2.81	6.37
4d	2.17	1.64	2.31	6.12
4e	2.35	1.75	2.88	6.98
4f	1.68	1.23	2.25	5.16
4g	2.21	1.55	2.01	5.77

Table 6.9: Cost J_{ITAE} for test case 4, SMC in MCLab.

Case	Cost in North	Cost in East	Cost in Heading	Total 10^3
4a	60	88	120	0.268
4b	85	127	124	0.336
4c	365	296	454	1.115
4d	379	305	441	1.125
4e	408	308	481	1.197
4f	304	232	424	0.960
4g	393	301	384	1.078

Table 6.10: Cost J_{ISE} for test case 4, SMC in MCLab.

Case	Cost in North	Cost in East	Cost in Heading	Total
4a	0.004	0.009	0.02	0.03
4b	0.006	0.01	0.01	0.02
4c	0.06	0.04	0.14	0.24
4d	0.07	0.04	0.08	0.19
4e	0.08	0.05	0.12	0.25
4f	0.04	0.03	0.08	0.15
4g	0.07	0.03	0.07	0.17

6.2.3 Summarized Performance

As mentioned in Section 5.1, test case a and b was meant for tuning purposes and hence not included among the comparison figures 6.6-6.8 in this section. It is however worth mentioning that the SMC with no overestimation of the inertia and damping matrices from test case 4a provided better performance than the PID-AFB in test case 3b when testing in calm seas.

Figures 6.6-6.8 shows the comparison of the best control strategies from test case 3 and 4 with respect to the costs J_{IAE},J_{ITAE} and J_{ISE}. By exposing the vessel to the harsh sea state with $H_s = 0.1$ m and $T_p = 1.5$ s in the MCLab, the SMC provided the best performance out of the three cost functions J_{IAE}, J_{ITAE} and J_{ISE}. In Figure 6.6 the cost with respect to IAE is shown. The PID-AFB with $\Delta K = 30$ kg had almost the same cost in heading as the SMC, while north and east position costs were worse. As shown in figures 6.3 and 6.5, the position and heading for both controllers follows a pattern for every wave train encountering the vessel. By looking closely on the east position in Figure 6.3, the position looks like it tends to be less oscillatory from time 300-360 seconds. This is also shown for the heading in Figure 6.5and by looking at prior behavior in Figure 6.5, this seem to repeat in intervals such as from time 0-70 seconds, 100-210 seconds. Both

control strategies seem to oscillate around the set point with similar variances of error but with different intervals of less oscillatory behavior. In spite of these observations, the SMC had lowest energy consumption in combination with the most precise control when comparing the best results from PID-AFB and SMC in figures 6.6-6.8.

In figure 6.7 the the best performance is obvious. The ITAE integrates the absolute error multiplied with the time. This explains the high cost values for the cost function with respect to the ITAE. With error over time, errors late in the simulations were punished more and this shows that the SMC has lower error than the PID-AFB over time. The last performance measurement, with J_{ISE}, has shown that the SMC provides gives the lowest cost when evaluated by this measure of performance. By this, the SMC provided the most accurate and green control for all test cases in harsh seas in the MCLab.

In retrospect of the experiments in the MCLab, it turned out that the weight of Cybership III is not the same as modeled in MCSim and used in the control systems. The vessel was found to weight $m = 87$ kg and this is 11 kg more than expected. The reason for this difference of 14% kg is that the team that developed the MCSim model and all matrices describing the vessel, inertia, damping, Coriolis etc. used information that originate from a report[1] of test cases performed on Cybership III at MARINTEK November 1988. At that time, there was different equipment mounted on the vessel e.g. batteries was not mounted on the vessel and a cable providing the electricity was connected and manually held above the water surface during tests. The batteries with other components currently mounted on Cybership III are shown in Figure B.9. When the best tuning strategy with SMC was overestimating the inertia with +40%, this corresponded to overestimating the mass to be $m \approx 106$ kg. The gain matrices obtained in the MCLab was tested with the controllers in MCSim and the results are shown in Figure B.6. The PID-AFB was tested with $\Delta K = 0$ kg and the estimated system's inertia and damping matrices $\hat{\boldsymbol{M}}$ and $\hat{\boldsymbol{D}}$ were chosen exactly the same as those used to model the process plant model of the vessel.

[1] This report is enclosed among the other attachments for this thesis as shown in Appendix A.

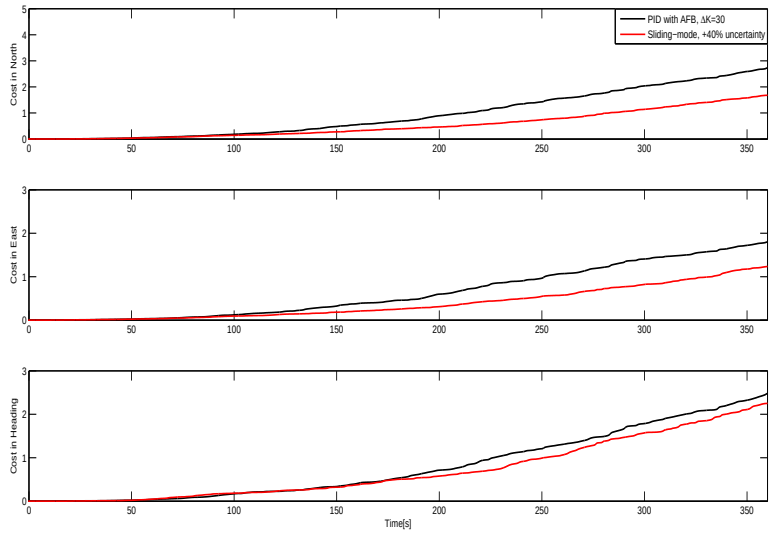

Figure 6.6: Comparison of test case 3e and 4f with respect to cost function $\boldsymbol{J}_{IAE}$. Significant wave height $H_s = 0.1$ and peak period of wave $T_p = 1.5$s. SMC is shown in the red line and PID-AFB in the black.

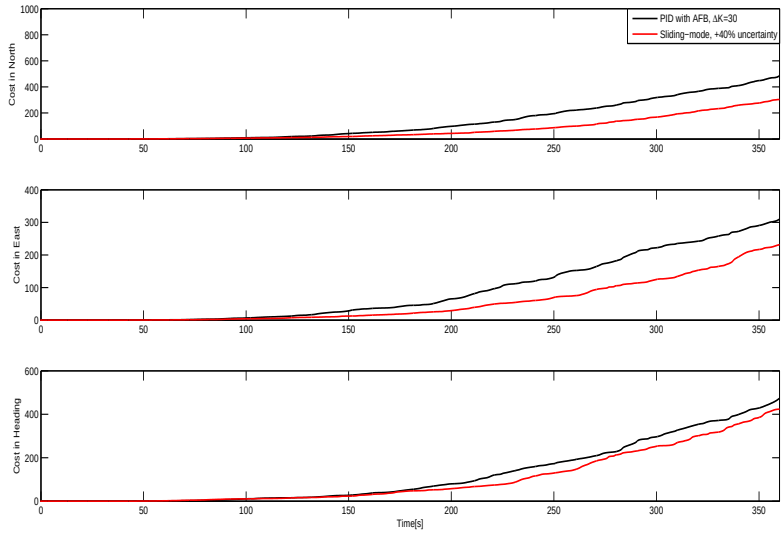

Figure 6.7: Comparison of test case 3e and 4f with respect to cost function $\boldsymbol{J}_{ITAE}$. Significant wave height $H_s = 0.1$ and peak period of wave $T_p = 1.5$s. SMC is shown in the red line and PID-AFB in the black.

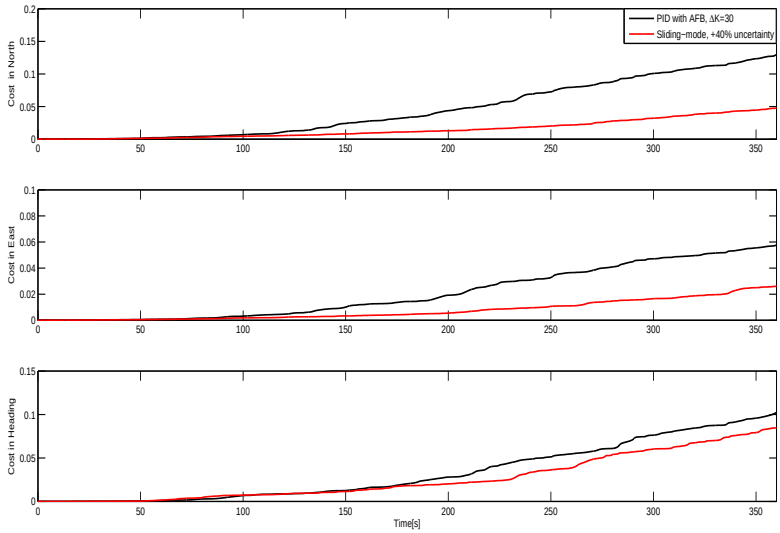

Figure 6.8: Comparison of test case 3e and 4f with respect to cost function $\boldsymbol{J}_{ISE}$. Significant wave height $H_s = 0.1$ and peak period of wave $T_p = 1.5$s. SMC is shown in the red line and PID-AFB in the black.

6.3 Discussion

6.3.1 Discussion of Results from MCLab

Finding which controllers out of PID-AFB and SMC that provided the best performance in extreme seas was done by measuring the electrical energy consumption from each of the three thrusters and multiplying it with the performance metrics IAE, ITAE and ISE. This gave a measure of how precise and at the same time energy saving the different tuning strategies was i.e. safer, smarter and greener. The tuning of the controllers was done by first finding the gain matrices for PID-AFB with Ziegler-Nichols inspired manual tuning, then using them to tune the SMC as proposed in Section 6.1.3. This way the control strategies has the same eigenvalues and are more comparable. Due to experiments in the model basin with the real ship model, individual readjustments of the gain matrices had to be done.

Table 6.11 summarizes the best test cases performed in the MCLab. The first two rows marked in gray represents the cost with respect to the IAE performance metric. The next two rows are white and shows the cost with respect to ITAE and so on. All test cases done with the first sea state tested are above the mid rule. Below the mid rule, the test cases performed with the harsh sea state are shown.

Table 6.11: Best performance for PID-AFB and SMC in MCLab summarized. The gray marked rows are test cases evaluated by the same performance metrics.

Cost Type	**Case**	**Sea State**	**Controller Type**	**Extra Mass/ Uncertainty** [kg] / [%]	**Total Cost**
J_{IAE}	3b		PID-AFB	30	2.18
J_{IAE}	4a	$H_s = 0.03$ m	SMC	0	1.55
J_{ITAE}	3b	$T_p = 0.8$ s	PID-AFB	30	356
J_{ITAE}	4a		SMC	0	268
J_{ISE}	3b		PID-AFB	30	0.04
J_{ISE}	4b		SMC	0	0.02
J_{IAE}	3e		PID-AFB	30	7.01
J_{IAE}	4f	$H_s = 0.1$ m	SMC	40	5.16
J_{ITAE}	3e	$T_p = 1.5$ s	PID-AFB	30	1267
J_{ITAE}	4f		SMC	40	960
J_{ISE}	3e		PID-AFB	30	0.29
J_{ISE}	4f		SMC	40	0.15

Test case 3a and 3b was meant for tuning purposes in order to obtain reasonable gain matrices for the calm sea state. It was found necessary to test the performance with the extra mass $\Delta K = 30$ kg added to the AFB in order to observe how the performance in the calm sea state was. By increasing the inertia when Cybership III was exposed to waves with $H_s = 0.03$ m and $T_p = 0.8$ s, the vessel performance was increased. This is shown in tables 6.5-6.7 where the total cost from test case a

to b was halved. A reason for test case b to give best performance may have been that since the environmental forces were not that strong and the system believed the model to be heavier than it was in reality, the system was more robust to the small disturbances from the waves and therefore did not use that much energy for small errors. Since the vessel turned out to actually be heavier than expected, the increase of the inertia is expected to have increased the accuracy of the vessel because of the inertia being wrongly estimated when modeled. However, only an extra mass of $\Delta K = 30$ kg was tested and there is no guarantee that this test case will give better performance than a test case with e.g. $\Delta K = 10$ kg or $\Delta K = 50$ kg. This result shows that by increasing the inertia of the vessel in this specific test environment, the control system ensured better performance than without.

In test case 3e, increasing the inertia with $\Delta K = 30$ kg provided the best performance. This tuning strategy clearly showed a better performance than test cases with $\Delta K = (0, 10, 50)$ kg, and the vessel controller was more robust to the wave forces acting on it. The controller has shown less oscillatory error of the position and heading when experiencing large wave trains encountering the vessel. Time after time the controller managed to stabilize when new waves encountered repeatably, without large overshoots. This result shows that by implementing AFB in surge and sway reduces unknown slowly varying disturbances from the generated waves, as Lindegaard (2003) also has shown.

Test case 3a and 3b, 4a and 4b were as mentioned, meant for tuning purposes only. Nevertheless it was interesting watching two different controllers operating in the same environment. By guessing that the inertia and damping of the vessel was perfect, the SMC has shown better performance than with 30% overestimation of the inertia and damping matrices. The reason for the SMC providing the best performance with 0% uncertainty in $\boldsymbol{M}$ and $\boldsymbol{D}$ may be because overestimating the inertia and damping can be risky if the guess of either damping, inertia or both are wrong. However, increasing the inertia with PID-AFB gave satisfactory performance and this means that overestimating the damping with the SMC can be the reason for bad performance of the SMC. The PID-AFB does not overestimate the damping matrix, and by increasing the inertia the performance was improved for the PID-AFB in calm seas. For the SMC, this narrows the reasons for the bad performance down to wrong estimations of the damping matrix $\boldsymbol{D}$.

The SMC uses a feed forward of the expected inertia $\hat{\boldsymbol{M}}$ and damping $\hat{\boldsymbol{D}}$ matrices and a wrong guess may result in bad performance when operating in calm seas as and not compensating for the wrongly estimated matrices. By overestimating the inertia of the vessel with +40% in test case 4f, the tuning strategy gave the best performance compared with 4c, 4d, 4e and 4g. As the vessel was found to be heavier than expected after the test cases, the SMC still showed best performance when overestimating the inertia with a mass of $m \approx 106$ kg. This mass is still much larger than the $m = 87$ kg that is the real vessel weight. This means that by guessing a larger inertia and damping, the vessel became more robust to the high waves with the peak period of $T_p = 1.5$ s.

An unexpected result was test case 4b showing better performance than test case 4a when calculating the cost for J_{ISE} as shown in Table 6.10. Table C.6 in Appendix C shows that test case 4a provides less error compared with test case 4b. This means that the latter uses less energy than test case 4a and hence by the cost function has shown to provide better performance with respect to energy consumption and accuracy.

When exposing Cybership III to irregular waves, the simulation time has to be of a certain length. If the time series were too short, the performance could give the wrong image of the performance of the controllers. An example is the vessel being exposed to wave trains of large waves for a certain time resulting in large motions for the vessel to compensate for thus a increased error. On the other hand, the vessel can be exposed to shorter waves leading to less oscillations of the states. Simulations should be performed long enough for the vessel to experience different types of waves so that the different tuning strategies are comparable. This could have been a limitation for the test cases performed at the MCLab. With more test time the simulations could have been tested for 30 minutes each test case in stead of six minutes that was done in this thesis.

Fossen (1991) and Hoang and Kreuzer (2008) had the aim of testing the SMC for ROVs and the results shown in this thesis has shown that SMC should be tested more for DP on ships in the future.

6.3.2 Comparison of Results from MCSim and Experiments in MCLab

In Chapter 5, the SMC and PID-AFB were tested in MCSim with three different sea states, calm, harsh and extreme (test case 1 and 2). In this chapter, test case 3 and 4 that were performed in the MCLab are presented. These test cases were performed when Cybership III was exposed to two different sea states, one calm and one harsh. The extreme sea state was not tested in the model basin due to facility limitations.

The results from test case 1 and 2 has shown that the SMC provided better performance for the first two sea states tested, while PID-AFB was best in extreme seas. Out of test case 3 and 4, the SMC provided best performance when tested for both sea states. In the MCSim tests, PID-AFB showed best performance out of the other tuning strategies for this controller when increasing the inertia as much as possible. On the other hand, the SMC showed best performance compared with the other tuning strategies for that controller when the inertia and damping matrices was expected to be perfectly estimated.

The PID-AFB provided best precision compared with other PID-AFB test cases and was most energy saving when operating with the increased mass of $\Delta K = 30$ kg in the MCLab. When testing the SMC in the calm sea state, expecting no overestimations of the inertia and damping matrices provided best results compared

with +30% overestimations. When testing the same controller with +40% overestimation of the inertia and damping in the harsh sea state, the SMC showed the best overall results, also compared with the PID-AFB. This contradicts the results found in MCSim when 0% uncertainty was best for the most harsh sea state. This observation may have many reasons. In MCSim, an increase of the virtual inertia $\boldsymbol{H}$ when using PID-AFB control provided better performance and the performance was improved for every test case increasing it. This did not work in the MCLab because the cost takes energy consumption into account and moving too much mass is very expensive.

A second observation was when choosing $\hat{\boldsymbol{M}}$ and $\hat{\boldsymbol{D}}$ the same as the system's inertia and damping matrices $\boldsymbol{M}$ and $\boldsymbol{D}$ used to design the process plant model. The SMC with 0% uncertainty performed better with this tuning strategy than with overestimations in MCSim. If the MCSim model was a good and precise model with realistic waves, the same tuning strategy should be the best when testing Cybership III in the model basin with the same waves acting on the vessel. The result was opposite, in the MCLab, the best test case was as shown in Table 6.11 below the mid rule, an uncertainty of +40%. The third observation was when testing the gain matrices used in MCLab in the MCSim model, they did neither give satisfactory nor same control. This observation is a proof of the difference between the MCSim model and the actual Cybership III as shown in Figure B.6. As mentioned in Section 6.2.3, the system matrices $\boldsymbol{M}$ and $\boldsymbol{D}$ used to develop MCSim and used by the controllers were not the same as in the actual vessel. In addition to these findings, it is believed that the waves generated in MCSim were not the same as the real waves generated in the MCLab.

By the above mentioned and discussed test cases, the SMC with overestimated inertia and damping matrices $\hat{\boldsymbol{M}}$ and $\hat{\boldsymbol{D}}$ of +40% has shown better performance than PID-AFB with $\Delta K = 30$ kg in the highest sea state that was possible to test Cybership III with in the MCLab. In Table 6.11 the SMC provided a lower cost than the PID-AFB in all test cases performed in harsh seas. The SMC provided 1.85 less cost when evaluated by J_{IAE}, 307 less cost when evaluated by J_{ITAE} and 0.14 less cost when evaluated by J_{ISE}.

This comparison of controllers could be tested more widely such as including more test cases and doing experiments with a different desired heading and introducing underestimations of the inertia and damping with the SMC.

The MCSim model is now experienced to not be comparable with Cybership III tested in the same environment. It does not exist any good thruster dynamics in MCSim closely related to the thruster dynamics on Cybership III. This means that the forces generated by the control system in MCSim are not sent through a thruster dynamics model comparable with the one on Cybership III such that the forces applied to the vessel in MCSim are not comparable with those generated in the MCLab. In addition, the observer in MCSim uses the commanded forces $\boldsymbol{\tau}_c$ directly from the controller as input, while the observer implemented on Cybership III uses the measured forces $\boldsymbol{\tau}_m$ generated by the thrust allocation. This difference in forces

applied to the vessel will make the vessel in the and MCSim model not comparable to Cybership III in the MCLab. The test results in Figure B.6 for when applying the gain matrices found from tuning in the MCLab to the controllers in MCSim showed that the models were not comparable. The reason for the performance seen in that figure is too low gains.

One similarity of the test cases done in the MCLab and MCSim was the tests cases 1a-1b and 2a-2b where the peak period of wave was chosen to be $T_p = 1.5$s in MCSim while in the MCLab chosen to be $T_p = 0.8$s. The reason for not choosing the same in the MCSim test cases was because the wave model in MCSim is not able to generate that low peak periods. Recall from Section 2.1.2, the peak wave frequency is outside the lookup tables for wave generation to the time domain and the RAOs are extrapolated.

The SMC with 0% uncertainty showed best performance in MCSim and in MCLab for the low sea state and the same controller with +40% overestimation provided best performance when testing the vessel in the harsh sea state in the MCLab.

Chapter 7

Conclusion and Future Work

7.1 Concluding Remarks

In this thesis, the SMC and PID-AFB were developed and compared in order to determine which control strategy provided the best performance during station keeping in extreme seas.

Tests were first performed in the Matlab/Simulink simulator MCSim, and afterwards as a model experiment in the MCLab. The performance in MCSim was evaluated by the performance metrics IAE, ITAE and ISE. The tests performed on the real vessel model in the MCLab was evaluated by another measure of performance, total energy consumption from the thrusters multiplied with IAE, ITAE and ISE separately. When the cost function was evaluated with respect to IAE, it was a product of IAE and the total energy consumed by the three thrusters mounted on Cybership III. Hence, the controllers are no longer only evaluated by the accuracy as in MCSim, but also by energy consumption. The performance metrics applied for evaluation of the test cases in MCSim could only determine if the test cases provided a safe DP operation or not. The aim of testing the controllers in the MCLab was to find a control strategy providing a safe and at the same time green operation.

By evaluating the results for the test cases performed in MCSim and the MCLab, the SMC showed best performance for all sea states except of those tested in extreme seas in MCSim. The PID-AFB with increased effective inertia of the vessel has shown to be more robust than the SMC when tested in extreme seas in MCSim. An increase of the extra mass ΔK to the inertia of the system improved the controller performance significantly in simulations. This controller was straightforward to implement and the challenge was choosing the extra mass added to the inertia used with the AFB. In MCSim the acceleration measurements had to be

filtered in order to achieve less noisy measurements. Acceleration noise was not a challenge when performing test cases in the MCLab due to low measurement noises. On the other hand, the SMC was more tricky to implement and to tune due to no experience with that type of controller. The chattering problem was solved by replacing the signum function used in the SMC control law by a hyperbolic tangent function providing more smooth control inputs.

The test results from the test cases performed in MCSim were not directly comparable with the results obtained in the MCLab. A test was performed in order to check how the gain matrices tuned in the MCLab would affect the controller performance when applied to the MCSim controllers. The controllers did not manage to counteract the waves and this strengthened the statement that the results from testing in MCSim and MCLab were not comparable. The reasons for this may be inaccurate model parameters, the lack of a proper thruster model, 3D effects of the waves in the basin, and reflections on the tank wall. The RAOs for the vessel modeled in MCSim were assumed to be for a different weight distribution than the actual vessel in the MCLab and this causes the vessel to to behave differently when exposed to waves. In order to achieve similar or the same vessel response to the waves, the RAOs in MCSim have to be developed for the same hull, weight, gravity etc. as Cybership III actually has.

Cybership III was recently weighted and it was 11 kg heavier than modeled in the controllers and in MCSim. The simulator MCSim was modeled with data from a report of Cybership III from 1988 as was mentioned in Section 6.2.3 and digitally attached, see Appendx A. The SMC has shown to be more robust than the PID-AFB when exposed to the harsh sea state in the MCLab. It is therefore no surprise that overestimating the mass and inertia of the vessel provides improved performance when the vessel actually is heavier than expected. However, the results has shown that the SMC provided the most safe, smart and green control when overestimating the system's inertia and damping matrices $\boldsymbol{M}$ and $\boldsymbol{D}$ with +40%. As mentioned in Section 6.3.2, the SMC provided in the harsh sea state 1.85 less cost when evaluated by J_{IAE}, 307 less cost when evaluated by J_{ITAE} and 0.14 less cost when evaluated by J_{ISE}.

By performing tests with Cybership III without the knowledge of having inaccurate models, this can be seen as an extra model uncertainty introduced to the vessel. Hence, the SMC has shown that it is more robust to model uncertainties than PID-AFB due to the fact that the vessel inertia was initially inaccurate modeled and tested. Assuming that robust controllers such as PID-AFB and SMC exposed to extreme seas continue to be researched , new control strategies improving todays DP systems for extreme seas may be found.

7.2 Lessons Learned

The work done during this master thesis assignment was very instructive. The test cases done in the MCLab had to be performed twice because the first test cases performed had too short time horizon. When working with irregular seas, the time horizon needs to be long enough so that the number of waves passed are representative of the sea state. However, even though the length of the test cases performed in the MCLab is believed to be sufficient, it could have been extended for future tests. The reason for this is because if the time horizon is long enough, wave trains does not contaminate test results such that different test cases are more comparable.

The difference between working in a Matlab/Simulink environment and with a real model experiment performed in a basin is enormous. When performing experimental tests in the MCLab, it is smart to start one week prior to the booked test period. Creating the communication between all units that has to communicate during tests can take time and if bugs appear, as they always do, extra days are valuable. Customizing the controllers with observer and reference model made in MCSim to fit with NIVeristand and developing the HMI interface takes time. The preliminary work linked up to the testing in the MCLab was done one week before the test week.

When tuning controllers in the model basin, it is important to start with very low gains to see how the vessel responds independent of if the gains were satisfactory in the MCSim tests. The first tests with Cybership III in the MCLab was performed with gain matrices obtained from tests in MCSim. Thin ropes should be attached to the vessel in order to counteract aggressive behavior due to large gain matrices. Analyzing plots after observing them in real-time on the NIVeristand HMI and on the actual vessel, gives a very intuitive understanding of the vessel motion relative to the time horizon e.g. how large oscillations in heading over a time horizon actually looks like on a vessel. This was noticed when processing results after test cases.

When first testing Cybership III in the model basin, the vessel did not behave as expected. The reason for this was found to be the thrusters not set in the correct position such that the controller thought the forces was applied to the correct angles, but every time a new error occurred the controller had to try to compensate for it.

The position reference system in the model basin was very unstable and sometimes the measurements froze. If the measurements freeze when the vessel was out of the desired set point, the vessel could collide with the walls when compensating for a constant error, break the markers and new tests had to be done. For future tests, extra days should be added to the original planned amount of test days.

7.3 Future Work

Suggested areas for future work are:

1. Update the process plant model in MCSim with new system matrices describing Cybership III as it is today and find new RAOs for Cybership III and implement them in the MCSim vessel model.
2. Design a model for thrust allocation and thruster dynamics in MCSim such that it is more comparable with experiments in the MCLab.
3. Compare the vessel response to the waves generated by the wave model in MCSim with the vessel response to the waves generated by the DHI Wave Synthesizer wave flap in the MCLab to check the credibility of the waves..
4. Extend test cases for both controllers with more uncertainties and extra inertia e.g. underestimation of inertia and damping matrix, and different angles for the waves encountering the vessel.
5. Extend the lengths for the test cases in MCLab when testing with irregular waves and repeat the experiment.

Bibliography

Agrachev, A. A., Sontag, E. D., Utkin, V. I., Morse, A. S., Sussmann, H. J., 2004. Nonlinear and Optimal Control Theory. Springer.

Alphatronmarine, 2015. DP vessel.
URL `http://www.marineinsight.com/wp-content/uploads/2011/08/Chloe_Candies.jpg`

Brodtkorb, A. H., Sørensen, A. J., Teel, A. R., 2014. Increasing the operation window for dynamic positioned vessels using the concept of hybrid control. In: International Conference on Ocean, Offshore and Arctic Engineering. ASME, San Francisco, California, USA.

Bryson, A. E., 2002. Applied Optimal Control. The Press Syndicate of The University Of Cambridge.

Fossen, T. I., 1991. Nonlinear modelling and control of underwater vehicles. Ph.D. thesis, Norwegian University of Science and Technology (NTNU), Trondheim, Norway.

Fossen, T. I., 2011. Handbook of Marine Craft Hydrodynamics and Motion Control. Wiley.

Fossen, T. I., Perez, T., 2010. Marine systems simulator.
URL `http://www.marinecontrol.org`

Fossen, T. I., Skjetne, R., Lindegaard, K. P. W., 2002. Inertia shaping techniques for marine vessels using acceleration feedback. In: Proceedings of the 15th IFAC World Congress. Barcelona, Spain

Fossen, T. I., Strand, J. P., jan 1999. Passive nonlinear observer design for ships using Lyapunov methods: full-scale experiments with a supply vessel. Automatica 35 (1), 3–16.

Hespanha, J., 2009. Linear systems theory. Princeton university press.

Hoang, N. Q., Kreuzer, E., 2008. A robust adaptive sliding mode controller for remotely operated vehicles. Technische Mechanik, 185 – 193.

Khalil, H. K., 2002. Nonlinear Systems. Prentice Hall.

Lindegaard, K.-P. W., 2003. Acceleration feedback in dynamic positioning. Ph.D. thesis, Norwegian University of Science and Technology (NTNU), Trondheim, Norway.

Nguyen, T. D., 2005. Design of hybrid marine control systems for dynamic positioning. Ph.D. thesis, National University of Singapore.

Nguyen, T. D., Sørensen, A. J., Tong Quek, S. T., 2007. Design of hybrid controller for dynamic positioning from calm to extreme sea conditions. Automatica 43 (5), 768–785.

NTNU, 2015. The marine cybernetics laboratory.
URL `http://www.ntnu.no/imt/lab/cybernetics`

Perez, T., Smogeli, Ø. N., Fossen, T. I., Sørensen, A. J., 2006. An overview of the marine systems simulator (mss): A simulink toolbox for marine control systems. Modeling, Identification and Control: Norwegian Research Bulletin 27 (4), 259–275.

Price, W. G., Bishop, R. E. D., 1974. Probabilistic theory of ship dynamics. Chapman and Hall.

Ruth, E., 2008. Propulsion control and thrust allocation of marine vessels. Ph.D. thesis, Norwegian University of Science and Technology (NTNU), Trondheim, Norway.

Seshagiri, S., Khalil, H., 2002. On introducing integral action in sliding mode control. In: Proceedings of the 41st IEEE Conference on Decision and Control. Las Vegas, Nevada, USA, pp. 1473 – 1478.

Slotine, J. J. E., Li, W., 1991. Applied Nonlinear Control. Prentice Hall.

Smogeli, Ø. N., Sørensen, A. J., Minsaas, K. J., 2008. The concept of anti-spin thruster control. Control Engineering Practice 16, 465 – 481.

Sørensen, A. J., 2013. Marine Control Systems: Propulsion and Motion Control of Ships and Ocean Structures Lecture Notes.

Sørensen, A. J., Strand, J., Nyberg, H., 2002. Dynamic positioning of ships and floaters in extreme seas. In: Proceedings of OCEANS'02 MTS/IEEE. Vol. 3. pp. 1849–1854 vol.3. Biloxi, Mississippi, USA

Steen, S., 2014. Experimental Methods in Marine Hydrodynamics. Department of Marine Technology, NTNU, Trondheim, Norway, lecture notes.

Torsethaugen, K., 2004. Simplified double peak spectral model for ocean waves. In: Proceedings of the 14th international offshore and polar engineering conference. International Society of Offshore and Polar Engineers, pp. 1 – 9. Mountain view, CA, USA

Appendices

Appendix A

Digital Attachments

The digital attachments for this thesis are shown in Table A.1. The Matlab/Simulink model with code used for tests in MCSim is found in Attachment 1. The Matlab/Simulink/NIveristand model with code used in the MCLab is included in Attachment 2. In Attachment 3, a report from 1988 is included to back up information. A video illustrating the equipment in MCLab and Cybership III in the model basin when performing test cases is found in Attachment 4.

Table A.1: Digital attachments.

Attachment	**Description**
1	MCSim Matlab/Simulink model with code
2	MCLab Matlab/Simulink/NIVeristand model with code
3	Report of Cybership III from 1988
4	Video illustrating tests and equipment in MCLab

Appendix B

Experiments in MCSim and MCLab

B.1 MCSim Software

Centre for autnomous marine operations and systems (AMOS) at NTNU has developed and uses a Matlab/Simulink simulator MCSim (Perez et al., 2006) for floaters and rigs as a part of the Marine System Simulator toolbox (MSS) (Fossen and Perez, 2010). The MSS toolbox consists of three toolboxes: Marine GNC (Guidance and Navigation Control), MCSim and DCMV (Dynamics and Control of Marine Vehicles) toolboxes. The MCSim toolbox is equipped with a vessel model, sensor module, simple observer, simple controller, simple thrust allocation and environmental forces as developing sea states, wind and current. The sensor module is faulty and the thrust allocation only adds a time delay to the forces applied and is not comparable with the real thruster system on Cybership III. The test platform MCSim is useful for this thesis because the simple controllers and observer can be replaced by own control systems, tested and tuned in an environment closely related to the environment at the Marine Cybernetics Laboratory, NTNU, where the final tests are to be done.

B.2 Simulation Results in MCSim

The results presented in this section are from simulations in MCSim when using PID-AFB and SMC. The tuning strategies presented in the following two subsections are those with the best performance for two sea states. In addition, gains

found by tuning in the MCLab has been applied to the controllers in MCSim for testing.

B.2.1 PID with Acceleration Feedback

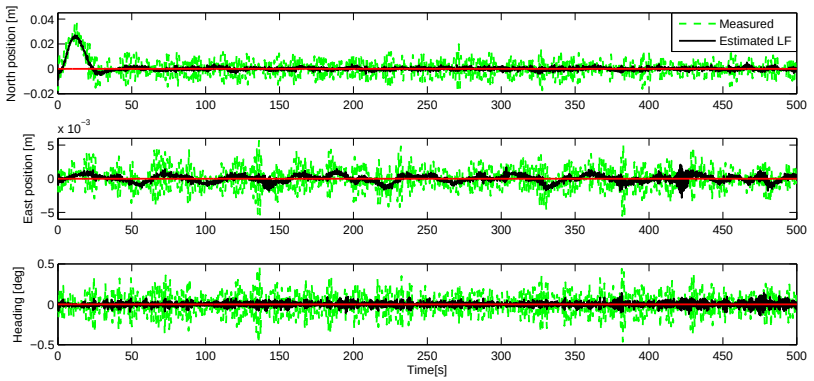

Figure B.1: Positions and heading in test case 1b. Significant wave height $H_s = 0.03$ m and peak period of wave $T_p = 1.5$ s. PID-AFB control with $\Delta K = 30$ kg.

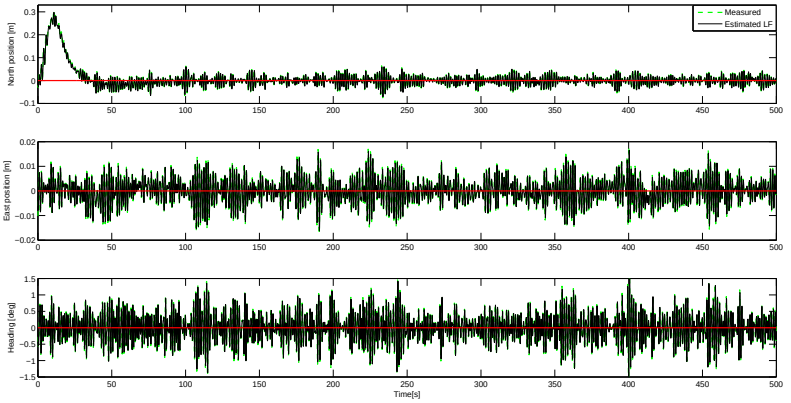

Figure B.2: Positions and heading in test case 1g. Significant wave height $H_s = 0.1$ m and peak period of wave $T_p = 1.5$ s. PID-AFB control with $\Delta K = 50$ kg.

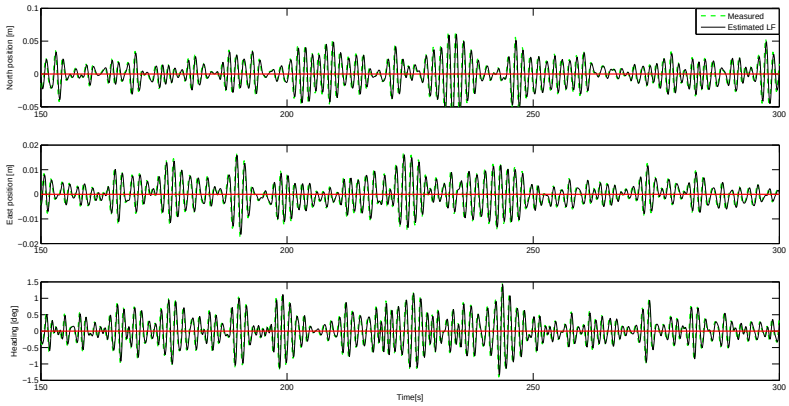

Figure B.3: Close view of positions and heading in test case 1g. Significant wave height $H_s = 0.1$ m and peak period of wave $T_p = 1.5$ s. PID-AFB control with $\Delta K = 50$ kg.

B.2.2 Sliding-mode Control

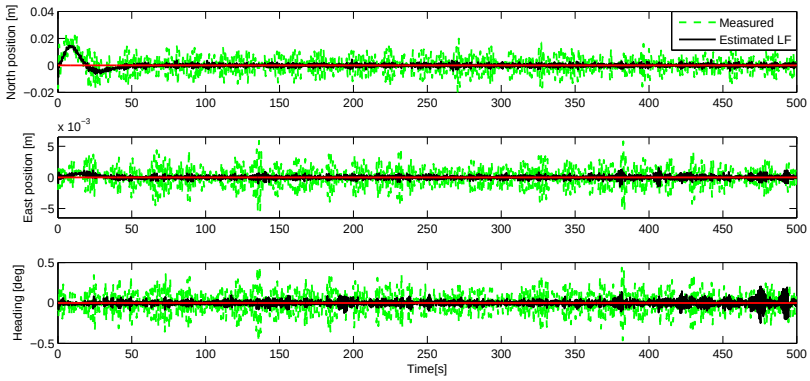

Figure B.4: Positions and heading in test case 2a. Significant wave height $H_s = 0.03$ m and peak period of wave $T_p = 1.5$ s. SMC with 0% uncertainty of $\boldsymbol{D}$ and $\boldsymbol{M}$.

B.2.3 MCLab Gains Applied in MCSim

The gain matrices obtained from tuning in the MCLab was applied to the controllers in MCSim and tested with the simulation time of 500 seconds. As shown in Figure B.6, the gain matrices are too low causing the vessel motion to become unstable. From time 190 seconds the controllers fails to maintain positions and

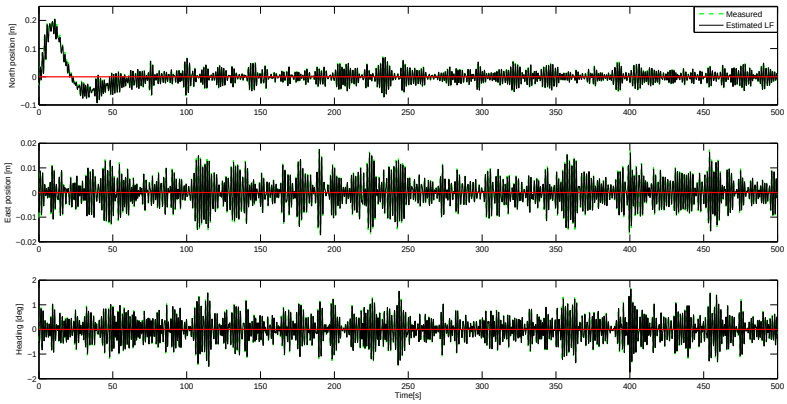

Figure B.5: Positions and heading in test case 2c. Significant wave height $H_s = 0.1$ m and peak period of wave $T_p = 1.5$ s. SMC with 0% uncertainty of $\boldsymbol{D}$ and $\boldsymbol{M}$.

heading. The largest overshoot seen in the north position is close to 2 m while the east position has 1 m overshoot. The heading also becomes more unstable towards the end of the simulation and the vessel heading is moving from side to side with larger oscillations for every time passing the desired heading angle of $\psi_d = 0°$. An overshoot of 2 m in the north position corresponds to 60 m on the full scale vessel.

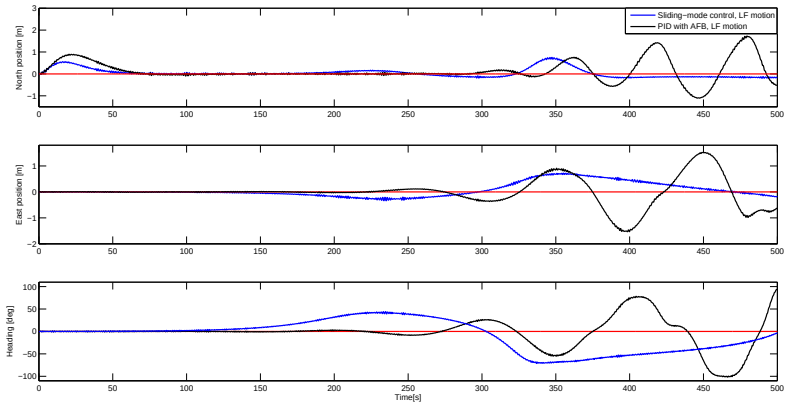

Figure B.6: Gain matrices obtained by tuning in the MCLab tested for controllers in MCSim causing unstable performance. Significant wave height $H_s = 0.1$ m and peak period of wave $T_p = 1.5$ s. SMC with 0% uncertainty of $\boldsymbol{D}$ and $\boldsymbol{M}$ and PID-AFB with $\Delta K = 50$.

B.3 MCLab

The MCLab is equipped with a model basin with Qualisys MCS, an operator PC , joystick, wave generator PC and one DHI Synthesizer wave flap. The model basin is dimensioned ($40 \times 6.5 \times 1.5$) m. A router distributes all data communication between, Cybership III, host PC and the camera PC via WLAN as shown in Figure 6.1. The Qualisys MCS is used to capture markers mounted on Cybership III as shown in Figure B.8 and are placed such that position and attitude can be read and forwarded first to the camera PC, then to the host PC. When the host PC receives measurements from the MCS system and data from Cybership III in real-time the measurements are shown on a NIVeristand HMI. The host PC is used to read measurements, change settings for the controllers and enable/disable forces distributed to the thrusters. A joystick communicating via bluetooth is available for manual control of the vessel. The wave generator PC is connected to the DHI wave synthesizer wave flap and is used to construct sea states by choosing spectrum type and wave parameters. The waves used in the model basin was irregular waves and the spectrum type was JONSWAP. For more information about the MCLab see NTNU (2015)

Figure B.7: MCLab model basin. Three Qualisys MCS units marked with red boxes.

B.4 Cybership III

Cybership III is a miniature model of a supply ship with the scaling factor $\alpha_s = 0.0290$ and has a mass of $m = 76$ kg, length of $L = 2.275$ m, breadth of $B = 0.437$ m and draught $T = 0.153$ m. The vessel is equipped with two main aft azimuth propellers and one fore azimuth thruster that are used as a bow thruster. Cybership III is equipped with an on board computer that communicates with a host PC via WLAN. The host PC that communicates with Cybership III is configured with NIVeristand software and the Matlab/Simulink control system is converted to C-code by this software and downloaded to the on board computer via the WLAN connection prior tests. An accelerometer is mounted on the vessel in order to measure acceleration in surge and sway. Four markers are mounted on the vessel as shown in Figure B.8 for the Qualisys MCS.

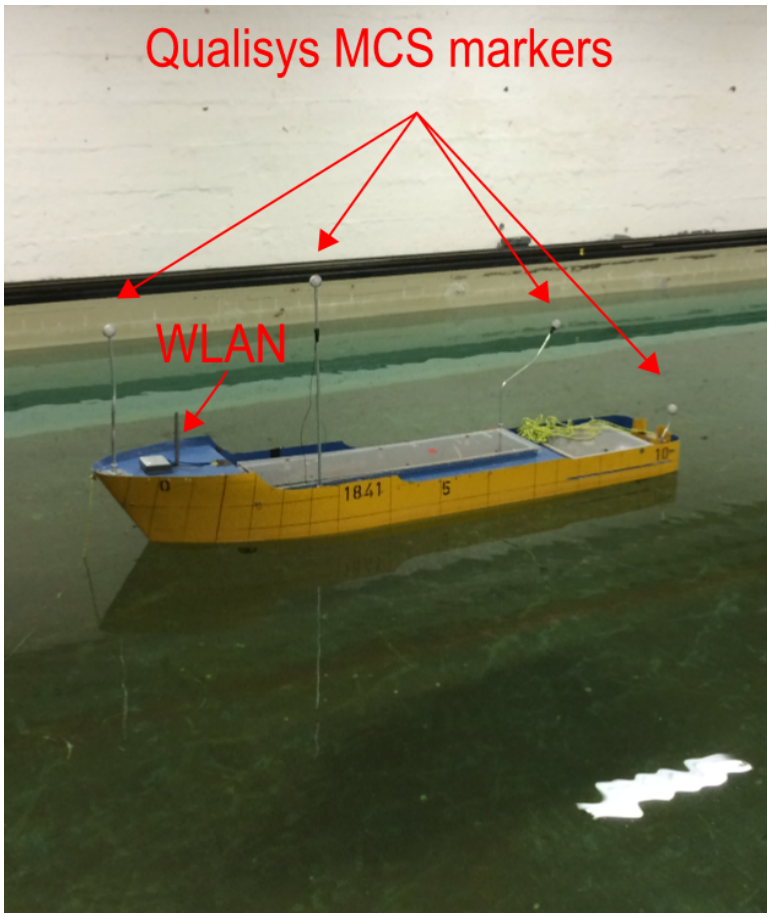

Figure B.8: MCS markers mounted on Cybership III.

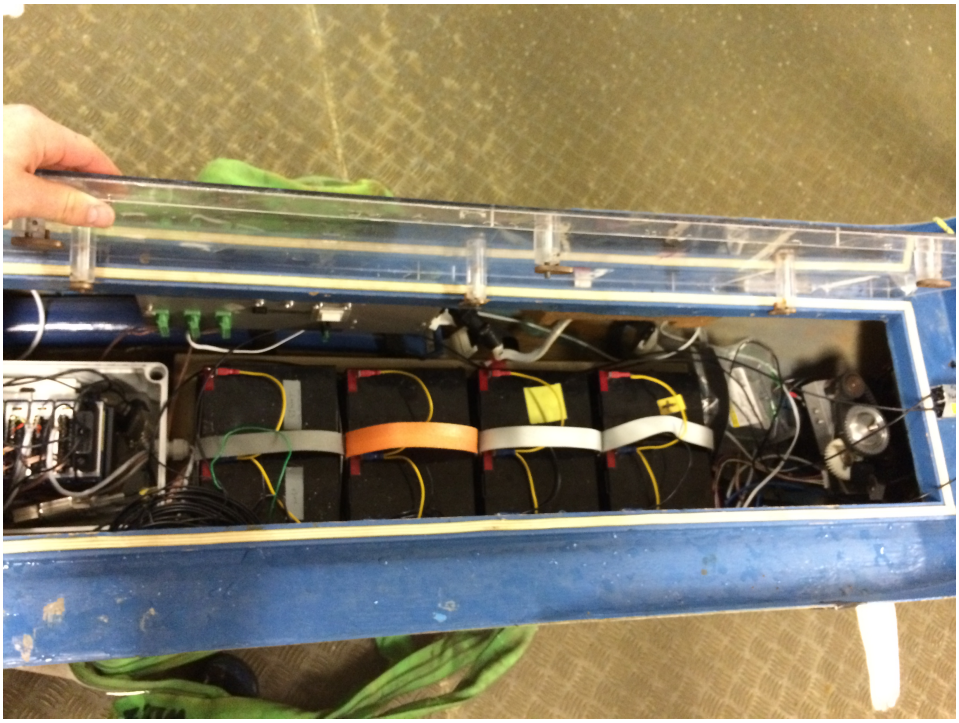

Figure B.9: Cybership III on board computer running on a QNX real-time operating system to the left followed by four batteries.

B.4.1 Thrust Allocation

The thrust allocation for Cybership III is briefly described here. The DP controller produces commanded forces in surge and sway, and a moment in yaw $\boldsymbol{\tau}_c = \begin{bmatrix} X & Y & N \end{bmatrix}^\top$. The thrust allocation distributes the commanded forces $\boldsymbol{\tau}_c \in \mathbb{R}^n$ to the actuators in the electrical system in terms of control inputs $u \in \mathbb{R}^r$. If $r > n$, the vessel is over-actuated and if $r < n$ the vessel is under-actuated. Cybership III is equipped with three azimuth propellers. Ruth (2008) proposed sectors that was better suited than others regarding the choice of the azimuth thruster angle. As shown in Figure B.10, azimuth 1 has the angle of $\alpha = 30°$, azimuth 2 has $\alpha = -30°$ and azimuth 3 has $\alpha = 90°$. The front thruster azimuth 3 is used as a bow thruster.

The thrusters does not understand how to distribute the forces and moment X, Y and N from $\boldsymbol{\tau}_c$ to rpm, thus a configuration of the thrusters forces and moments has to be made. The actuator forces are:

$$\boldsymbol{\tau} = \boldsymbol{T}(\boldsymbol{\alpha})\boldsymbol{K}\boldsymbol{u} \tag{B.1}$$

The thrust configuration matrix $\boldsymbol{T}(\boldsymbol{\alpha})$ corresponds to the forces in x and y direction and the moment with respect to the azimuth thrusters angles. By generating the configuration matrix in (A.2), the control input vector $\boldsymbol{u}$ can be generated and used for commanded rps to the thrusters. $\boldsymbol{K}$ is a diagonal thrust coefficient matrix. Figure B.10 shows the position of the thrusters and by generating the following thrust configuration matrix:

$$\boldsymbol{T}(\boldsymbol{\alpha}) = \begin{bmatrix} cos(30°) & cos(-30°) & cos(90°) \\ sin(30°) & sin(-30°) & sin(90°) \\ l_{1,x}sin(30°) - l_{1,y}cos(30°) & l_{2,x}sin(-30°) - l_{2,y}cos(-30°) & l_{3,x}sin(90°) - l_{3,y}cos(90°) \end{bmatrix}$$

the thrust configuration matrix becomes:

$$\boldsymbol{T}(\boldsymbol{\alpha}) = \begin{bmatrix} 0.8660 & 0.8660 & 0 \\ 0.5 & -0.5 & 1 \\ -0.3097 & 0.3097 & 0.76 \end{bmatrix}. \tag{B.2}$$

Recall from Figure 1.3 that the commanded forces are sent through the thrust allocation part of the DP system and the control input $\boldsymbol{u}$ is generated:

$$\boldsymbol{u} = \boldsymbol{K}^{-1}\boldsymbol{T}^{\dagger}(\alpha)\boldsymbol{\tau} \tag{B.3}$$

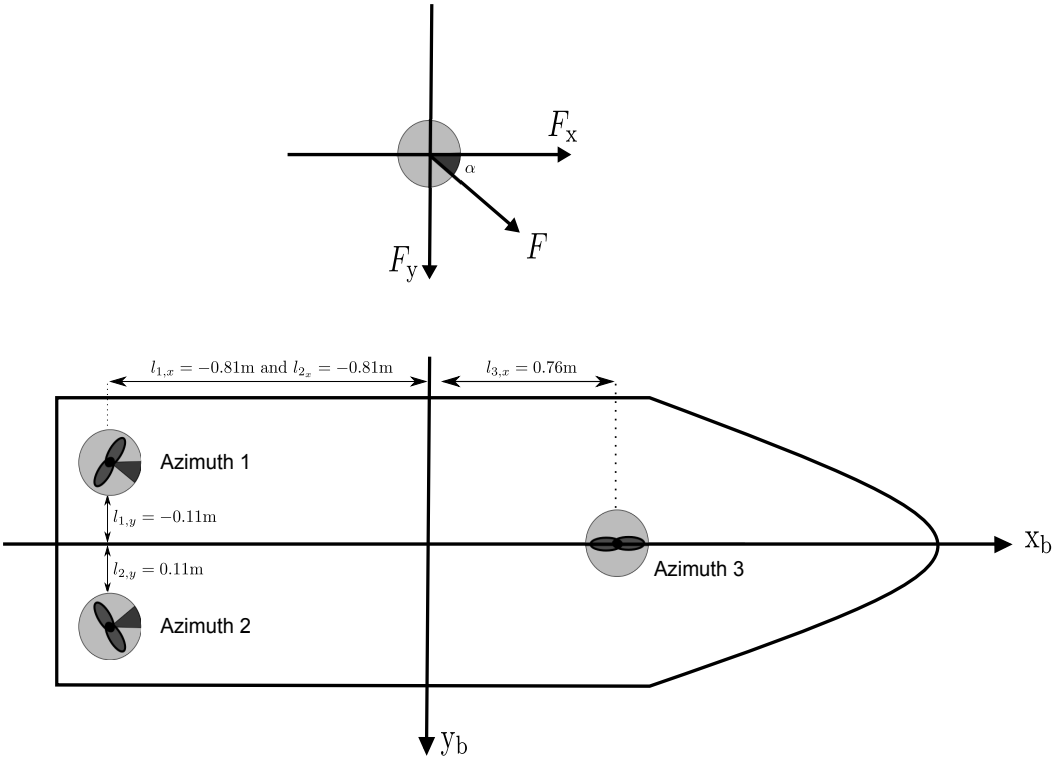

Figure B.10: Cybership III thrust allocation.

Appendix C

Performance Metrics

C.1 Measures of Performance

This section summarizes the methods used to measure the performance of Cybership III in order to find the control strategy that provides best performance with respect to energy consumption and precision. First, measures of performance such as ISE, IAE and ITAE are explained, then these measures of performance are adapted to a cost function. This cost function is the main measure of performance for the test cases of Cybership III in the MCLab.

C.1.1 ISE, IAE and ITAE

ISE, IAE and ITAE are measures of performance used to determine the precision of controllers. ISE integrates the square of the error over time meaning that large errors will be penalized more than smaller ones. IAE integrates the absolute error over time and does not add any weight to the errors. ITAE integrates the absolute error multiplied by the time and errors that exists after far out in a time series will be weighted more than errors appearing early on in the simulation. These performance metrics only evaluates the error of the positions and heading, therefore good results implies a safe operation.

$$\boldsymbol{ISE} = \int_0^t \epsilon^2 dt \tag{C.1}$$

$$\boldsymbol{IAE} = \int_0^t |\epsilon| dt \tag{C.2}$$

$$\boldsymbol{ITAE} = \int_0^t t|\epsilon| dt \tag{C.3}$$

These measures of performance are to be adapted by a cost function in the following subsection.

Tables of ISE, IAE and ITAE

The following tables are results from test case 3 and 4 at the MCLab.

Table C.1: IAE for test case 3, PID-AFB in MCLab.

Case	**North** [m]	**East** [m]	**Heading** [rad/s]	**Total**
3a	8.44	6.71	5.22	20.37
3b	4.40	5.52	3.40	13.32
3c	12.87	6.48	10.72	30.07
3d	12.54	6.96	9.64	29.14
3e	11.32	7.47	10.28	29.07
3f	12.50	7.08	10.46	30.04

Table C.2: ITAE for test case 3, PID-AFB in MCLab.

Case	**North** [m] 10^3	**East** [m] 10^3	**Heading** [rad/s] 10^3	**Total** 10^3
3a	1.47	1.12	0.88	3.46
3b	0.73	0.90	0.63	2.26
3c	2.34	1.22	1.73	5.27
3d	2.35	1.30	1.64	5.29
3e	2.00	1.28	1.96	5.24
3f	2.25	1.31	1.79	5.35

Table C.3: ISE for test case 3, PID-AFB in MCLab.

Case	**North** [m]	**East** [m]	**Heading** [rad/s]	**Total**
3a	0.34	0.21	0.12	0.67
3b	0.08	0.12	0.06	0.26
3c	0.77	0.18	0.51	1.46
3d	0.63	0.21	0.40	1.24
3e	0.54	0.24	0.42	1.2
3f	0.73	0.22	0.48	1.43

Table C.4: IAE for test case 4, SMC in MCLab.

Case	North [m]	East [m]	Heading [rad/s]	Total
4a	2.75	3.96	5.08	11.79
4b	2.91	4.33	4.68	11.92
4c	7.36	5.96	10.56	23.88
4d	7.69	5.81	8.19	21.69
4e	7.95	5.95	9.77	23.67
4f	6.32	4.65	8.47	19.44
4g	7.18	5.02	6.52	18.72

Table C.5: ITAE for test case 4, SMC in MCLab.

Case	North [m] 10^3	East [m] 10^3	Heading [rad/s] 10^3	Total 10^3
4a	0.46	0.67	0.92	2.05
4b	0.59	0.88	0.87	2.34
4c	1.37	1.11	1.71	4.19
4d	1.34	1.08	1.57	3.99
4e	1.38	1.04	1.63	4.05
4f	1.14	0.87	1.59	3.60
4g	1.26	0.98	1.25	3.49

Table C.6: ISE for test case 4, SMC in MCLab.

Case	North [m]	East [m]	Heading [rad/s]	Total
4a	0.03	0.07	0.12	0.22
4b	0.04	0.18	0.09	0.31
4c	0.22	0.16	0.52	0.90
4d	0.26	0.15	0.30	0.71
4e	0.29	0.17	0.41	0.87
4f	0.18	0.1	0.32	0.60
4g	0.23	0.11	0.22	0.56

C.1.2 Cost

A cost function (C.9) is made in order to measure the performance of the PID-AFB and SMC strategies. The cost function is the product of IAE, ITAE, ISE multiplied with the total energy of thruster 1, 2 and 3 for every time step. This

gives a measure how precise the controller is in addition to how much energy it spends on it. With this cost function, the measure of performance determines if the control strategy is smart by the best possible combination of a green and safe operation.

By logging the power consumption from each of the three thrusters on Cybership III, the energy can be found by:

$$\boldsymbol{E} = \int_0^t P(\tau)d\tau \tag{C.4}$$

The power was found by using the measured rpm together with motor constants from the data sheet in Figure C.1. The motor constants corresponding to the thrusters mounted on Cybership III are within the yellow marked box.

The power for each thruster was found by first computing voltage and current. From motor data nr. 15 the voltage was found:

$$\text{Speed constant} = 491 = \frac{rpm}{V} \implies V = \frac{rpm}{491} \tag{C.5}$$

The current was found by using motor data nr. 14:

$$\text{Torque constant} = 19.4 = \frac{mNm}{A} \implies A = \frac{mNm}{19.4} \tag{C.6}$$

In addition, the speed/torque gradient was found from motor data nr. 5:

$$\text{speed/torque gradient} = 8.45 = \frac{rpm}{mNm} \implies \frac{rpm}{8.45} \tag{C.7}$$

And the power is then:

$$P = \frac{rpm^2}{491 \times 8.45 \times 19.4} \tag{C.8}$$

Defining $\boldsymbol{E}_{tot} := \boldsymbol{E}_{thruster1} + \boldsymbol{E}_{thruster2} + \boldsymbol{E}_{thruster3}$ and $\boldsymbol{M}$ as the measure of performance with respect to $\tilde{\boldsymbol{\eta}}$, the cost function becomes:

$$\boldsymbol{J}_j = \sum_{i=1}^{n} \boldsymbol{E}_{tot,i}\boldsymbol{M}_{j,i} \tag{C.9}$$

with n as the number of iterations and $\boldsymbol{M}$ as the measure of performance with j=ISE, ITAE and IAE. This cost function evaluates the different test cases in Chapter 6 in order to determine which control strategy is best suitable for Cybership III.

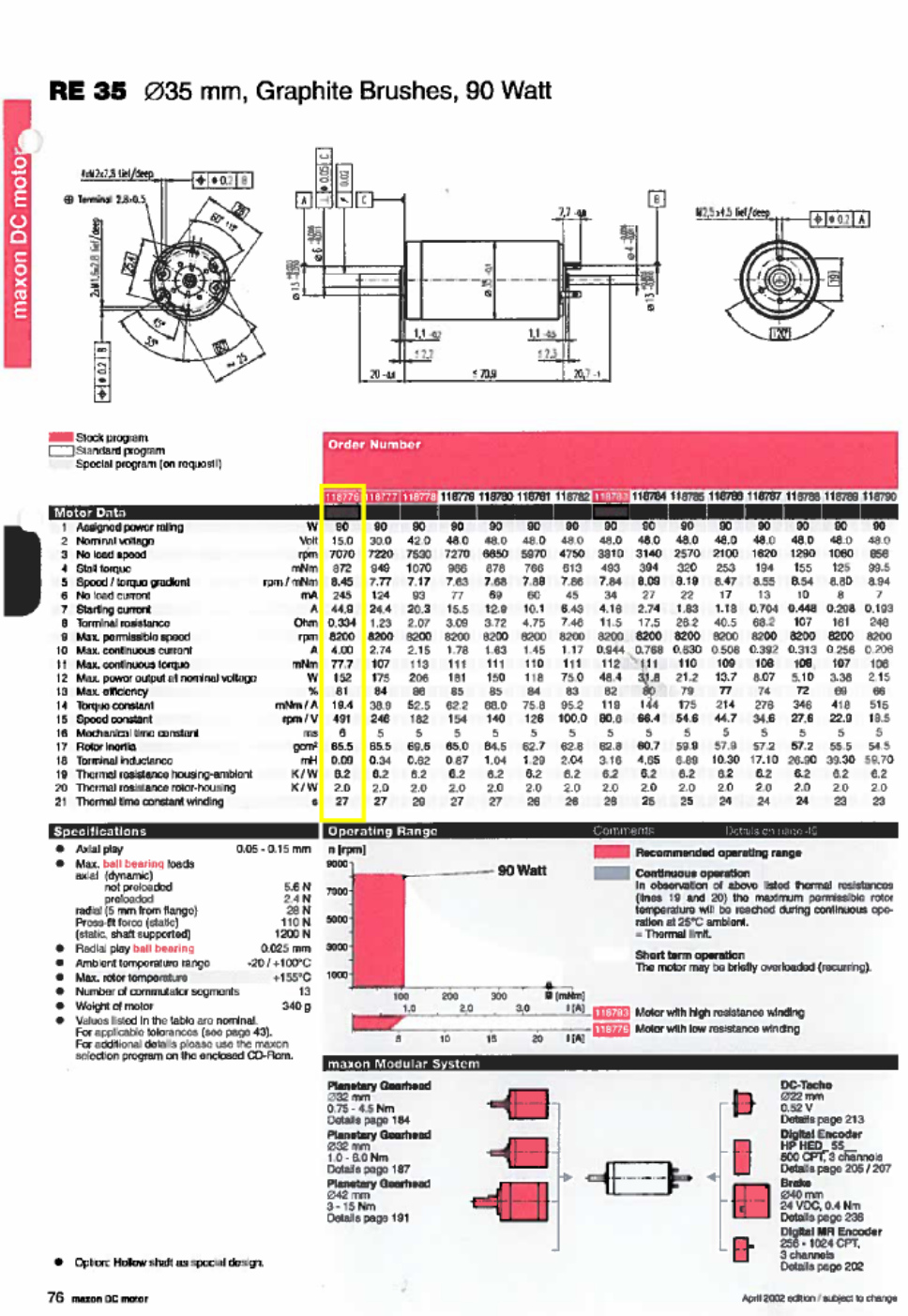

	Motor Data		118778	118777	118779	118778	118780	118781	118782	118783	118784	118785	118786	118787	118788	118789	118790
1	Assigned power rating	W	90	90	90	90	90	90	90	90	90	90	90	90	90	90	90
2	Nominal voltage	Volt	15.0	30.0	42.0	48.0	48.0	48.0	48.0	48.0	48.0	48.0	48.0	48.0	48.0	48.0	48.0
3	No load speed	rpm	7070	7220	7530	7270	6850	5970	4750	3810	3140	2570	2100	1620	1290	1060	856
4	Stall torque	mNm	872	949	1070	986	878	766	613	493	394	320	253	194	155	125	99.5
5	Speed / torque gradient	rpm / mNm	8.45	7.77	7.17	7.63	7.68	7.88	7.86	7.84	8.09	8.19	8.47	8.55	8.54	8.80	8.94
6	No load current	mA	245	124	93	77	59	60	45	34	27	22	17	13	10	8	7
7	Starting current	A	44.9	24.4	20.3	15.5	12.9	10.1	8.43	4.16	2.74	1.83	1.18	0.704	0.448	0.268	0.193
8	Terminal resistance	Ohm	0.334	1.23	2.07	3.09	3.72	4.75	7.46	11.5	17.5	26.2	40.5	68.2	107	161	246
9	Max. permissible speed	rpm	8200	8200	8200	8200	8200	8200	8200	8200	8200	8200	8200	8200	8200	8200	8200
10	Max. continuous current	A	4.00	2.74	2.15	1.78	1.63	1.45	1.17	0.944	0.768	0.630	0.508	0.392	0.313	0.256	0.206
11	Max. continuous torque	mNm	77.7	107	113	111	111	110	111	112	111	110	109	108	108	107	106
12	Max. power output at nominal voltage	W	152	175	206	181	150	118	75.0	48.4	31.8	21.2	13.7	8.07	5.10	3.38	2.15
13	Max. efficiency	%	81	84	86	85	85	84	83	82	80	79	77	74	72	69	66
14	Torque constant	mNm / A	19.4	38.9	52.5	62.2	68.0	75.8	95.2	119	144	175	214	276	346	418	515
15	Speed constant	rpm / V	491	246	182	154	140	126	100.0	80.0	66.4	54.6	44.7	34.6	27.6	22.9	18.5
16	Mechanical time constant	ms	6	5	5	5	5	5	5	5	5	5	5	5	5	5	5
17	Rotor inertia	gcm²	65.5	65.5	69.5	65.0	64.5	62.7	62.8	62.8	60.7	59.9	57.9	57.2	57.2	55.5	54.5
18	Terminal inductance	mH	0.09	0.34	0.62	0.87	1.04	1.29	2.04	3.16	4.65	6.89	10.30	17.10	26.90	39.30	59.70
19	Thermal resistance housing-ambient	K / W	6.2	6.2	6.2	6.2	6.2	6.2	6.2	6.2	6.2	6.2	6.2	6.2	6.2	6.2	6.2
20	Thermal resistance rotor-housing	K / W	2.0	2.0	2.0	2.0	2.0	2.0	2.0	2.0	2.0	2.0	2.0	2.0	2.0	2.0	2.0
21	Thermal time constant winding	s	27	27	29	27	27	26	26	26	25	25	24	24	24	23	23

Specifications	
Axial play	0.05 - 0.15 mm
Max. ball bearing loads	
axial (dynamic)	
not preloaded	5.6 N
preloaded	2.4 N
radial (5 mm from flange)	28 N
Press-fit force (static)	110 N
(static, shaft supported)	1200 N
Radial play ball bearing	0.025 mm
Ambient temperature range	-20 / +100°C
Max. rotor temperature	+155°C
Number of commutator segments	13
Weight of motor	340 g

- Values listed in the table are nominal. For applicable tolerances (see page 43). For additional details please use the maxon selection program on the enclosed CD-Rom.

Figure C.1: Datasheet for maxon DC motors.

Appendix D

Additional Derivations

D.1 Nonlinear Passive Observer Passivity Analysis

This section continous the passivity analysis in Chapter 3. For simplicity, a state state representation of (3.1a), (3.1b) and (3.1e) results in:

$$\dot{\boldsymbol{\eta}}_0 = \boldsymbol{A}_0\boldsymbol{\eta}_0 + \boldsymbol{B}_0\boldsymbol{R}(\mathrm{y}_3)\boldsymbol{\nu} \tag{D.1}$$
$$\mathbf{y} = \boldsymbol{C}_0\boldsymbol{\eta}_0 \tag{D.2}$$

with

$$\boldsymbol{\eta}_0 = \left[\boldsymbol{\xi}^\top \boldsymbol{\eta}^\top\right]^\top,\ \boldsymbol{A}_0 = \begin{bmatrix} \boldsymbol{A}_\omega & \mathbf{0}_{6\times3} \\ \mathbf{0}_{3\times6} & \mathbf{0}_{3\times3} \end{bmatrix}, \tag{D.3}$$

$$\boldsymbol{B}_0 = \begin{bmatrix} \mathbf{0}_{6\times3} \\ \boldsymbol{I}_{3\times3} \end{bmatrix} \text{ and } \boldsymbol{C}_0 = \begin{bmatrix} \boldsymbol{C}_\omega & \boldsymbol{I}_{3\times3} \end{bmatrix}. \tag{D.4}$$

Applying the same simplification for the observer equations:

$$\dot{\hat{\boldsymbol{\eta}}}_0 = \boldsymbol{A}_0\hat{\boldsymbol{\eta}}_0 + \boldsymbol{B}_0\boldsymbol{R}(\mathrm{y}_3)\hat{\boldsymbol{\nu}} + \boldsymbol{K}_0(\boldsymbol{\omega}_0)\tilde{\mathbf{y}} \tag{D.5}$$
$$\mathbf{y} = \boldsymbol{C}_0\hat{\boldsymbol{\eta}}_0 \tag{D.6}$$

with

$$\hat{\boldsymbol{\eta}}_0 = \begin{bmatrix} \hat{\boldsymbol{\xi}}^\top & \hat{\boldsymbol{\eta}}^\top \end{bmatrix}^\top \text{ and } \boldsymbol{K}_0(\boldsymbol{\omega}_0) = \begin{bmatrix} \boldsymbol{K}_1(\boldsymbol{\omega}_0) \\ \boldsymbol{K}_2 \end{bmatrix}. \tag{D.7}$$

The resulting error dynamics is stated by Fossen (2011):

$$\dot{\tilde{\boldsymbol{\eta}}}_0 = \left[\boldsymbol{A}_0 - \boldsymbol{K}_0(\boldsymbol{\omega}_0)\boldsymbol{C}_0\right]\tilde{\boldsymbol{\eta}}_0 + \boldsymbol{B}_0\boldsymbol{R}(\mathrm{y}_3)\tilde{\boldsymbol{\nu}} \tag{D.8}$$

$$\dot{\tilde{\boldsymbol{b}}} = -\boldsymbol{T}_b^{-1}\tilde{\boldsymbol{b}} - \boldsymbol{K}_3\tilde{\mathbf{y}} \tag{D.9}$$

$$\boldsymbol{M}\dot{\tilde{\boldsymbol{\nu}}} = -\boldsymbol{D}\tilde{\boldsymbol{\nu}} + \boldsymbol{R}^\top(\mathrm{y}_3)\tilde{\boldsymbol{b}} - \boldsymbol{R}^\top(\mathrm{y}_3)\tilde{\boldsymbol{b}} - \boldsymbol{R}^\top(\mathrm{y}_3)\boldsymbol{K}_4\tilde{\mathbf{y}}. \tag{D.10}$$

Defining a new state vector:

$$\tilde{\boldsymbol{x}} := \begin{bmatrix} \tilde{\boldsymbol{\eta}}_0 \\ \tilde{\boldsymbol{b}} \end{bmatrix}, \tag{D.11}$$

which gives:

$$\dot{\tilde{\boldsymbol{x}}} = \boldsymbol{A}\tilde{\boldsymbol{x}} + \boldsymbol{B}\boldsymbol{R}(\mathrm{y}_3)\tilde{\boldsymbol{\nu}} \tag{D.12}$$

$$\tilde{\boldsymbol{z}} = \boldsymbol{C}\tilde{\boldsymbol{x}} \tag{D.13}$$

with

$$\boldsymbol{A} = \begin{bmatrix} \boldsymbol{A_0} - \boldsymbol{K}_0(\boldsymbol{\omega}_0)\boldsymbol{C}_0 & \mathbf{0}_{9\times 9} \\ -\boldsymbol{K}_3\boldsymbol{C}_0 & -\boldsymbol{T}^{-1} \end{bmatrix},\ \boldsymbol{B} = \begin{bmatrix} \boldsymbol{B}_0 \\ \mathbf{0}_{3\times 3} \end{bmatrix}, \boldsymbol{C} = \begin{bmatrix} \boldsymbol{K}_4\boldsymbol{C}_0 & -\boldsymbol{I}_{3\times 3} \end{bmatrix}. \tag{D.14}$$

As a part of the Lyapunov analysis, the error dynamics needs to satisfy the Kalman-Yakubovich-Popov (KYP) lemma in order to be passive (Khalil, 2002). By this, the matrix pairs $(\boldsymbol{A}_0, \boldsymbol{B}_0)$ needs to be controllable and $(\boldsymbol{A}_0, \boldsymbol{C}_0)$ must be observable. The controllability and observability matrices must have full rank.